NASA/TM—2017-219379

Control and Non-Payload Communications (CNPC) Prototype Radio Validation Flight Test Report

Kurt A. Shalkhauser, Joseph A. Ishac, and Dennis C. Iannicca
Glenn Research Center, Cleveland, Ohio

Steven C. Bretmersky
MTI Systems, Inc., Cleveland, Ohio

Albert E. Smith
University of South Carolina, Columbia, South Carolina

July 2017

NASA STI Program . . . in Profile

Since its founding, NASA has been dedicated to the advancement of aeronautics and space science. The NASA Scientific and Technical Information (STI) Program plays a key part in helping NASA maintain this important role.

The NASA STI Program operates under the auspices of the Agency Chief Information Officer. It collects, organizes, provides for archiving, and disseminates NASA's STI. The NASA STI Program provides access to the NASA Technical Report Server—Registered (NTRS Reg) and NASA Technical Report Server—Public (NTRS) thus providing one of the largest collections of aeronautical and space science STI in the world. Results are published in both non-NASA channels and by NASA in the NASA STI Report Series, which includes the following report types:

- TECHNICAL PUBLICATION. Reports of completed research or a major significant phase of research that present the results of NASA programs and include extensive data or theoretical analysis. Includes compilations of significant scientific and technical data and information deemed to be of continuing reference value. NASA counter-part of peer-reviewed formal professional papers, but has less stringent limitations on manuscript length and extent of graphic presentations.

- TECHNICAL MEMORANDUM. Scientific and technical findings that are preliminary or of specialized interest, e.g., "quick-release" reports, working papers, and bibliographies that contain minimal annotation. Does not contain extensive analysis.

- CONTRACTOR REPORT. Scientific and technical findings by NASA-sponsored contractors and grantees.

- CONFERENCE PUBLICATION. Collected papers from scientific and technical conferences, symposia, seminars, or other meetings sponsored or co-sponsored by NASA.

- SPECIAL PUBLICATION. Scientific, technical, or historical information from NASA programs, projects, and missions, often concerned with subjects having substantial public interest.

- TECHNICAL TRANSLATION. English-language translations of foreign scientific and technical material pertinent to NASA's mission.

For more information about the NASA STI program, see the following:

- Access the NASA STI program home page at http://www.sti.nasa.gov

- E-mail your question to help@sti.nasa.gov

- Fax your question to the NASA STI Information Desk at 757-864-6500

- Telephone the NASA STI Information Desk at 757-864-9658

- Write to:
  NASA STI Program
  Mail Stop 148
  NASA Langley Research Center
  Hampton, VA 23681-2199

NASA/TM—2017-219379

Control and Non-Payload Communications (CNPC) Prototype Radio Validation Flight Test Report

Kurt A. Shalkhauser, Joseph A. Ishac, and Dennis C. Iannicca
Glenn Research Center, Cleveland, Ohio

Steven C. Bretmersky
MTI Systems, Inc., Cleveland, Ohio

Albert E. Smith
University of South Carolina, Columbia, South Carolina

National Aeronautics and
Space Administration

Glenn Research Center
Cleveland, Ohio 44135

July 2017

Acknowledgments

The National Aeronautics and Space Administration thanks the faculty and staff of the Avionics Engineering Center at the Ohio University Russ College of Engineering and Technology for their institutional support, enabling us to successfully operate the Albany, Ohio, ground station described in this report. NASA also expresses gratitude to the management and staff of Cedar Fair Entertainment Company (Cedar Fair, L.P.) for logistical support at the Cedar Point amusement park, and for permission to access the Lake Erie shoreline to operate the Sandusky, Ohio, ground station.

This report contains preliminary findings, subject to revision as analysis proceeds.

This work was sponsored by the Transformative Aeronautics Concepts Program.

Level of Review: This material has been technically reviewed by technical management.

Available from

NASA STI Program
Mail Stop 148
NASA Langley Research Center
Hampton, VA 23681-2199

National Technical Information Service
5285 Port Royal Road
Springfield, VA 22161
703-605-6000

This report is available in electronic form at http://www.sti.nasa.gov/ and http://ntrs.nasa.gov/

Control and Non-Payload Communications (CNPC) Prototype Radio Validation Flight Test Report

Kurt A. Shalkhauser, Joseph A. Ishac, and Dennis C. Iannicca
National Aeronautics and Space Administration
Glenn Research Center
Cleveland, Ohio 44135

Steven C. Bretmersky
MTI Systems, Inc.
Cleveland, Ohio 44135

Albert E. Smith
University of South Carolina
Columbia, South Carolina 29208

Summary

This report provides an overview and results from the unmanned aircraft (UA) Control and Non-Payload Communications (CNPC) Generation 5 prototype radio validation flight test campaign. The radios used in the test campaign were developed under cooperative agreement NNC11AA01A between the NASA Glenn Research Center and Rockwell Collins, Inc., of Cedar Rapids, Iowa. Measurement results are presented for flight tests over hilly terrain, open water, and urban landscape, utilizing radio sets installed into a NASA aircraft and ground stations. Signal strength and frame loss measurement data are analyzed relative to time and aircraft position, specifically addressing the impact of line-of-sight terrain obstructions on CNPC data flow. Both the radio and flight test system are described.

1.0 Introduction

The potential applications of unmanned aircraft (UA) to new commercial and U.S. Government services are developing rapidly, and UA developers are preparing to demonstrate these services within the United States. Public safety is paramount; to achieve these important new capabilities and enable growth in the domestic UA industry, NASA is working with other U.S. Government agencies to provide technical solutions for safe operation of UA in the national airspace. Through these efforts, NASA will demonstrate the communications system throughput and reliability capabilities needed for remote control of an unpiloted aircraft.

Data from the NASA testing directly supports the RTCA, Inc., Special Committee SC–228 development of the Command and Control (C2) Data Link Minimum Operational Performance Standards (MOPS) (Terrestrial) document, which was prepared for the Federal Aviation Administration (FAA) as RTCA Paper No. DO–362 (Ref. 1). Working closely with the RTCA, NASA has executed flight tests in multiple environments and conditions to accumulate the data needed for systems studies, link budget development, UA-related investigations, and MOPS requirements validation. This report presents a description of the Control and Non-Payload Communications (CNPC) radios, an overview of the airborne and ground measurement systems, and a discussion of the flight parameters used during flight testing.

Signal strength measurement data for the air-ground CNPC radio channels are presented and discussed for multiple test locations, radio waveforms, radio output power levels, flight conditions, aircraft altitudes, and ranges. The effects of line-of-sight obstructions between the ground station and aircraft antennas are demonstrated. CNPC data flow between a single aircraft and ground station (referred to as "point-to-point mode") is analyzed. CNPC data flow from a single ground station to multiple aircraft (networked mode) is also presented.

2.0 Control and Non-Payload Communications (CNPC) Radio Development

Through a cost-sharing cooperative agreement with Rockwell Collins, Inc., the NASA Glenn Research Center designed a prototype UA CNPC system that will allow safe and efficient communications within the L-band and C-band spectrum allocations. The system was based on initial "seed" requirements from RTCA, Inc., Special Committee 203 (SC–203), and is on a path to FAA certification.

The CNPC radio development was accomplished through a series of evolutionary upgrades to the CNPC radio waveform and radio hardware. Table I describes the general technical progression of the radios, beginning from a point-to-point L-band demonstration through dual-band radios offering multi-aircraft control and networked handoff capability (Refs. 2 and 3). The Rockwell Collins/NASA CNPC radio tray is shown in Figure 1.

Figure 1.—Control and Non-Payload Communications (CNPC) radio tray including L-band radio (left) and C-band radio (right) with attendant cabling and interface components.

TABLE I.—EVOLUTION OF PROTOTYPE UNMANNED AIRCRAFT (UA) CONTROL AND NON-PAYLOAD COMMUNICATIONS (CNPC) RADIO

Generation 1	L-band only, single aircraft, single ground station, point-to-point CNPC
Generation 2	C-band, single aircraft, multiple ground stations (networked mode) added; in-flight “handoffs” between ground stations
Generation 3	Capability added for multiple aircraft
Generation 4	Data rates updated to perform testing for preliminary command and control (C2) Minimum Operational Performance Standards (MOPS); data rates adjustable
Generation 5	Data rates and waveforms updated to align with final C2 MOPS; used to perform C2 MOPS verification and validation tests

TABLE II.—TYPES OF COMMUNICATIONS TRAFFIC IN UNMANNED AIRCRAFT (UA) SERVICE CLASSES

Service class	Telemetry	Voice	Navigational aids	Aircraft targets	Weather radar
1	✓				
2	✓	✓			
3	✓	✓	✓	✓	
4	✓	✓	✓	✓	✓

2.1 Service Classes and Data Classes

RTCA SC–228 recognizes that different UA will have varying capabilities for differing CNPC data requirements. As a first step to identifying those requirements, SC–228 defined four service classes (Table II) based on the types of UA communications traffic that would be used. For example, a small UA operating in a remote area at low altitude may only require uplink control and downlink telemetry services (service class 1), but a larger UA operating over a long range and high altitude would require all types of communications services (service class 4).

Glenn performed an extensive analysis of the traffic types for each service class of UA to determine the minimum data rates required. The analysis included data requirements for the airfield departure, en route, and airfield arrival phases of flight. The analysis also included UA operations in both manual (by a ground-based pilot manipulating UA control surfaces in near real time) and automatic modes (by adjustments of flight waypoints for an autopiloted UA). This analysis accounted for the raw payload data, header compression, and overhead for transport and network layer headers and security. These data rates were then converted to user payload bytes per CNPC frame assuming 20-Hz operation for the departure and arrival phases and 15-Hz operation for the en route phase (5 Hz are reserved for the en route acquisition of other ground stations to enable handoffs). The user payload sizes identified in the analysis were then verified using a combination of specialized testing using the Generation 4 (Gen 4) radios and simulations.

The results of the analysis indicated that a minimum of four data classes could efficiently support the four services during various phases of flight. The analysis was based on a set of assumptions about the size and rates for each of the traffic types that may not be representative of the needs all UA. Therefore, a set of data classes were defined for the (Generation 5) prototype radio to provide varying levels of user payload sizes that a UA manufacturer could choose from to support their UA's specific requirements (Table III).

Table IV shows a mapping, based on the data requirements analysis, of the SC–228-defined service classes to the data classes. This table also provides the estimated average percentage of payload bits utilized for each service class, operating mode, and phase of flight.

TABLE III.—CONTROL AND NON-PAYLOAD COMMUNICATIONS (CNPC) DATA CLASSES

Data class	User payload, bytes/frame[a]
1	44
2	100
3	160
4	216

[a]Includes L2 header(s) but excludes bytes for acquisition, preamble, midambles, postamble, forward error correction, and cyclic redundancy check.

TABLE IV.—SERVICE-CLASS TO DATA-CLASS MAPPING

Service class	Aircraft control	Phase of flight	Uplink			Downlink		
			Data class	Utilization, percent	Rate, Hz	Data class	Utilization, percent	Rate, Hz
1	Auto	Departure	1	56	20	1	39	20
		En route	1	31	15	1	37	15
		Arrival	1	88	20	1	45	20
	Manual	Departure	2	46	20	2	62	20
		En route	1	72	15	1	87	15
		Arrival	2	82	20	2	83	20
2	Auto	Departure	2	84	20	2	78	20
		En route	2	93	15	2	95	15
		Arrival	2	98	20	2	81	20
	Manual	Departure	3	66	20	3	77	20
		En route	3	69	15	3	74	15
		Arrival	3	88	20	3	88	20
3	Auto	Departure	2	85	20	3	86	20
		En route	2	95	15	4	82	15
		Arrival	2	97	20	3	88	20
	Manual	Departure	3	69	20	4	86	20
		En route	3	73	15	4	96	15
		Arrival	3	91	20	4	96	20
4	Auto	Departure	2	85	20	3	90	20
		En route	2	95	15	4	86	15
		Arrival	2	97	20	3	91	20
	Manual	Departure	3	69	20	4	89	20
		En route	3	73	15	4	99	15
		Arrival	3	91	20	4	98	20

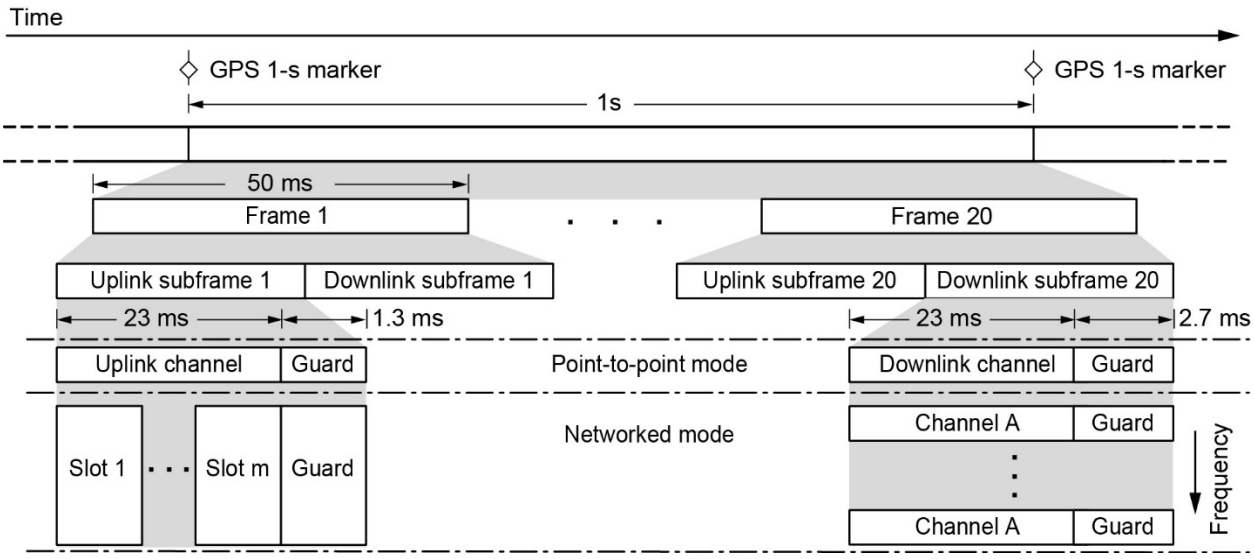

Figure 2.—Waveform overview.

2.2 Waveform Description

The basic structure of the Gen 5 prototype radio waveform has not changed substantially from the original (Generation 1) radio. Each second of time is divided into twenty 50-ms frames in order to support a maximum message rate of 20 messages per second. Time division duplexing is used to further subdivide each of these frames into an uplink subframe and a downlink subframe, as shown in Figure 2.

The Gen 5 waveform supports either point-to-point or networked modes of operation. In the point-to-point mode, a single ground station radio communicates to a single UA radio using up to all 20 frames, employing one of the point-to-point waveform modes in the uplink and one in the downlink. The networked mode of operation is designed to allow a set of ground station radios (acting as one) to communicate to multiple UA radios. For the uplink, this is achieved by using one of the networked uplink modes that use time division multiple access to divide the uplink subframe into slots that are each assigned to an individual UA. For the Gen 5 prototype system, one CNPC radio can provide uplink communications for up to 24 individual UAs ($m = 24$). In the downlink, multiple frequency division multiple access channels are used to support multiple UAs. Therefore, one Gen 5 CNPC radio would be required for each simultaneous UA downlink. In the future, multiple receivers will probably be incorporated into each radio, enabling a single radio to support networked mode operation in a ground station.

2.3 Waveform Modes

The Gen 5 prototype radio waveform supports the four data classes through different waveform modes as indicated in Table V. For the downlink and point-to-point uplink, a separate waveform mode is defined for each data class. The bandwidth and data rate of each of these modes are adjusted to provide the required user payload size per frame. The networked uplink waveform modes operate differently. These modes are defined by the number of slots provided. The data rate and bandwidth are adjusted to provide the same number of bits per user slot. For example, the 12-slot uplink has twice the bandwidth and data rate of the six-slot uplink, but the total number of bits per user slot remains the same. In the networked uplink, data classes are supported by allocating multiple slots, with data class 1 utilizing one slot and data class 3 utilizing three adjacent slots.

TABLE V.—GENERATION 5 CONTROL AND NON-PAYLOAD COMMUNICATIONS (CNPC) WAVEFORM MODES

Communication direction	Waveform mode[a]	Data class	Slots	Bandwidth, kHz	Physical data rate, kbps
Downlink and point-to-point uplink	A	1	---	30	34.5
	B	2	---	60	69
	C[a]	3[a]	---[a]	90[a]	103.5[a]
	D[a]	4[a]	---[a]	120[a]	138[a]
Networked uplink	UL3	1 to 3	3	90	103.5
	UL6	1 to 3	6	180	207
	UL9	1 to 3	9	270	310.5
	UL12	1 to 3	12	360	414
	UL15	1 to 3	15	450	517.5
	UL18	1 to 3	18	540	621
	UL21	1 to 3	21	630	724.5
	UL24[a]	1, 2[a], and 3[a]	24[a]	720[a]	828[a]

[a]Only these waveforms were implemented in the prototype radio.

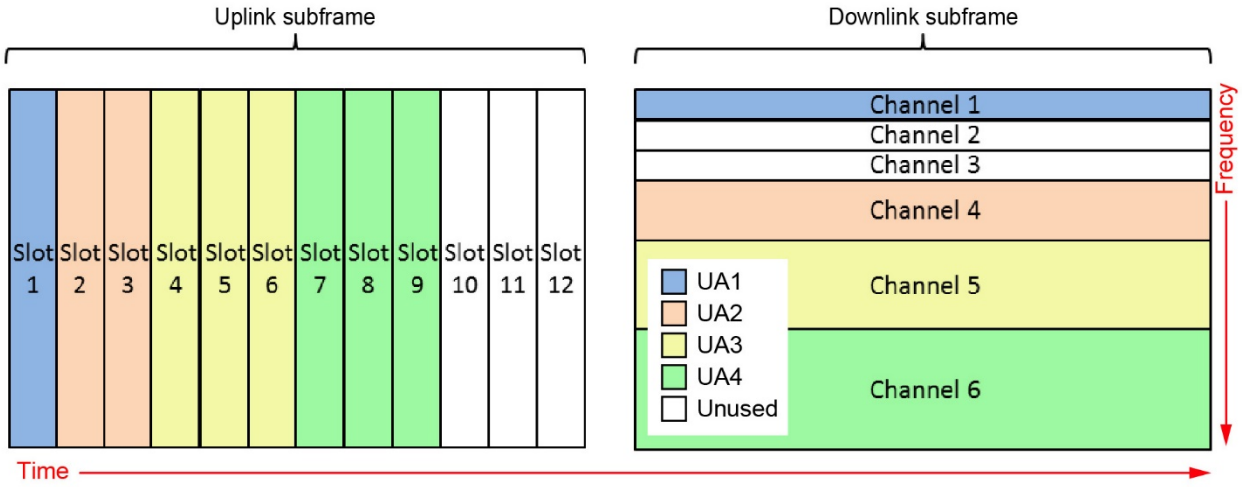

Figure 3.—Example of networked Control and Non-Payload Communications (CNPC) frame usage for four unmanned aircraft (UA). It is not a requirement for the uplink and downlink subframes to utilize the same spectrum. The downlink channels also need not use contiguous spectrum.

Figure 3 shows a single frame of an example networked CNPC system supporting four UAs. The uplink is configured for the 360-kHz 12-slot mode, whereas six downlink channels are allocated in the same spectrum. In this example, UA1 requires data class 1 for the uplink and downlink and is allocated one uplink slot and one 30-kHz downlink channel. UA2 uses two uplink slots and one 60-kHz downlink channel to support its requirement for data class 2 uplink and downlink. UA3 receives three uplink slots and transmits in one 90-kHz downlink channel for data class 3. UA4 requires a data class 3 uplink and a data class 4 downlink, and as such is allocated three uplink slots and one 120-kHz downlink channel.

All waveform modes are modulated using Gaussian minimum shift keying (GMSK), which is a continuous-phase modulation with a constant power envelope. The waveforms can be configured to operate over a range of frequencies and output powers. The L-band is configurable for frequencies between 961 to 974 MHz, with output powers of approximately 0.25 to 6 W. The C-band radio is capable of operating at frequencies from 5031 to 5090 MHz at approximately 0.5 to 25 W.

The constant power envelope of GMSK modulation reduces the complexity of the radio transmitter amplifiers, but at 1 bit per symbol, GMSK only offers bandwidth efficiency of 1.15 bits/Hz. Future radios would likely incorporate more efficient modulation techniques to conserve frequency spectrum while improving data throughput.

3.0 Test System Description

A diagram of the CNPC radio validation test system is presented in Figure 4. The primary elements of the system are the test aircraft and ground station, both of which are monitored and controlled by a centralized test operations center at Glenn. One pair of CNPC radios (one L-band and one C-band) was installed in both the test aircraft and at each ground station to establish bidirectional radio connectivity, allowing researchers to simultaneously monitor both air-to-ground and ground-to-air signal propagation characteristics in both frequency bands. The equipment used in these tests was selected for prototyping purposes only, with the objective of recording the performance of the air-to-ground radio links. Antenna types, antenna placement, and transmit power levels are not necessarily those to be used in the future deployed system.

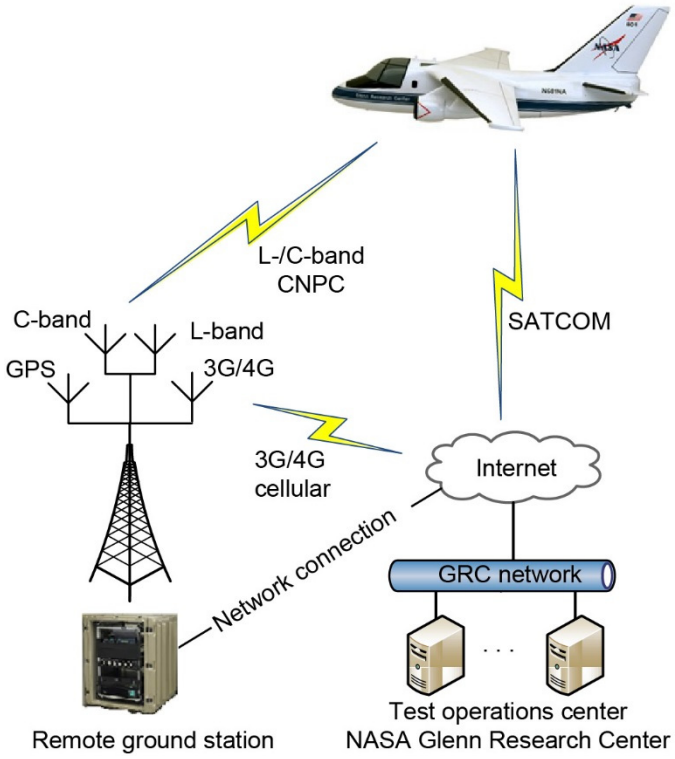

Figure 4.—Control and Non-Payload Communications (CNPC) baseline radio test system. GPS, Global Positioning System; SATCOM, satellite communications.

In order to capture data in a specific terrain setting, a ground station was placed in one of three unique geographic locations and the planned aircraft flight pattern shifted according to that location. For flight tests over hilly terrain, ground station 2 (GS2) was installed at the Ohio University Gordon K. Bush Airport in Albany, Ohio (airport designation: KUNI). For flight tests over urban environments and capturing airfield departure and standard climb-out to class A airspace, ground station 1 (GS1) at Glenn's Lewis Field campus in Cleveland, Ohio, was used. For the over-water tests, a mobile equipment trailer with an extendable antenna mast (designated ground station 3 (GS3)) was temporarily positioned at the extreme western edge of Lake Erie in Sandusky, Ohio. Each ground station was equipped with an Internet connection for remote control, monitoring, programming, and test operations. A commercial, satellite-based communications link was used to coordinate test operations between Glenn's test operations center and the test aircraft.

3.1 Description of Airborne Platform Used in Validation Testing

A Lockheed model S–3B Viking aircraft owned by Glenn (FAA aircraft registration number N601NA) was used for all of the CNPC radio flight tests. The twin-turbofan jet research aircraft had been used extensively for the channel sounding measurements and for numerous developmental CNPC radio flight tests.

The S–3B aircraft possessed multiple features supporting the CNPC radio flight testing:

- A high-mount cantilever wing—provided an unobstructed radiofrequency (RF) line-of-sight path between the airborne CNPC radio test antennas and the ground stations during level flight and light banking
- Wingspan—68 ft, 8 in.
- Long-range flight (endurance) capability—typical duration of 2 to 4 hr
- Large, pressurized cabin—accommodates four-person crew (pilot, co-pilot, and two research personnel)
- Commercial satellite communications (SATCOM) link for experiment coordination with ground station operators
- In-cabin equipment racks, ample research electrical power, and Global Positioning System (GPS) test support accommodations
- Excellent flight stability and maneuverability—standard rate turns at 20° to 30° aircraft banking, maximum 60° bank turns, and sustained 10° bank (slip) possible
- Maximum true airspeed—360 kt (414 mph, 185 m/s) at 29 kft (8839 m)
- Cruise speed—250 kt (287 mph, 128 m/s)
- Minimum airspeed—120 kt (138 mph, 61 m/s)
- Range—over 1000 nmi
- Service ceiling—29,000 ft (8839 m)

The airborne research equipment consisted of one L-band and one C-band CNPC radio, electrical power supply hardware, GPS and time server equipment, computers, and networking equipment. These components were mounted in two 19-in.-wide equipment racks within the pressurized volume in the rear of the aircraft.

Flight-qualified, low-profile, omnidirectional, 0.25-wave monopole antennas were permanently mounted on the underside of the S–3B aircraft. One antenna serves the L-band transmit/receive function, and one antenna serves the C-band transmit/receive function. These antennas were connected to the radio

by customized, aircraft-grade, fully shielded coaxial cables with low insertion loss, allowing each radio system to be operated without the need for additional signal amplification. When landing gear is stowed for level flight, both antennas have a full hemisphere field of view (in the “downward” or nadir direction) that is unobstructed by protuberances from the aircraft. Figure 5 shows the locations of the CNPC antennas and the underside geometry of the S–3B test aircraft. The CNPC antennas are positioned slightly right of the aircraft centerline to reduce coupling to adjacent aircraft antennas. Aircraft CNPC antennas are shown in Figure 6.

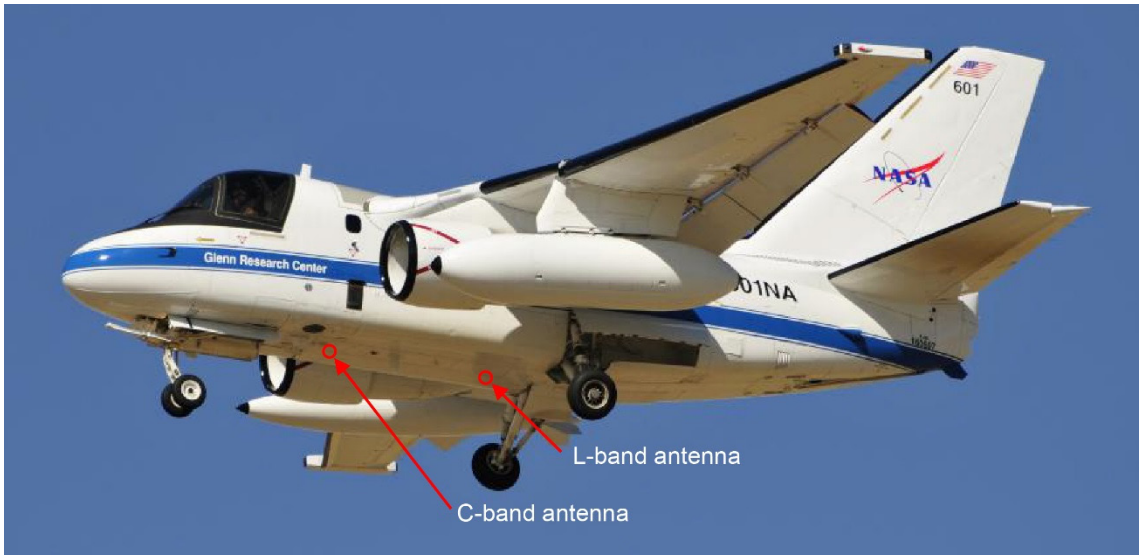

Figure 5.—NASA S–3B Viking test aircraft showing approximate Control and Non-Payload Communications (CNPC) antenna mounting locations.

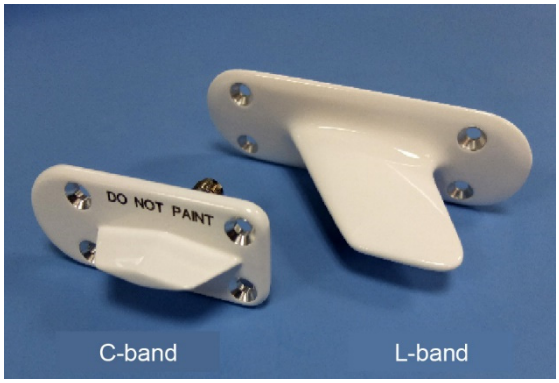

Figure 6.—Aircraft Control and Non-Payload Communications (CNPC) antennas.

3.2 Description of Ground Stations Used in Validation Testing

Three separate ground stations were used in the validation testing, each prepared and operated by Glenn. Each ground station was connected to the Internet through either a hard-wired host-site network or a 3G/4G cellular network, which allowed full control and monitoring from Glenn's test operations center. A firewall or gateway was responsible for managing the networks provided by the 3G/4G connection and the host network at the installation site. In situations where both existed, the gateway used the cellular network as a backup. Had the host network experienced an outage or other disruption, the gateway would have automatically switched to the cellular connection. The cellular modem was selected to provide data access using one of several cellular service providers, depending on service available at the specific ground station location.

An uninterruptible power supply (UPS) delivered 120-V power to three load circuits, two of which were remotely controllable. The Load 1 circuit fed the power supply for the radios and radiation safety indicator. The Load 2 circuit was connected to the Ethernet switch and the computer, which allowed for power cycling (yielding a reboot of the computer) if necessary. The Load 3 circuit, which was not switchable, provided continuous power to the cellular modem and the firewall. In the event of a prime power (mains) loss at the ground station installation site, the 1350 W UPS had the battery capacity to provide backup power to the ground station for approximately 30 min. During this time, operators would have secured all test data and performed a controlled shutdown of the network and computer. Figure 7 illustrates the internal connections and interfaces for the ground station.

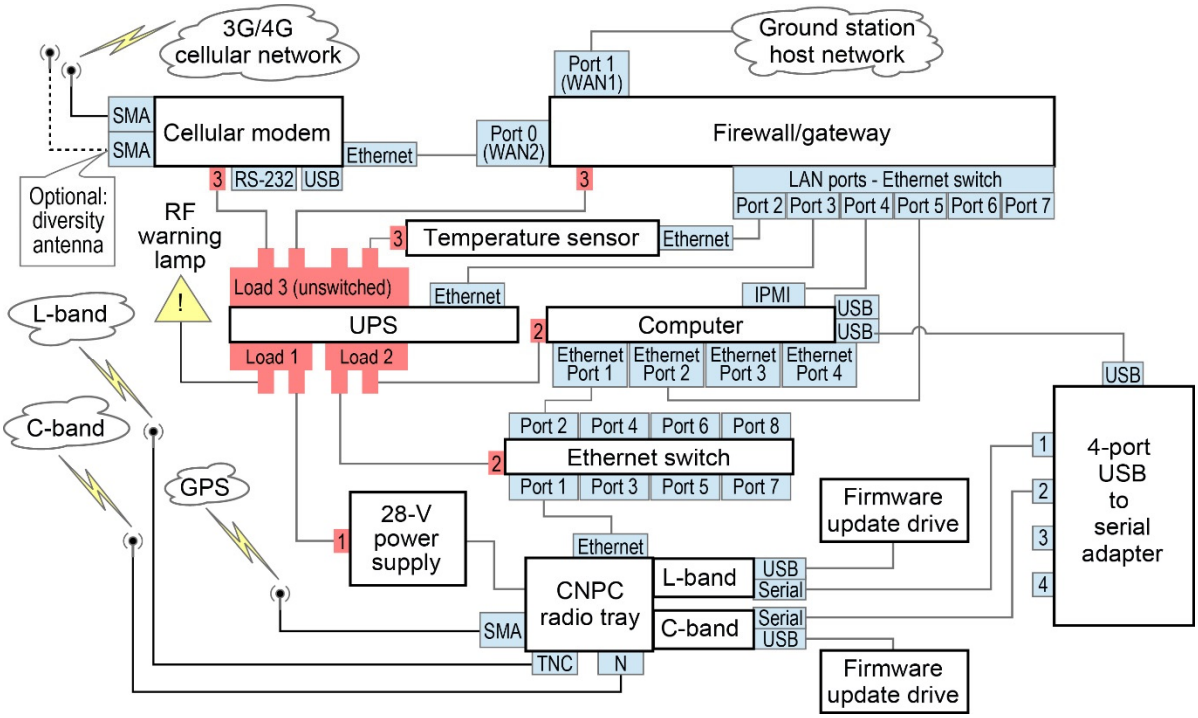

Figure 7.—NASA Control and Non-Payload Communications (CNPC) ground station. SMA, SubMiniature version A; LAN, local area network; RF, radiofrequency; TNC, Threaded Neill-Concelman; UPS, uninterruptible power supply; USB, Universal Serial Bus; WAN, wide area network.

A GPS antenna fed the GPS signal to the CNPC radio, which was used as a time server for the ground station computer and cellular modem. This allowed the equipment internal to the ground station to be time synchronized as well as synchronized with the aircraft, other ground stations, and test equipment at the various test locations. This synchronization was necessary for measuring data flow latency throughout the ground station network.

The computer had an Intelligent Platform Management Interface (IPMI) that permitted remote monitoring and control of the computer without the use of the operating system. In the event of a computer failure, the ground station systems could have been powered down and rebooted and had errors logged via the IPMI.

Figure 8 shows the ground station equipment in the transport case at a typical installation site. All antenna, power, and network cabling exiting the case to external locations are visible at the lower right. Figure 9 shows the L-band and C-band antennas installed at the Ohio University airport in Albany, Ohio, as configured for the validation flight tests. Figure 10 shows the L-band and C-band antennas installed at Glenn's Lewis Field campus in Cleveland, Ohio.

Figure 8.—Transportable ground station.

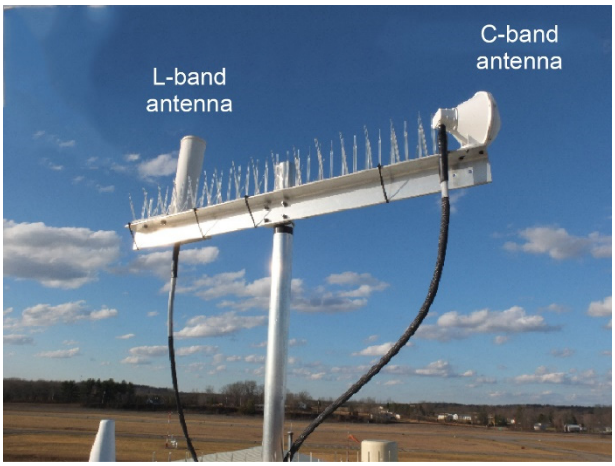

Figure 9.—Ground station 2 (GS2) antennas installed at Ohio University airport.

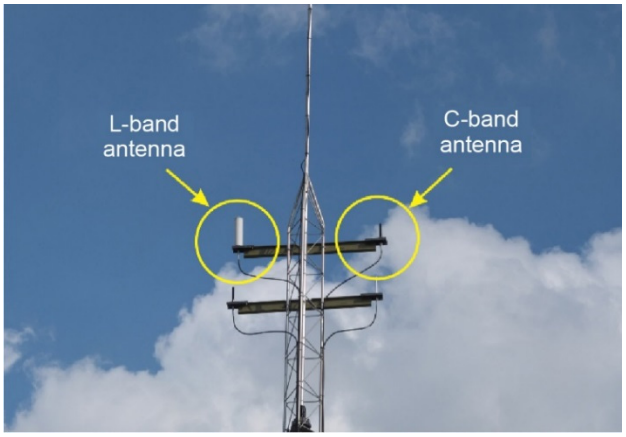

Figure 10.—Ground station 1 (GS1) antennas installed at NASA Glenn's Lewis Field campus.

3.2.1 Ground Station Locations

Ground station site selection for the validation testing was influenced by many factors but was primarily driven by local terrain features and the ability to establish the line-of-sight CNPC radio connection between the aircraft radio and the ground station radio in that particular terrestrial setting. Unique propagation and dispersive signal propagation conditions were expected in each location.

Frequency authorizations were obtained for the NASA CNPC flight test operations in multiple areas across the contiguous United States. Validation testing occurred in two of those flight zones, indicated by the 190-km-radius circles shown in Figure 11. GS1 and GS2 were at the center of the flight zones. GS3 was a mobile terminal that also operated within the authorized Cleveland Hopkins International Airport (destination code: CLE) flight zone. Table VI lists location details for the ground stations used in the validation testing.

Figure 11.—U.S. map identifying test locations with Control and Non-Payload Communications (CNPC) frequency authorizations; 190-km-radius flight zones are shown; GS, ground station. Map image from National Atlas (Ref. 4).

TABLE VI.—VALIDATION FLIGHT TEST GROUND STATION LOCATIONS

Test date	Ground station location	Latitude	Longitude	Flight setting	Ground elevation (above MSL[a]), ft	Antenna height (AGL[b]), ft
February 19, 2016 February 23, 2016	GS2[c] Albany, Ohio	39°12'38.63" N	82°13'28.84" W	Hilly terrain	765	47
March 1, 2016 March 3, 2016	GS3[d] Sandusky, Ohio	41°28'40.6" N	82°40'34.4" W	Open, fresh water	851	50
March 7, 2016	GS1[e] Cleveland, Ohio	41°24'41.77" N	81°52'14.57" W	Airport/urban	750	47.5

[a]Mean sea level.
[b]Above ground level.
[c]Ground station 2.
[d]Ground station 3.
[e]Ground station 1.

Figures 12 to 16 provide gain patterns for the aircraft and ground station radio antennas. The performance data were supplied by the antenna manufacturer as a general description only, realizing that RF performance after installation will likely be different than shown.

(Note: The vertical plane C-band ground station antenna performance for GS2 and GS3 was not available at the time of this report; the radiation pattern was assumed to be similar to the horizontal performance.)

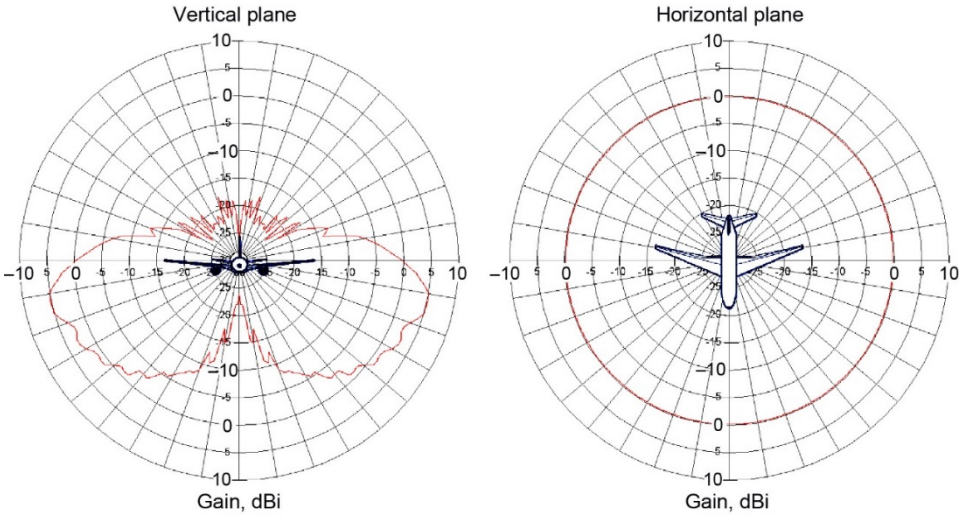

Figure 12.—C-band aircraft antenna gain patterns.

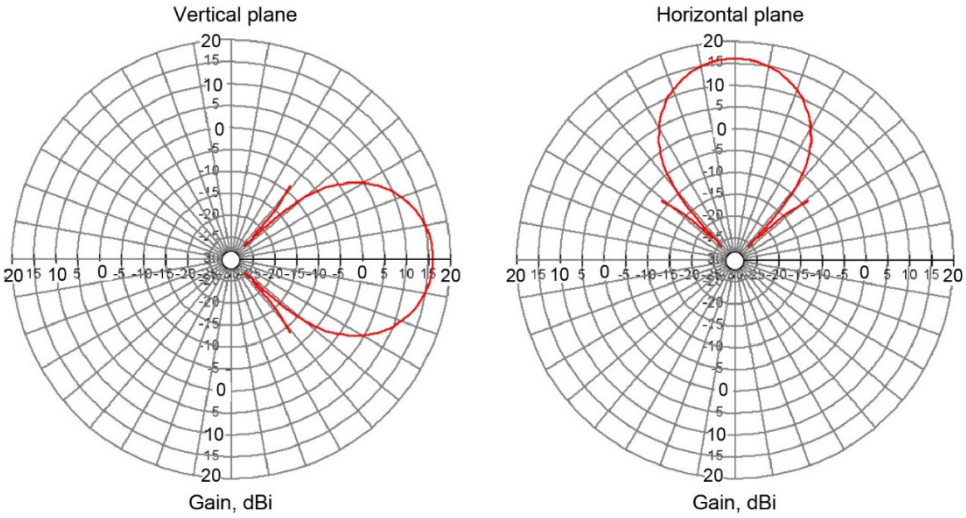

Figure 13.—C-band ground station antenna gain patterns for ground station 2 (GS2) and ground station 3 (GS3). (a) Vertical estimated. (b) Horizontal-manufacturer data.

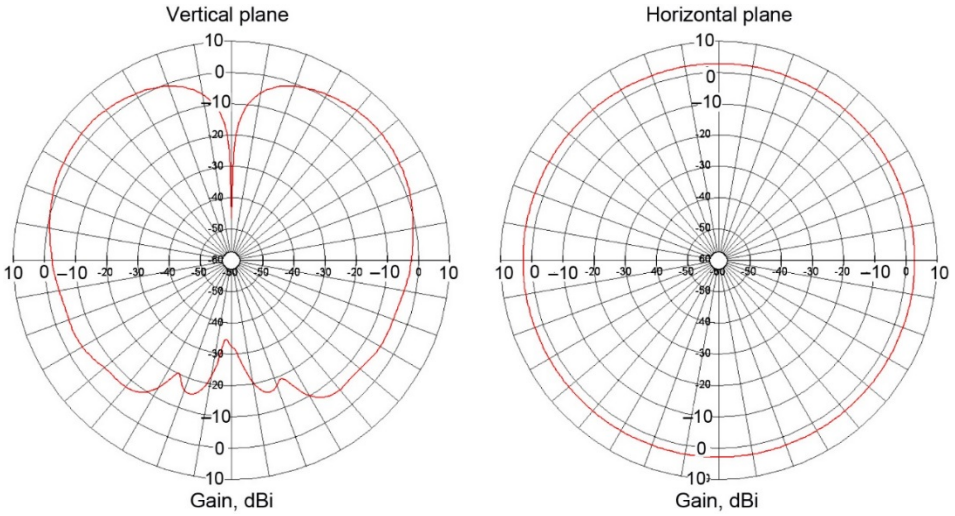

Figure 14.—C-band ground station antenna gain patterns for ground station 1 (GS1).

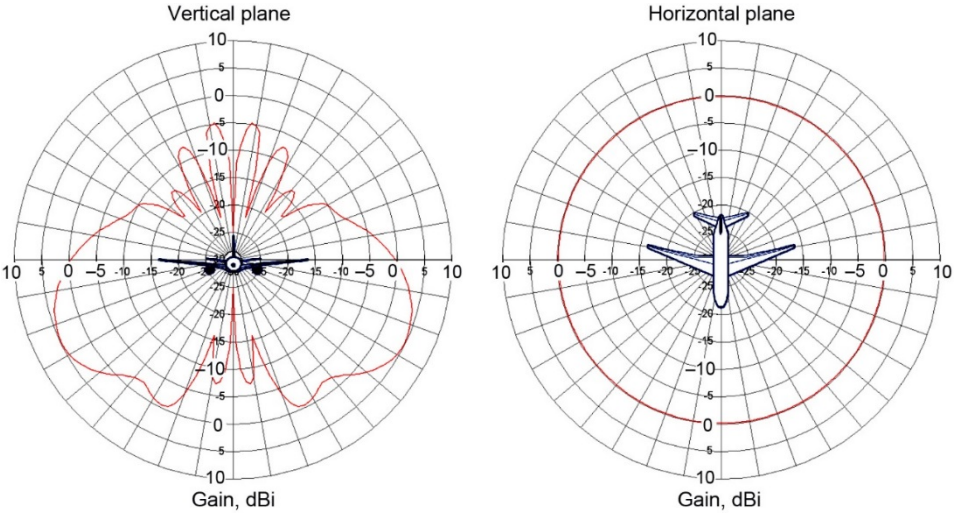

Figure 15.—L-band aircraft antenna gain patterns.

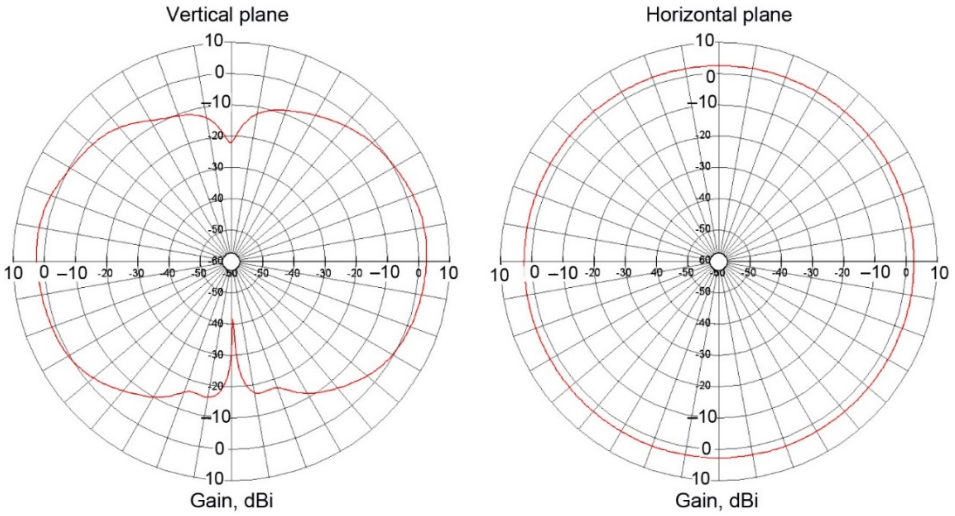

Figure 16.—L-band ground station antenna gain patterns.

3.2.2 Control and Non-Payload Communications (CNPC) Radio Transmission Spectrum

The CNPC radios operated using GMSK modulation to produce an output signal spectra similar to that shown in Figure 17. The trace shown is for a C-band radio, shown operating at the 5060-MHz center frequency. L-band radio output is similar. The ordinate axis is for scale only. The radios were operated in data class 3 service with the 90-kHz channel bandwidth waveform, offering a 103,500 bits/s symbol rate.

For all validation flight tests, the CNPC radios were operated within their respective frequency authorizations. C-band radios were operated at an uplink center frequency of 5060 MHz; L-band radios were operated at a center frequency of 968 MHz for both up and down links. For the validation flight tests, the CNPC radios were operated at the output power levels shown in Table VII. Insertion losses imposed by the coaxial cable runs between each radio and its associated antenna are included in the table.

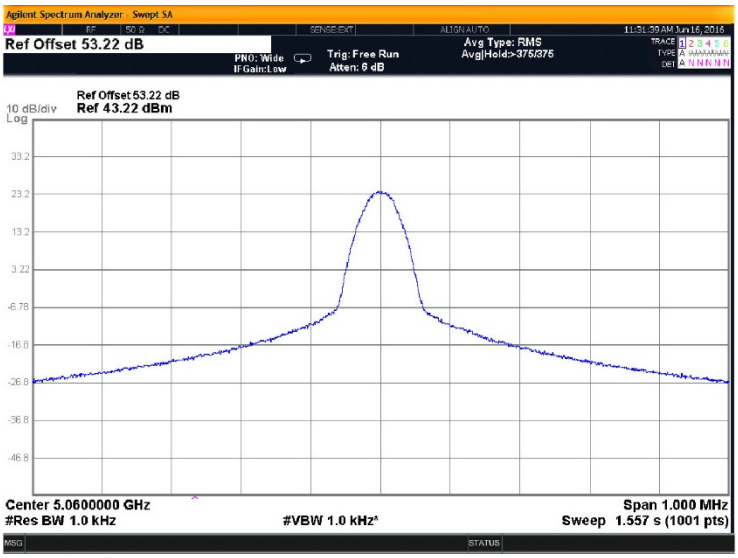

Figure 17.—Control and Non-Payload Communications (CNPC) radio output signals; 90-kHz mode.

TABLE VII.—GROUND STATION RADIO ANTENNA TYPES AND RADIO OUTPUT POWER LEVELS

Application	CNPC[a] radio number	Frequency, MHz	Radio output, dBm	Radiofrequency (RF) cable losses, S21, dB	Power input to antenna		Notes
					dBm	W	
S–3B aircraft	E03	968	38.1	1.4	36.7	4.68	4.5-dBi omnidirectional blade monopole
		5060	43.4	3.2	40.2	10.4	5-dBi omnidirectional blade monopole
GS1[b], Cleveland, Ohio (departure/ascent)	E01	968	37.3	2.9	34.4	2.75	2-dBi omnidirectional dipole
		5060	43.5	5.7	37.8	6.02	4.1-dBi omnidirectional dipole
GS2[c], Albany, Ohio Test MN2 (hilly terrain)	E05	968	37.1	2.7	34.4	2.75	2-dBi omnidirectional dipole
		5060	44.2	6.5	37.7	5.89	16-dBi lensed horn directional
GS3[d], Sandusky, Ohio Test MN1 (over water)	E09	968	37.7	2.7	35	3.16	2-dBi omnidirectional dipole
		5060	44	6.5	37.5	5.62	16-dBi lensed horn directional

[a]Control and Non-Payload Communications.
[b]Ground station 1.
[c]Ground station 2.
[d]Ground station 3.

3.3 Data Acquisition and Control Environment Description

The flight test network architecture consisted of three major components: the control element, the ground station(s), and the mobile node (router) aboard the aircraft. Within the control element network was the Mobile Internet Protocol version 6 (IPv6) home agent (HA) and one or more correspondent nodes (CNs) that needed to communicate with the mobile node.

The HA was placed in the control element network, or "home network," and was used as a central communications point for contacting the mobile node. The HA maintained a binding database of a mobile node's current foreign network address, or care-of address (CoA). The bindings map the home address (HoA), a known address in the home network, to the shifting CoA in the foreign network in order to transparently reroute traffic from external users.

Each ground station served as a broker providing a UA with its foreign network IPv6 address. This was done by means of an IPv6 access router (AR), which communicated with the aircraft through the prototype CNPC radio. Router Advertisements (RAs) were then used to provide the UA with a network address. The aircraft communicated to the ground station using the same CNPC radio link. A Mobile IPv6 router attached to the radio allowed the mobile network to communicate with the home network seamlessly. This allowed the various components behind the mobile router (MR) to be addressed directly by using a predefined static mobile network prefix. Users did not need to know the dynamic addressing schemes used at the various ground stations because the devices could always be reached via their mobile network prefix address.

3.3.1 Internetworking

In a deployed environment, communication between endpoints would be expected to eventually utilize IPv6 end to end, without the need for any encapsulation of traffic within legacy Internet Protocol version 4 (IPv4) packets for transmission across the Internet. However, the wide area network (WAN) used during testing did not support routing IPv6 traffic natively between all ground stations. In order to emulate a complete native IPv6 environment, "6in4" (Protocol 41) tunnels were created between the HA and the ground station computer systems to allow for utilization of the readily available IPv4 backhaul communications networks. Although there are several alternative ways to configure the test architecture to transmit IPv6 packets across an IPv4 network, the 6in4 approach reduced configuration complexity and eliminated the need for devices between the HA and ground station computer to be IPv6 compatible.

The home network and the ground stations were each protected by a dedicated firewall system that served as both an IPv4 network firewall and a virtual private network (VPN) gateway to secure the transmission of data across the Internet. Each ground station utilized an IPv4 IPsec VPN connection to communicate with the home network and carry the 6in4 traffic between the HA and the ground station computer where it was unencapsulated back to native IPv6 packets.

Although the prototype flight architecture implemented this 6in4 encapsulation in order to ensure complete compatibility with an expected future implementation, the terrestrial IPv4 IPsec VPN link over the Internet had no design relevance to the CNPC security architecture recommendations under evaluation by these experiments. The additional overhead of the VPN gateways and IPv4 VPN link were negligible across the high-capacity landline connection.

3.3.2 Addressing Scheme

The home network and ground stations were designed to support a dual-stack IPv4/IPv6 environment in order to support direct communications with legacy devices such as UPS battery backup network interfaces or out-of-band management interfaces on the ground station computers that may not support

IPv6. In addition, an IPv4 addressing scheme was needed to serve as an endpoint for the 6in4 tunnels between the HA and the ground station computer.

The ground station computers were configured to use the RA daemon in order to support IPv6 neighbor discovery across the RF link by multicasting periodic RA packets every 10 s. The remote aircraft computer, upon receipt of one of these RA packets, would be able to self-configure its IPv6 CoA and begin communicating with the ground station as well as the HA, at the network layer.

3.3.3 Network Mobility Concept

The Mobile IPv6 design allowed the aircraft to maintain seamless network layer communications between the pilot's ground control station and the onboard avionics systems as the UAs transitioned between ground stations. This design resulted in a few dropped packets during the transition, but the established sessions continued on without needing to reconnect. This method eliminated the relatively costly procedure of tearing down and reestablishing active IPsec sessions.

The Mobile IPv6 network shown in Figure 18 started configuring itself after the CNPC radios connected. Then the ground station AR sent an RA via the CNPC radios to the MR. The MR, using the RA, created a CoA, providing the MR with a global address that allowed communication between the MR and HA.

The MR then sent a binding update (BU) that contained the MR's HoA and CoA to the HA, providing the HA with MR's latest point of attachment to the network. The HoA is a global address from the home network (located in the control element) address space and was used by the HA to identify the MR. After authenticating the BU, the HA replied with a binding acknowledgment (ACK) and created an IPv6 dynamic tunnel between the HA and the MR through which any traffic between the CN and the MR traveled.

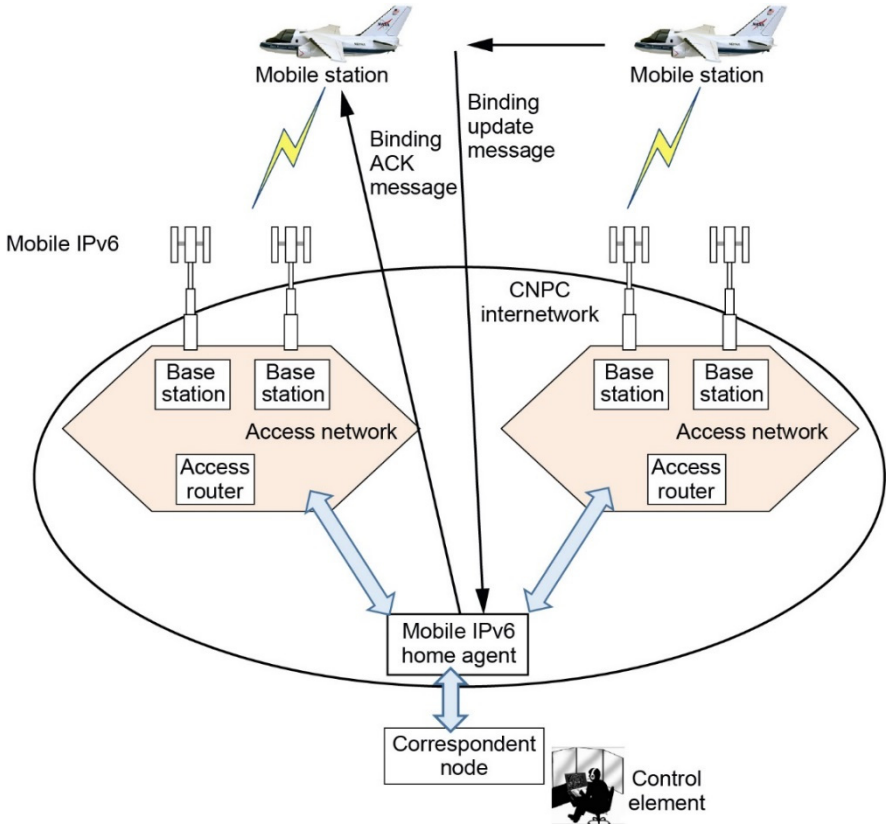

Figure 18.—Mobile Internet Protocol version 6 (IPv6) layer 3 networking scheme. ACK, acknowledgment; CNPC, Control and Non-Payload Communications.

The validation testing described in this report used only one ground station at a time, using the system described previously. However, this mobile network architecture was developed and tested to allow seamless and reliable handoffs between multiple ground stations to enable extended range operations (Ref. 3).

3.3.4 Robust Header Compression (ROHC)

ROHC is a 2001 specification used to reduce the size of network protocol headers across a single data communication link. There has been significant interest in compressing headers in situations where communication links have limited capacity or where the ratio of header to payload is large. In the Unmanned Aircraft Systems (UAS) CNPC waveform, reducing this overhead is of critical importance because the link is limited in capacity and the anticipated nature of communication is a large number of relatively short messages, each message with an associated set of protocol headers. Given the degree of real-time sensitivity, the traffic should be moved forward expeditiously.

The ROHC specification defines a process that will, under ideal circumstances, compress the IPv6 header to 1 or 2 bytes. It does this by establishing "sessions" between the ROHC compressor and ROHC decompressor operating at the two endpoints. The state is maintained at both endpoints, and the compressor begins removing invariant or predictable components in the header, obviating the need to pass those fields across the communication link. Because the decompressor shares the same session and state as the compressor it can reconstruct those headers upon arrival.

3.3.5 End-to-End Network Security

IPsec is a security extension to the Internet Protocol (IP) that provides end-to-end security protection of network layer traffic in a standard fashion. It allows for mutual authentication of nodes at the establishment of a session and periodic renegotiation of cryptographic keys used during an ongoing session. Mechanisms are available to provide confidentiality, data integrity, data origin authentication, nonrepudiation, and antireplay capabilities. IPsec can be used in two different modes: "transport," which protects data communications between two hosts, and "tunnel," which protects communications between two gateways, allowing for secure communications between one or more hosts on each side of the tunnel. In addition, IPsec offers transport and tunnel modes with two protocols: authentication headers (AH) and Encapsulating Security Payload (ESP).

For the architecture to provide secure transmission over the CNPC network while maximizing the capability of ROHC to compress as much of the header stack as possible, the IPsec ESP transport mode was utilized to transmit packets between the CN (behind the HA) and the MR or other destination aboard the UA. Once the Mobile IPv6 tunnel was established between the HA and the MR, and traffic destined for one of the preconfigured security endpoints was detected by the operating system, an Internet Key Exchange version 2 (IKEv2) session was automatically established to negotiate a set of IPsec associations between the pilot station and the UA system(s). All packets subsequently transmitted over this Mobile IPv6 tunnel after IPsec ESP transport mode security associations are established were encrypted, and the communications were securely authenticated with strong cryptographic algorithms.

The testing utilized 256-bit Elliptic Curve Digital Signature Algorithm (ECDSA) certificates on the endpoint systems for authentication of the CNPC link. IKEv2 negotiation used 128-bit Advanced Encryption Standard in Galois/Counter Mode (AES–GCM) with a 64-bit Cryptographic Message Authentication Code (CMAC) for session establishment. ESP was also configured to use 128-bit AES–GCM for encryption and 64-bit CMAC for authentication of packets.

4.0 Flight Test Campaign

The validation flight tests were conducted during a 3-month period (February to April 2016) in the airspace above Ohio and the adjoining Lake Erie area. The objective of the testing was to collect in-flight data measuring the operating range and data throughput capabilities of the CNPC system. From this data, UAS designers and operators would be able to assess the capability of the CNPC link to safely support the C2, air traffic control (ATC) and pilot communication, and detect-and-avoid functions needed for future UAS operation. Flight tests were flown at representative ranges and altitudes that were envisaged by SC–228 as being of interest and that would offer UAS operational utility.

The flight path for each validation test was tailored to account for the terrain setting, weather conditions, frequency authorization restrictions, and limitations imposed by FAA and local ATC authorities. For each test flight, the NASA research aircraft was piloted between pairs of preselected waypoints at a fixed range from the ground station. Aircraft altitude, attitude, and airspeed were held nearly constant between waypoints to create a one-way flight "segment" of nominally 3.5 min. After completing a flight segment, the aircraft maneuvered to travel the same flight path between waypoints, but in the opposite direction. This technique was intended to determine the impact of asymmetrical installation of the CNPC antenna on the aircraft. During these flight segments, the aircraft traveled transverse to the direction of RF radiation from the ground station, thereby presenting the port and starboard sides of the aircraft to the ground station antenna.

The test aircraft flew the path between each pair of waypoints, not only in two directions, but also at multiple altitudes to capture the effects of terrain obstruction at multiple elevation angles, multipath reflections, and signal dispersion. Flight segments were flown at ranges of 35 (points A and B), 65 (points C and D), and 100 nmi (points E and F) from the ground station to examine different received signal strengths.

In addition to transverse flight paths, an inbound or outbound segment was flown at each test location. Test data from these flight paths often provided valuable information on multipath interference as well as maximum CNPC radio range. Table VIII summarizes flight altitudes, ranges, and flight paths.

TABLE VIII.—VALIDATION FLIGHT TEST SUMMARY

Hilly terrain (L-band and C-band)			
Waypoints	A, B	C, D	E, F
Range, nmi	35	65	100
Altitude, ft	----------	17,500	17,500
	14,000	14,000	15,500
	----------	10,000	13,500
	7,500	6,500	----------
	3,500	----------	----------
Inbound descending, fresh water (L-band and C-band)			
Waypoints	A,B	C,D	E,F
Range, nmi	35	65	100
Altitude, ft	----------	----------	17,000
	----------	10,500	11,500
	5,000	6,500	7,000
	3,000	3,500	----------
	1,500	----------	----------
Standard departure (L-band and C-band), outbound ascending, runs 1 and 2			
Reduced-power flight range demonstration (L-band only)			
Flight path		Altitude, ft	
Outbound		11,600	
Inbound		11,600	
Transverse segments at range of 20, 25, 30, 35, 40, 45, 50, and 56 nmi		11,600	
Networking/multiuser test (L-band only)			
Flight path		Altitude, ft	
25-nmi radius orbit		8,500	

The complete set of CNPC radio data from the validation flight testing is presented in the appendix. This data set includes a compilation of data from the validation flight tests at various altitudes and ranges, in hilly, urban, and over-water terrain settings, and in both C-band and L-band.

4.1 Validation Flight Test Results and Analysis

4.1.1 Hilly Terrain Setting, February 19, 2016

Figure 19 presents the flight track of the NASA aircraft over hilly terrain in southern Ohio. For these tests, GS2 at the Ohio University airport was used. The complete flight path of the aircraft includes all reversals, ascent and descent maneuvers, and range changes. Figure 20 displays the same flight track viewed from a low altitude to show the flight path at various test altitudes. Waypoints are identified as A to E. The flight segments between waypoints precisely represent the locations where RF data were captured for evaluation.

Each flight segment highlighted in a flight track plot corresponds directly to data plots for both the ground-to-air and air-to-ground radio links. Separate data plots are presented for each direction of aircraft travel between the waypoints, for each test altitude, and for ranges of 35, 65, and 100 nmi from the ground station.

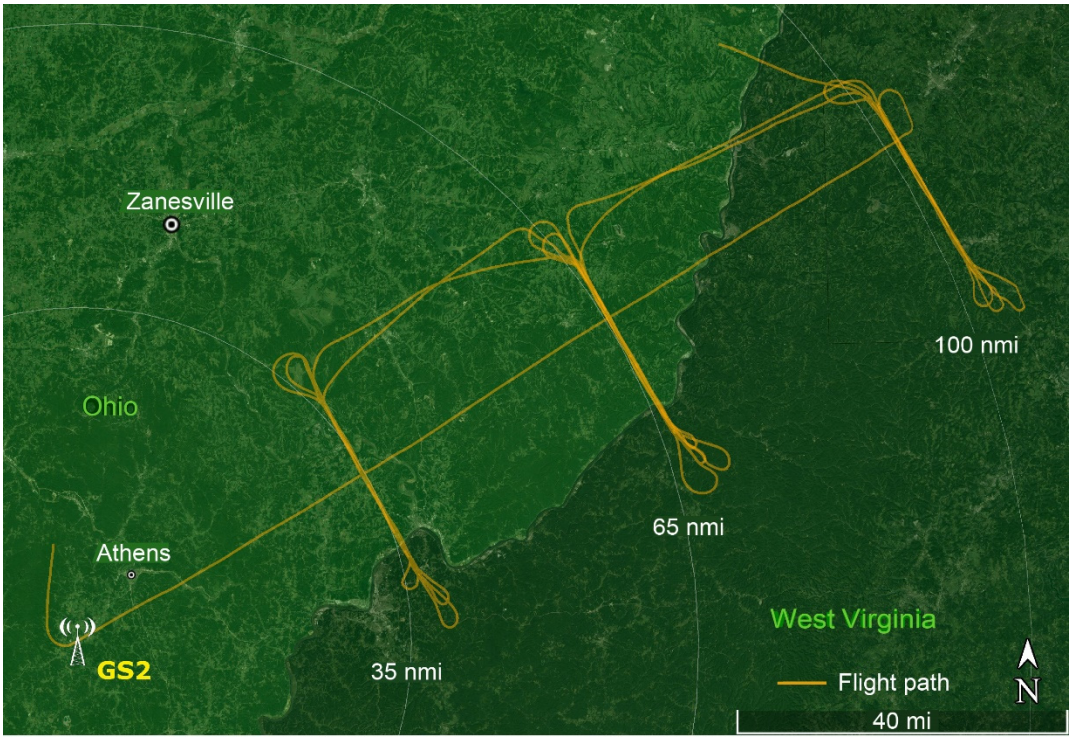

Figure 19.—Flight path over hilly terrain on February 19, 2016. Image ©2016 GoogleEarth (Ref. 5).

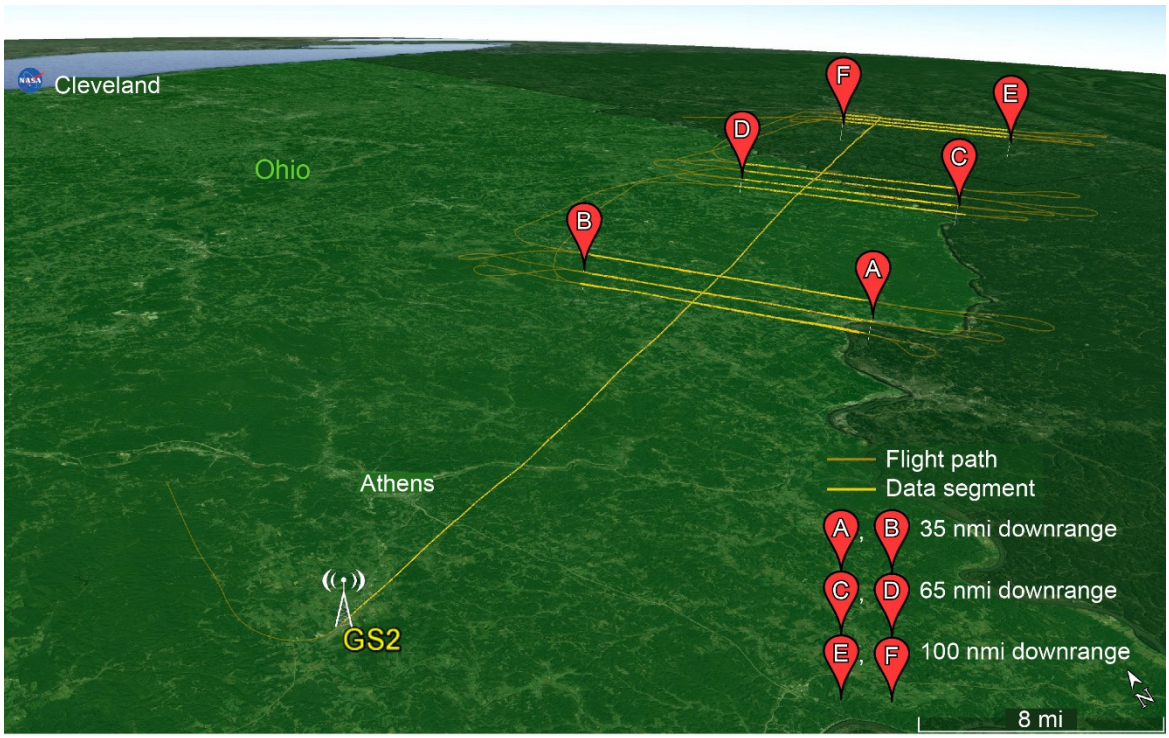

Figure 20.—Perspective view of flight path over hilly terrain highlighting data capture segments on February 19, 2016. Image ©2016 GoogleEarth (Ref. 5).

4.1.1.1 C-Band Radio Performance Over Hilly Terrain

Figure 21 presents typical flight segment data using the C-band CNPC radios. In both plots, the aircraft was traveling transverse to the radiation path at a distance 100 nmi downrange from GS2 and was traveling in the same direction, moving from waypoint E to F, but at two different altitudes.

Signal strength values measured at the radio receivers are plotted along the vertical axis for both the uplink (ground-to-air) path and downlink (air-to-ground) path in Figure 21. The uplink and downlink traces are nearly identical, indicating remarkable similarity in performance. The signal strength data were measured on each data frame at 20 times/s, then plotted as an average value every 1 s to time correlate with aircraft flight parameters. All signal strength traces are for the point-to-point, 90-kHz-wide data channel at the 103,500 bits/s symbol rate (waveform C), as requested by SC–228. The RF channel was centered near the 5060-MHz frequency for these tests.

Directly below the signal strength traces are the percentages of data frame loss averaged over 1 s at the ground and aircraft receivers. Where the CNPC radio link was transferring all data without error, the data are presented as 0 percent frame loss and no trace is visible on the grid. Where errors occurred in the radio link, the lost frame data created a narrow, visible vertical line, or “impulse,” ranging from 0 to 100 percent, where the latter represents a total loss of radio link.

Aircraft parameters are plotted in the lowest portion of each figure. The range plot is the slant range between the ground station and aircraft, calculated by the CNPC radios from when the message preamble arrived. Because each path between waypoints was flown as a line segment rather than as an arc segment, the range plot predictably shows small variation across the test period.

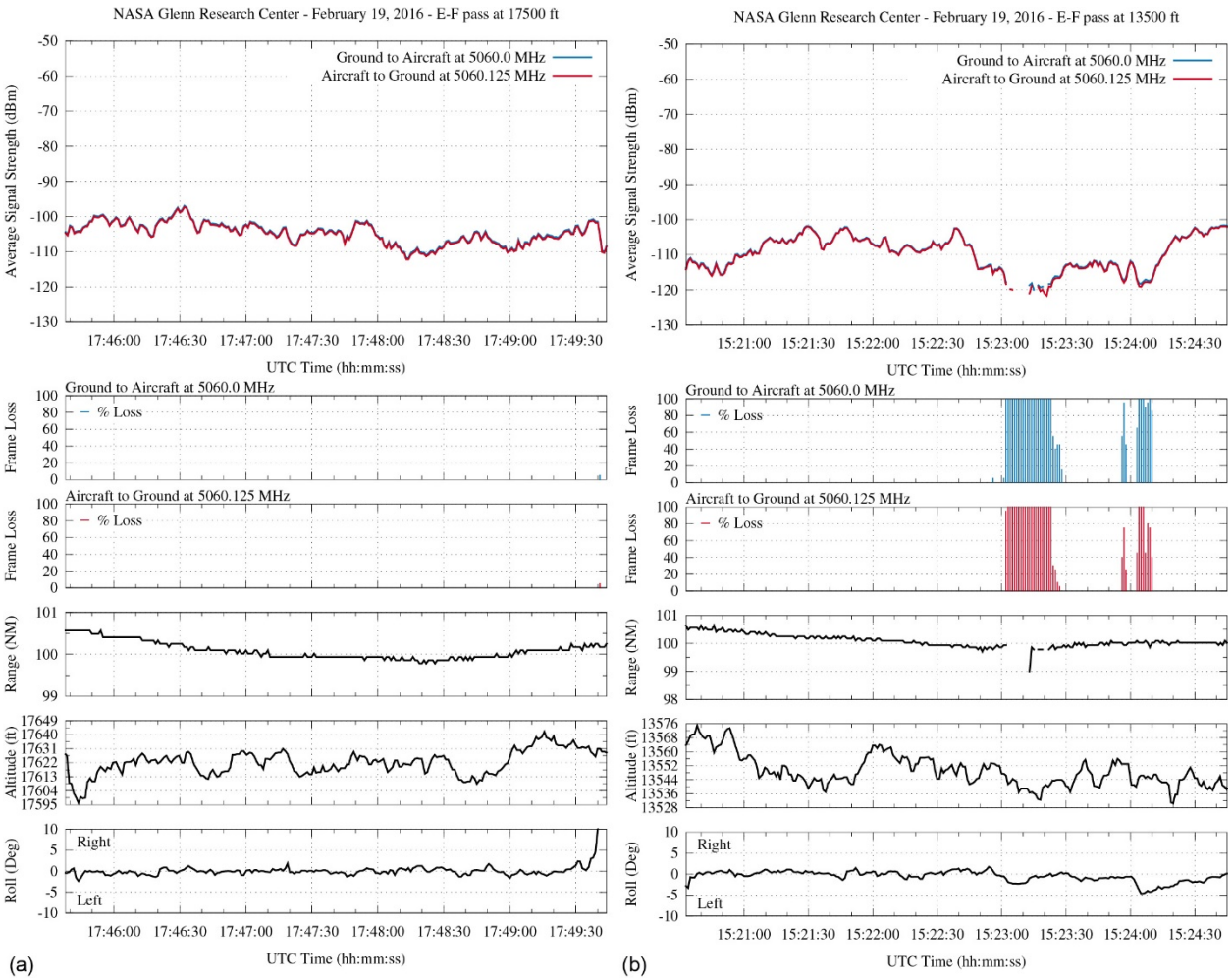

Figure 21.—C-band signal strength and frame loss over hilly terrain. (a) At 100-nmi range and 17,500-ft altitude. (b) At 100-nmi range and 13,500-ft altitude.

Aircraft altitude and roll angle data were drawn from aircraft onboard instrumentation. Aircraft altitudes are presented as height above mean sea level (MSL). In most cases, the aircraft was maintained in level flight with less than 3° of roll angle. All data in all traces were time synchronized with GPS-based timing information.

The obvious difference between the plots in Figures 21(a) and (b) is the frame losses at an altitude of 13,500 ft. These losses were caused by terrain obstructions (hills) that interrupted the line-of-sight path between the ground station and aircraft antennas. Aircraft altitudes were intentionally selected to yield elevation angles of less than 2° above the horizon for the tests, causing these terrain-induced RF propagation issues.

Similar signal strength and frame loss characteristics existed for the aircraft at the much smaller range of 35 nmi (Fig. 22). In this example, the aircraft was traveling the same direction (waypoint A to B) at the same nominal downrange distance, but again at two different altitudes. The frame loss traces for both the uplink and downlink are 0 percent at 14,000 ft, but frame losses are clearly evident for when the aircraft was operating at an altitude of 3500 ft.

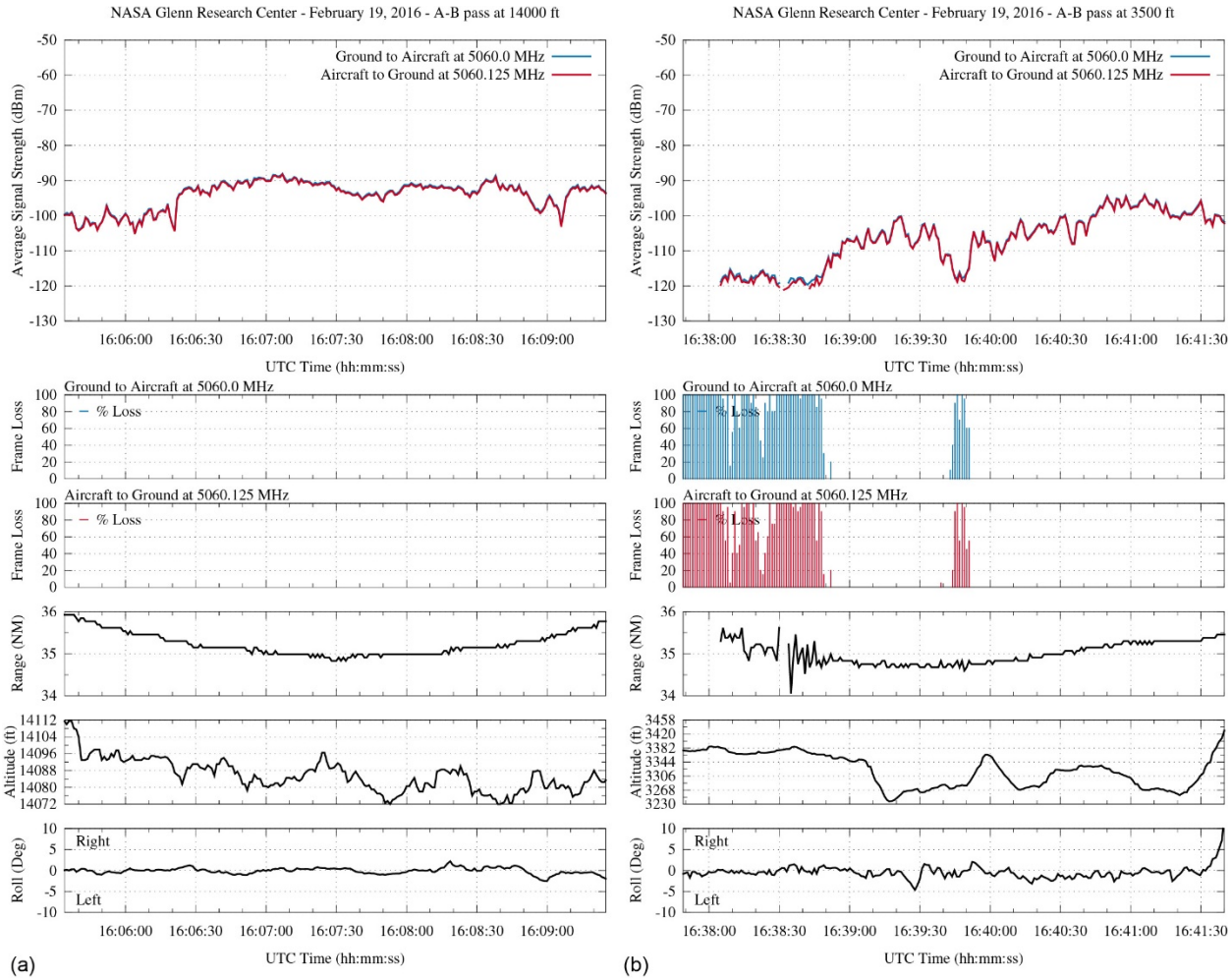

Figure 22.—C-band signal strength and frame loss over hilly terrain. (a) At 35-nmi range and 14,000-ft altitude. (b) At 35-nmi range and 3500-ft altitude.

4.1.1.1.1 Frame Loss Versus Bearing Angle

To demonstrate the repeatability of the measurement systems and to further examine the influence of terrain on the CNPC signal, the validation test data were reprocessed and replotted versus the absolute bearing (azimuth angle between true north and compass direction as viewed from the ground station antenna). Figure 23 is used to visualize this approach. In this figure, flight data are presented versus time, with the full flight segments highlighted. In contrast, the data in the bearing plots are presented versus compass angle and are truncated to the subsegments within the range limits (divergent "walls").

Figure 24 presents the signal strength and frame loss data for three flight altitudes at a downrange distance of 100 nmi. Both flight directions are presented, showing the similarity of results for flying from waypoint E to F, or on the reverse heading from F to E. The results indicate that a significant interruption to the CNPC signal occurred at an altitude of 13,500 ft between bearing ranges of approximately 59.3° to 60.2°, whereas the higher altitude runs were mostly unaffected. The frame losses occurred in both flight directions. Signal strength traces at all altitudes show a slight reduction of received power over the 59.3° to 60.2° range.

Figure 25 presents similar bearing data for the uplink signal path. As expected, the frame losses occur over the same angular range.

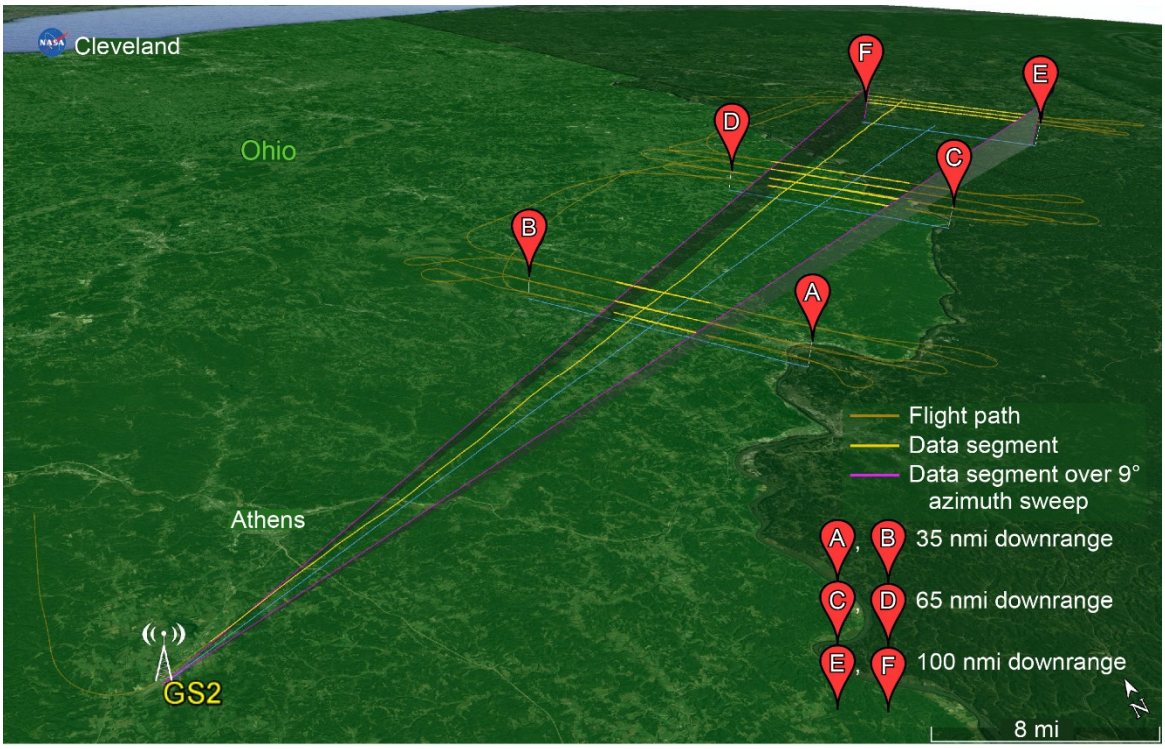

Figure 23.—Perspective view of flight path over hilly terrain showing 56° to 66° bearing range limits. Image ©2016 GoogleEarth (Ref. 5).

Figure 24.—Downlink C-band signal strength and frame loss versus bearing angle over hilly terrain at 100-nmi range.

Figure 25.—Uplink C-band signal strength and frame loss versus bearing angle over hilly terrain at 100-nmi range.

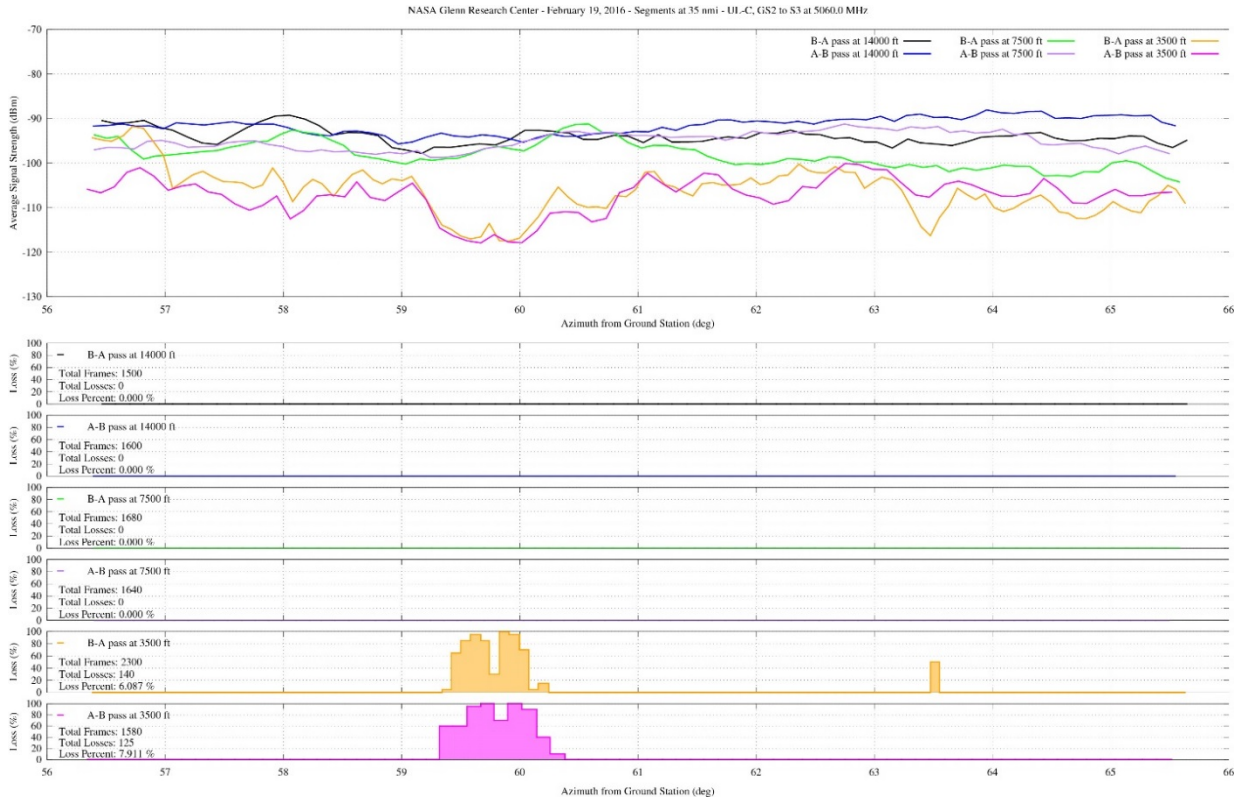

Figure 26.—Uplink C-band signal strength and frame loss versus bearing angle over hilly terrain at 35-nmi range.

Figure 26 presents the signal strength and frame loss data for three flight altitudes and two flight directions at a downrange distance of 35 nmi. Again the results indicate that a significant interruption to the CNPC signal occurred at the lowest test altitude in the 59.3° to 60.2° bearing range, the same as shown in the previous figures. In this case, the higher altitude runs were mostly unaffected. The frame losses again occurred in both flight directions.

The bearing plots offer another valuable piece of information about the CNPC RF link. As noted in Section 3.1, the aircraft CNPC antennas were mounted slightly to the right of aircraft centerline, which places the antennas farther from the ground station (on the "distant" side of the aircraft) during the E-to-F passes, and closer to the ground station (on the "closer" side of the aircraft) during the F-to-E passes. Cursory examination of the traces indicates that, for this particular aircraft, the aircraft antenna mounting asymmetry had little effect on the CNPC link performance.

Although terrain obstruction is a likely cause of deteriorating CNPC link performance, there are other factors that can influence signal propagation. Multipath interference, for example, is predicted to have a significant impact on CNPC signals.

4.1.1.1.2 Frame Loss Duration and Excess Path Loss (EPL) Observations

A cursory examination of frame-loss events was conducted on the C-band, uplink, hilly terrain data, with the intent of quantifying the duration of random losses during a flight segment. In this case, random loss events were defined as those situations where the aircraft was within radio range and on a line-of-sight path from the ground station but an unexpected frame loss occurred because of some other cause. Signal loss caused by obstructions, such as flying behind hills, or flying beyond the sensitivity of the radio receivers, was not included in the EPL study. Another objective of the examination was to gain

general knowledge of the RF power margin required in the CNPC radio link budget to possibly overcome the random frame-loss events.

Figure 27(a) presents the signal strength received at the aircraft radio, with respect to time, during a typical flight segment. This flight segment was flown at a range of 100 nmi from the ground station and at a MSL altitude of 13 500 ft, which intentionally subjects the RF signal to partial terrain obstruction (higher flight altitudes did not yield any random signal losses.) The theoretical received power P_r was calculated by first using a free-space attenuation model to determine path loss $L_{\text{path loss}}$. Then, transmit power P_t, transmitter and receiver cable losses $L_{\text{tx cable}}$ and $L_{\text{rx cable}}$, and transmitter and receiver antenna gains G_{tx} and G_{rx} were included with the path loss to produce the standard link budget given in Equation (1):

$$P_r = P_t + G_{\text{tx}} + G_{\text{rx}} - L_{\text{tx cable}} - L_{\text{rx cable}} - L_{\text{path loss}} \tag{1}$$

The theoretical received power, in the absence of constructively interfering multipath rays, is a maximum upper boundary for the measured received power because it assumes that there are constant maximum gains from both antennas. The antenna gains depend heavily on orientation, and are therefore not constant during flight test segments. It should also be noted that often the theoretical received power does not appear to change during a single flight-path segment. This is due to the negligible change in the actual distance of the aircraft from the ground station.

Figure 27(b) contains percent frame loss with respect to time, identifying when data were not fully passed from the transmitter to the receiver. The receiver expects to receive 20 frames/s, and any less than that would indicate link loss. The percentage quantifies the severity of link loss (50 percent being 10 frames lost out of the 20 frames sent). In Figure 27 there are five distinct periods of signal loss, with individual durations ranging from 0.05 to 21.7 s. The cause of the 21.7-s loss event has been determined to be terrain obstruction.

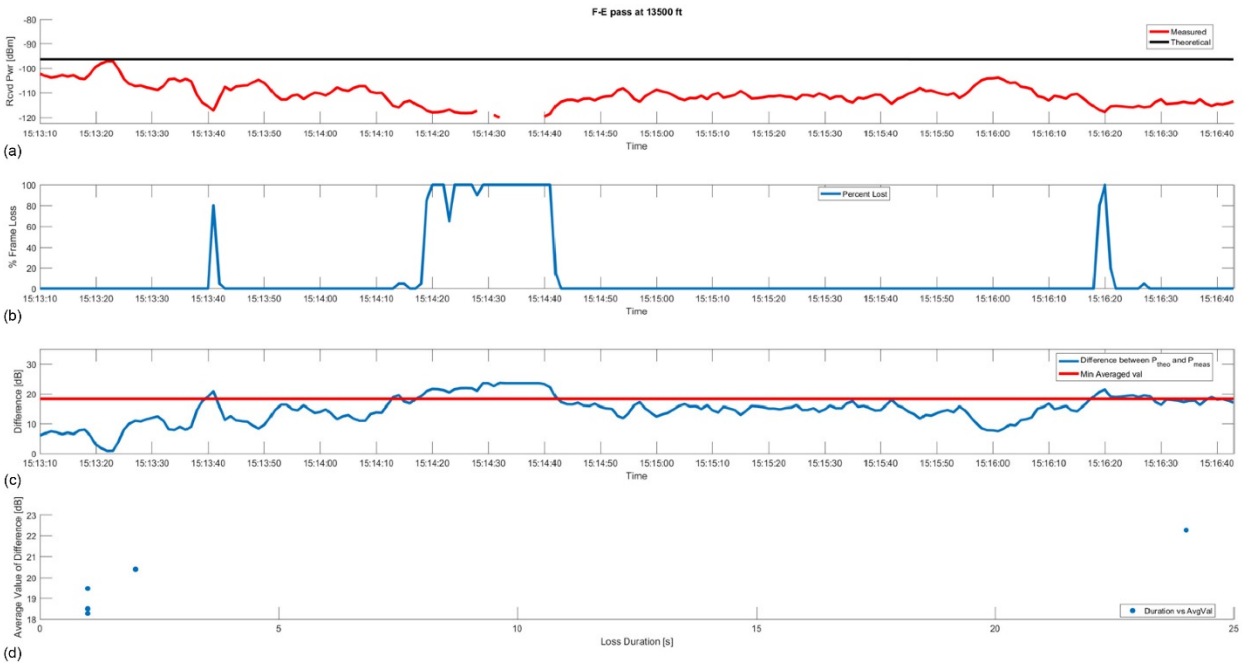

Figure 27.—Frame loss durations and excess path loss (EPL) for flight segment at 100-nmi range and 13,500-ft altitude. (a) Signal strength received at aircraft radio. (b) Percent frame loss with respect to time. (c) Difference between measured received power and theoretical received power. (c) Scatter plot of five frame-loss events.

Figure 27(c) presents the difference between the measured received power and the theoretical received power based on the free-space attenuation model, as shown in Equation (2):

$$\Delta P_r = P_{r,\text{theoretica l}} - P_{r,\text{measured}} \tag{2}$$

The difference, or EPL, corresponds to additional losses not predicted by the free-space model, such as atmospheric effects, suboptimal antenna gains, and obstructions. There is an artificial limit of difference in power level because the radio's sensitivity is –120 dBm. If the radio had no data recorded for received power, a radio received power value of –120 dBm was assumed. During a loss event, the EPL values were collected and averaged to produce a single power difference average value for that loss duration. The minimum value of these averages was then used as an EPL threshold value. With the smallest average EPL difference plotted that caused a loss event, any larger values of EPL should be a loss event as well.

Figure 27(d) contains a scatter plot of the five frame-loss events, showing the average EPL values and corresponding loss durations. In this example, the EPL threshold value was 18.3 dB for the 0.4-s loss event at time 15:13:40. If the terrain-induced loss event occurring between 15:14:19 and 15:14:41 was excluded from the analysis, the highest average value of EPL would have been 20.4 dB for the 1.3-s event at 15:16:20. This example implies that if at least 20.4 dB of margin is included in the CNPC link budget to cover path losses above the free-space attenuation model, the radio link will probably not have encountered random frame-loss events in this flight segment. This value compares favorably with the signal fading and link budget study described in Appendix L of Reference 1.

It is recommended that a thorough analysis of frame-loss events be conducted to correlate the CNPC frame loss data during this flight campaign to more advanced signal propagation models. Applying a fixed value of margin in the CNPC link budget is likely a far too conservative approach for many flight situations.

4.1.1.2 L-Band Radio Performance Over Hilly Terrain

The NASA S–3B aircraft and ground stations were all equipped to simultaneously and independently collect CNPC radio validation data in both the C-band and L-band. Flight paths, test altitudes, terrain settings, and all other parameters were, therefore, identical for the L-band and C-band tests. Like the C-band tests, all signal strength traces are for the point-to-point, 90-kHz-wide data channel at the 103,500 bits/s symbol rate (waveform C), as requested by SC–228. The RF channel was centered at a frequency of 968 MHz for the L-band tests.

Figures 28 and 29 present the L-band bearing plots for ranges of 100 and 35 nmi over the same flight path segments shown previously for the C-band. In these traces there are no significant signal strength reductions like those observed near the 60° bearing in C-band plots. The authors believe that the longer wavelength of the L-band signal allows improved propagation performance through vegetation near the terrain obstructions encountered at low elevation angles. Signal strength near the 65° bearing has dropped to the sensitivity limit of the radios, indicated by the increase in frame losses (Fig. 28). At a range of 35 nmi, the reduction in free space loss yielded a higher received signal strength and fewer frame losses at the 65° bearing (Fig. 29).

Figure 28.—Uplink L-band signal strength and frame loss versus bearing angle over hilly terrain at 35-nmi range.

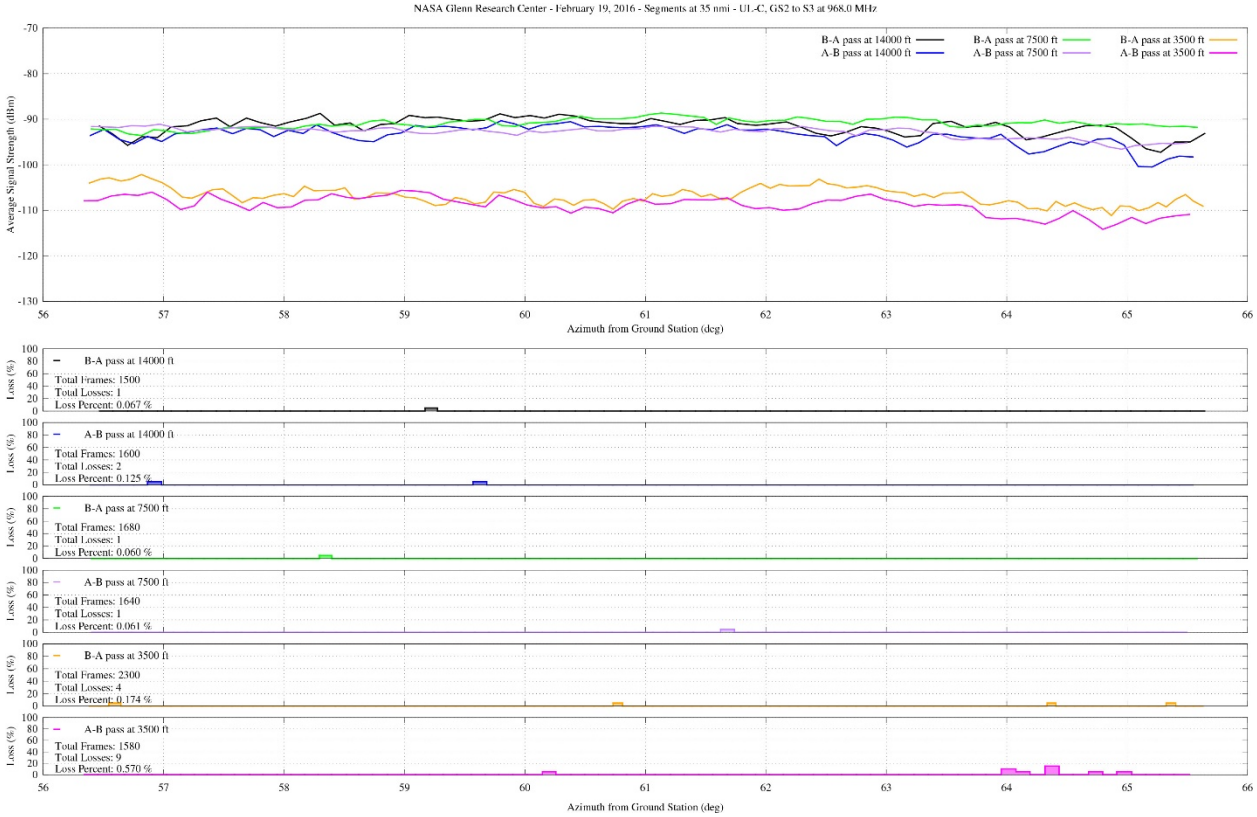

Figure 29.—Uplink L-band signal strength and frame loss versus bearing angle over hilly terrain at 35-nmi range.

4.1.2 Fresh-Water Setting, March 1, 2016

Figure 30 presents the flight track of the NASA aircraft over open, fresh water above Lake Erie along the Ohio coastline and immediately south of the U.S.-Canada border. The complete flight path of the aircraft includes all reversals, ascent and descent maneuvers, and range changes. Figure 31 is the same flight track viewed from a low altitude to show the flight path at various test altitudes. For these tests, the portable GS3 equipment, located along the Lake Erie shoreline in Sandusky, Ohio (lower left of figure), was used.

Figure 30.—Flight path over fresh water on March 1, 2016. Image ©2016 GoogleEarth (Ref. 5).

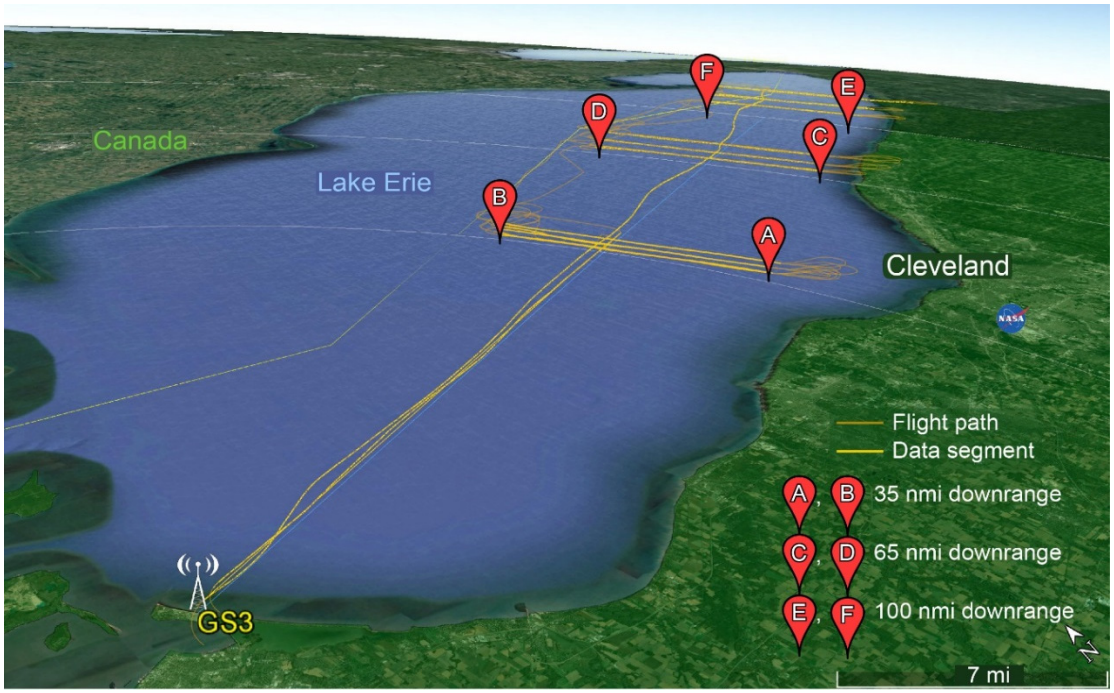

Figure 31.—Perspective view of flight path over fresh water highlighting data capture segments, March 1 and 3, 2016. Image ©2016 GoogleEarth (Ref. 5).

Flight operations and CNPC link testing above the Lake Erie surface were conducted in a fashion nearly identical to those over hilly terrain. The ground station hardware and electronics used for fresh-water testing used radios, antennas, cables, and other systems with the same configurations, operating frequencies, power settings, and model numbers as in the hilly terrain setting. By sheer luck, the lake surface was open water with no ice cover, which is highly unusual for early March. Winds were from the northeast, creating 2- to 3-ft waves on the lake surface for the duration of the tests.

The fresh-water setting and the position of the ground station directly along the Lake Erie shoreline offered the ability to perform the flight tests without any manmade structures or natural terrain obstructions. Taking advantage of this arrangement, the test altitudes at each range were reduced by several thousand feet to investigate lake surface effects on the CNPC signals.

4.1.2.1 C-Band and L-Band Radio Performance Over Fresh Water

Figure 32 presents typical flight segment data using the C-band CNPC radios over fresh, open water. The lowest over-water test altitudes at 100 and 35 nmi are presented for comparison with the hilly terrain plots. For the 100-nmi downrange segment shown in Figure 32(a), the 7000-ft altitude is a full 6500 ft lower than that flown in hilly conditions, yet delivers reliable CNPC data transfer across the segment. Similarly, the 35-nmi downrange segment shown in Figure 32(b) was flown at 1500 to 2000 ft lower than in hilly conditions and did not experience frame loss.

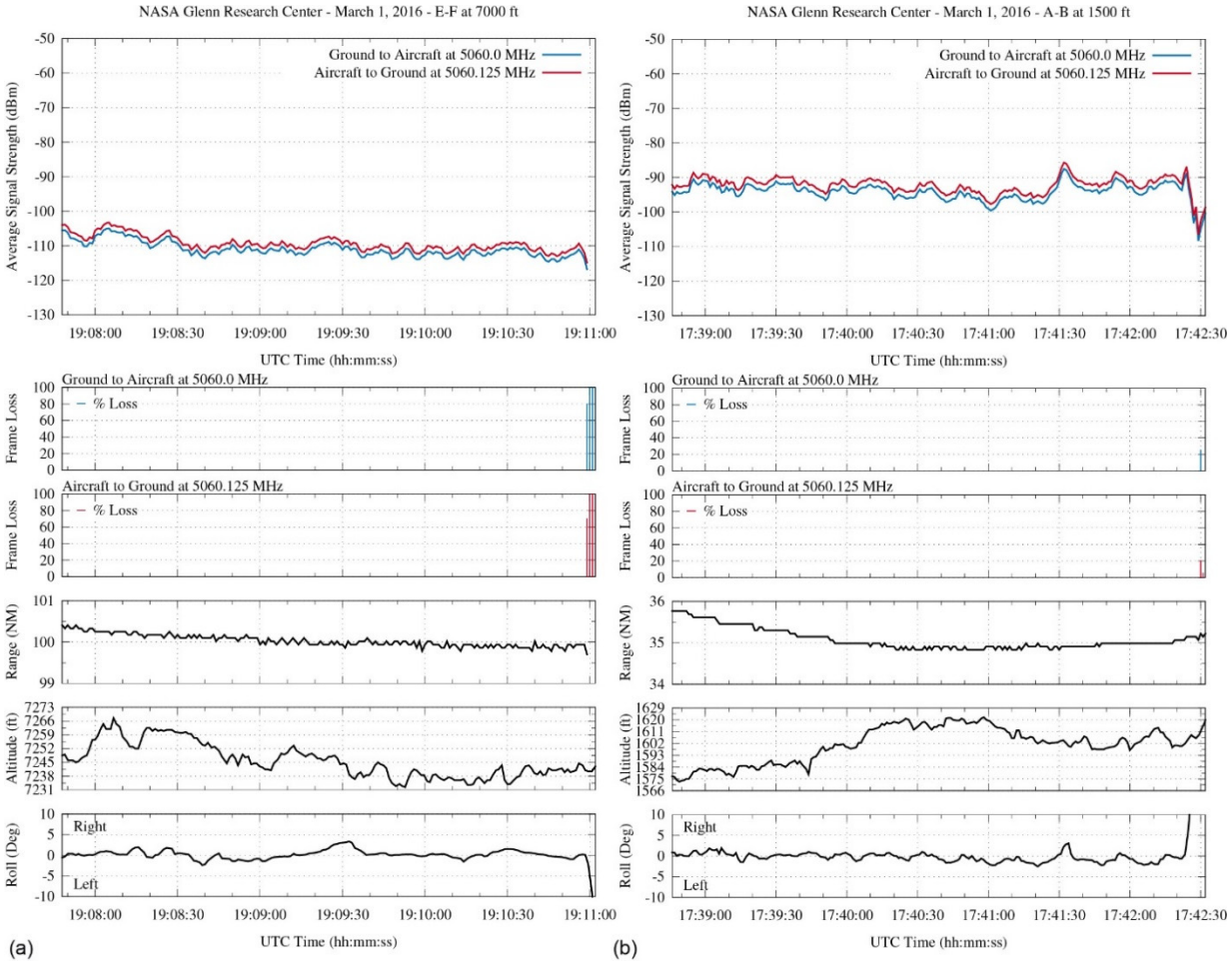

Figure 32.—C-band signal strength and frame loss over open water. (a) At 100-nmi range and 7000-ft altitude. (b) At 35-nmi range and 1500-ft altitude.

Figure 33 presents flight segment data recorded using the L-band radios during the same flight tests. Once again, the line-of-sight path was unobstructed even at the low altitudes, allowing uninterrupted CNPC communications.

The uplink and downlink signal strength traces have nearly identical characteristics, tracking within approximately 1 dB throughout the entire set of tests. The offset in the C-band data is being reviewed and is suspected to be the result of thermal conditions at the Sandusky ground station.

(Note: Flight segments over Lake Erie were sometimes truncated to avoid international airspace boundaries. Higher values of roll angle in the figures indicate aircraft maneuvering. Frame losses observed at the beginning or end of flight segments are due to airframe shadowing, and are most prevalent in C-band test results.)

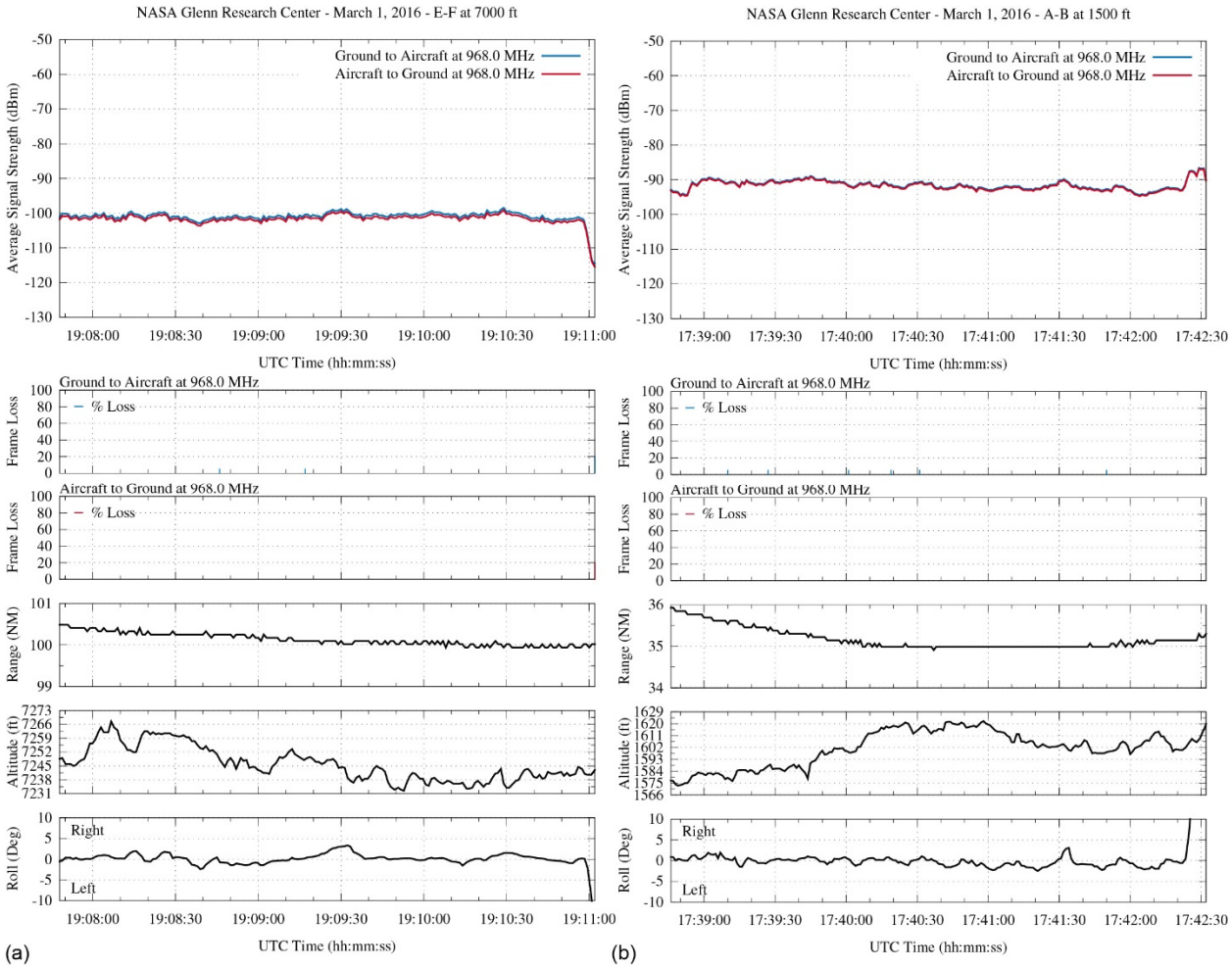

Figure 33.—L-band signal strength and frame loss over open water. (a) At 100-nmi range and 7000-ft altitude. (b) At 35-nmi range and 1500-ft altitude.

In addition to the transverse flight segments described previously, the aircraft also executed an outbound run, flying overhead of the ground station on a fixed outbound heading through the ground station antenna main beam. The C-band data from this flight segment are presented in Figure 34(a). The measured signal strength data show a characteristic pattern of cyclical nulls, commonly associated with two-ray multipath interference. At the relatively close range of this test, the null depth generally remained above the sensitivity threshold of the radios, allowing most data to pass with very low frame loss. The L-band data are presented in Figure 34(b). Once again, the null pattern is observed, but with fewer cycles because of the longer radio wavelength. This time a null at 05:44:00 clearly resulted in frame loss. Future investigations should examine deliberate aircraft flights at the null distances to determine the impact on CNPC, if any.

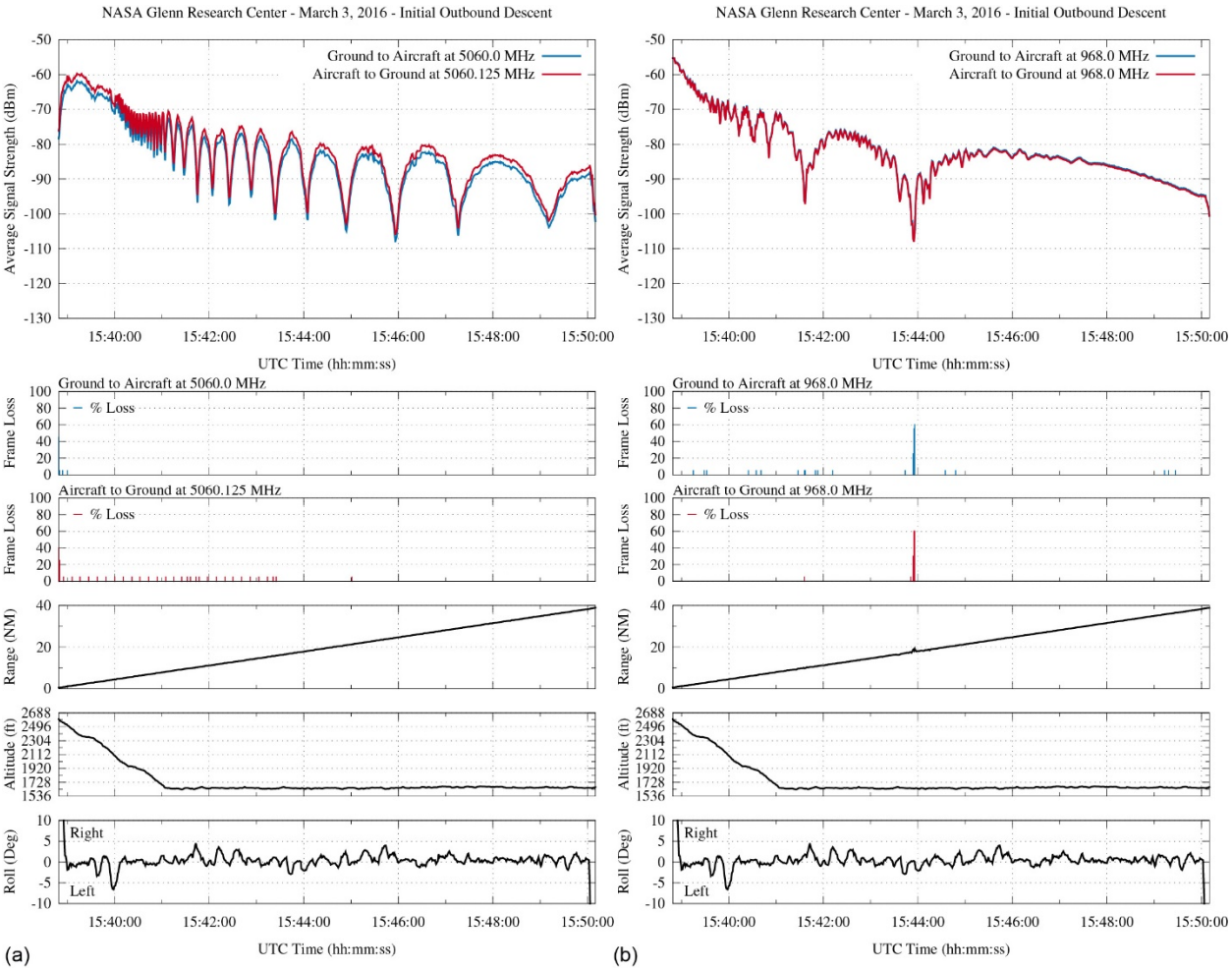

Figure 34.—Signal strength and frame loss over open water during outbound overflight. (a) C-band. (b) L-band.

4.1.3 Validation Flight Test Data for Standard Airport Departure/Ascent, March 7, 2016

Figure 35 presents the flight track of the NASA aircraft over northwest Ohio during two ATC-directed standard departures from Cleveland Hopkins International Airport and ascent to Class A airspace. The complete flight path of the aircraft includes reversals and airport approach maneuvers. The two outbound flight segments precisely represent the locations where RF data were captured for evaluation.

Figure 36 presents C-band validation flight test data during airfield departure, and Figure 37 presents corresponding L-band flight test data. Test results for the C-band indicate that the aircraft could ascend to a 20,000-ft cruising altitude with low frame losses before reaching a downrange distance of 50 nmi from the airfield. Data show that ATC-directed course changes result in aircraft roll, which often disrupts the CNPC signal (time 18:39:00 in Fig. 36). Multipath interference, such as that occurring near time 18:51, also disrupts the CNPC link for brief periods. L-band test results display many of the same properties.

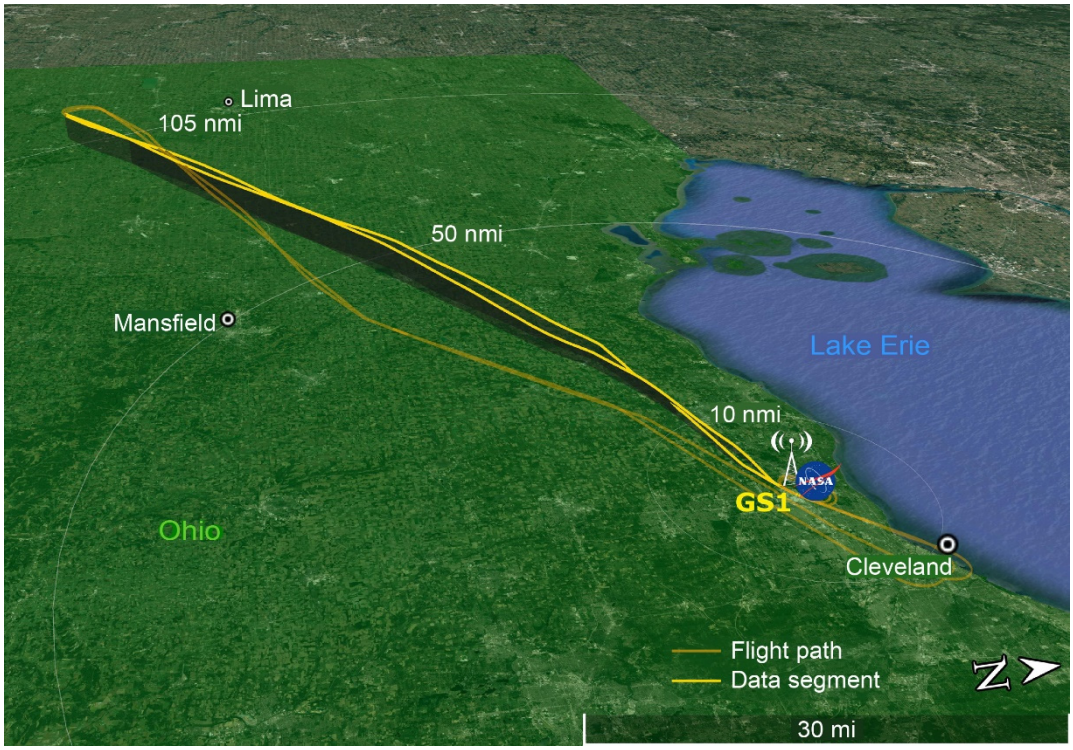

Figure 35.—Perspective view of flight path during standard airport departure. Image ©2016 GoogleEarth (Ref. 5).

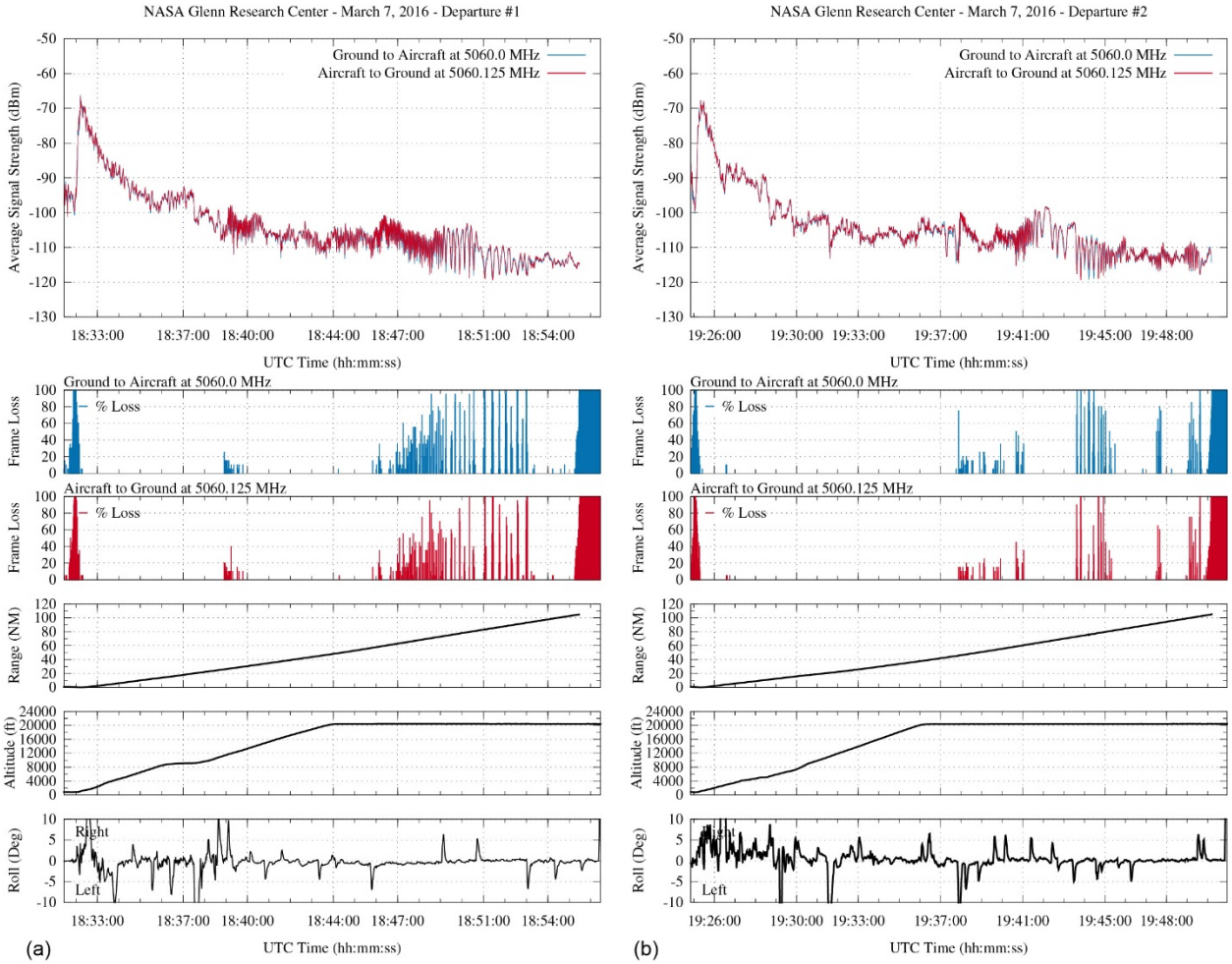

Figure 36.—C-band signal strength and frame loss. (a) During controlled airfield standard departure 1. (b) During controlled airfield standard departure 2.

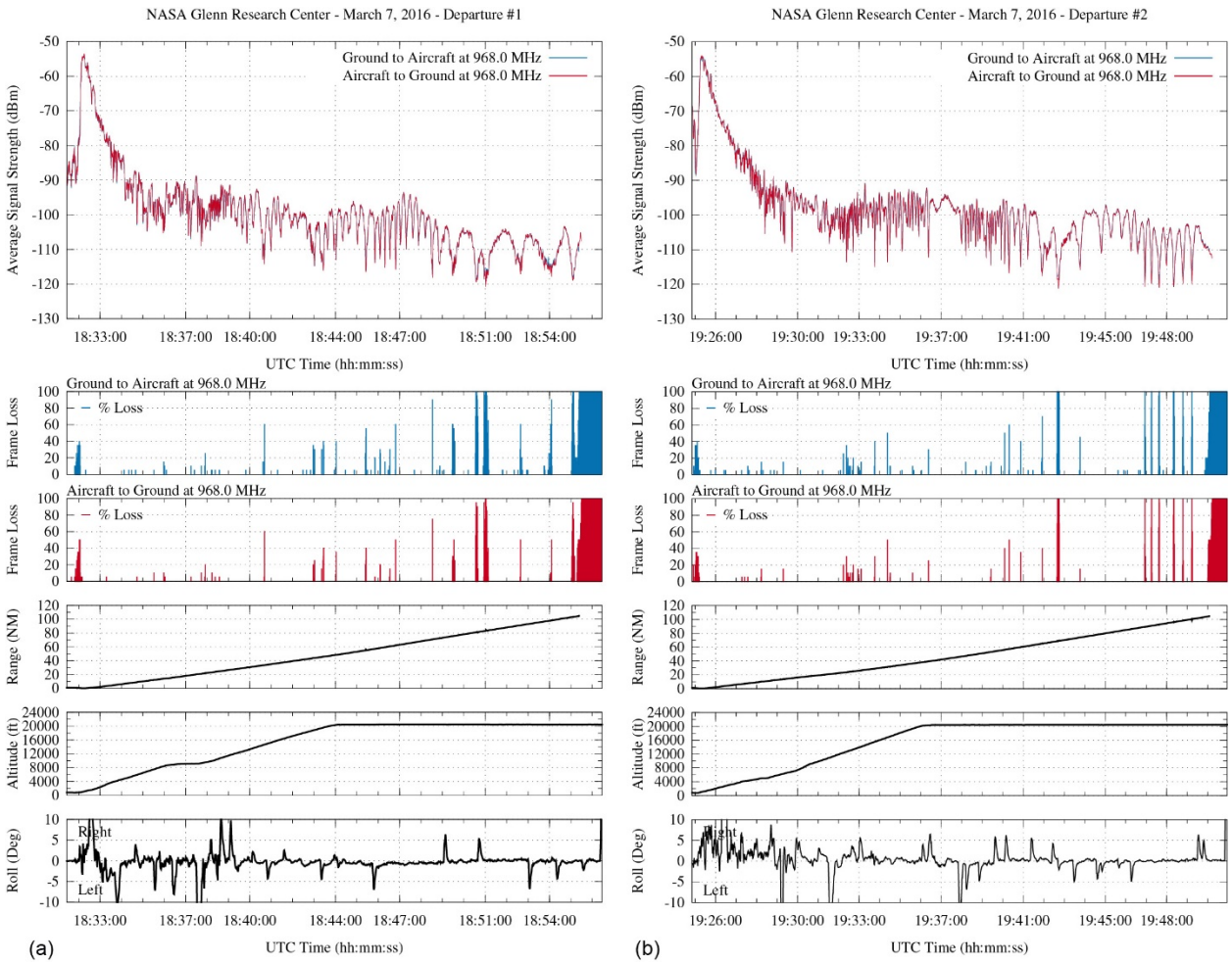

Figure 37.—L-band signal strength and frame loss. (a) During controlled airfield standard departure 1. (b) During controlled airfield standard departure 2.

4.2 Flight Test Data for Reduced-Power Flight Range Demonstration, April 28, 2016

A separate flight test was performed to demonstrate the CNPC range at reduced transmitter power level. For this test, the output RF power level from both airborne and ground station L-band radios were each reduced to deliver only 10 mW of RF power at the antenna inputs. Transmit power was reduced through a combination of radio power control adjustments, exploiting cable losses, and supplemental in-line attenuation. The aircraft was flown on outbound and inbound headings, then through a serpentine pattern, all over the same hilly terrain used in the validation testing. The aircraft altitude was held at approximately 11,600 ft for all tests. The complete flight path for the 10-mW demonstration test is shown in Figure 38. Data capture segments are highlighted in Figure 39. No C-band data were collected during this test flight.

Figures 40 and 41 present flight test data for portions of the L-band 10-mW demonstration flight over hilly terrain. Outbound and inbound runs indicate the presence of a substantial multipath interference at approximately 22 to 27 nmi downrange, likely caused by a ground reflection. Transverse segments flown at ranges of 25 and 50 nmi show the typical frame losses inside (Fig. 41(a)) and outside (Fig. 41(b)) of the affected flight area.

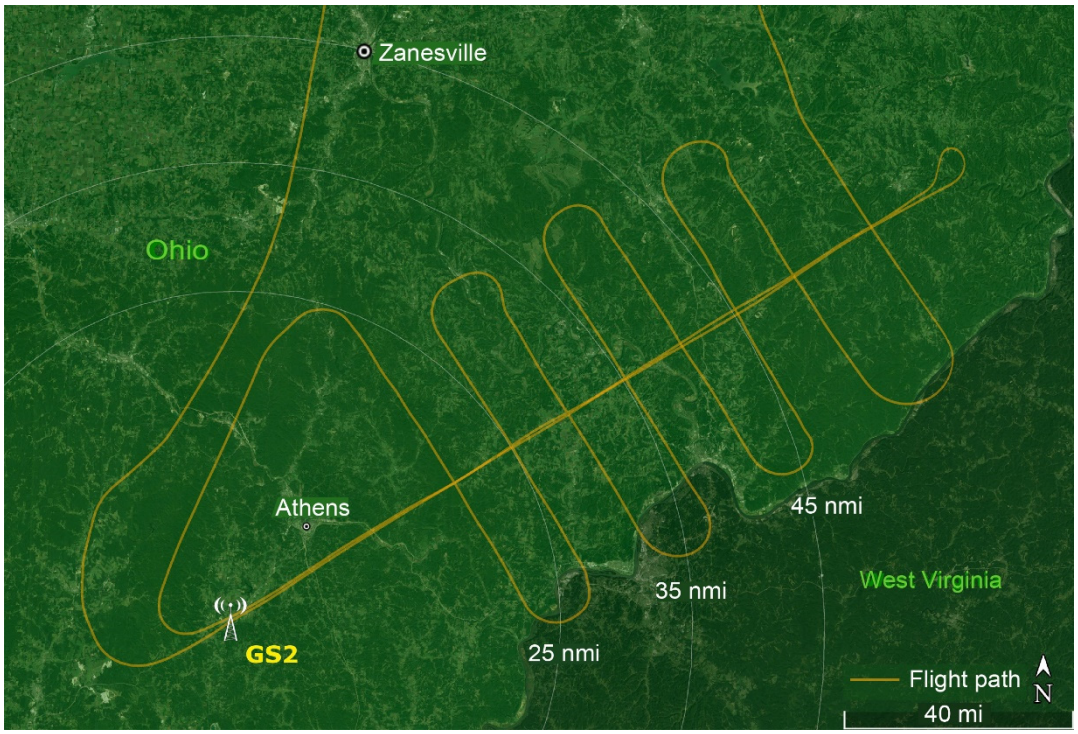

Figure 38.—Flight path over hilly terrain for 10-mW radio test on April 28, 2016. Image ©2016 GoogleEarth (Ref. 5).

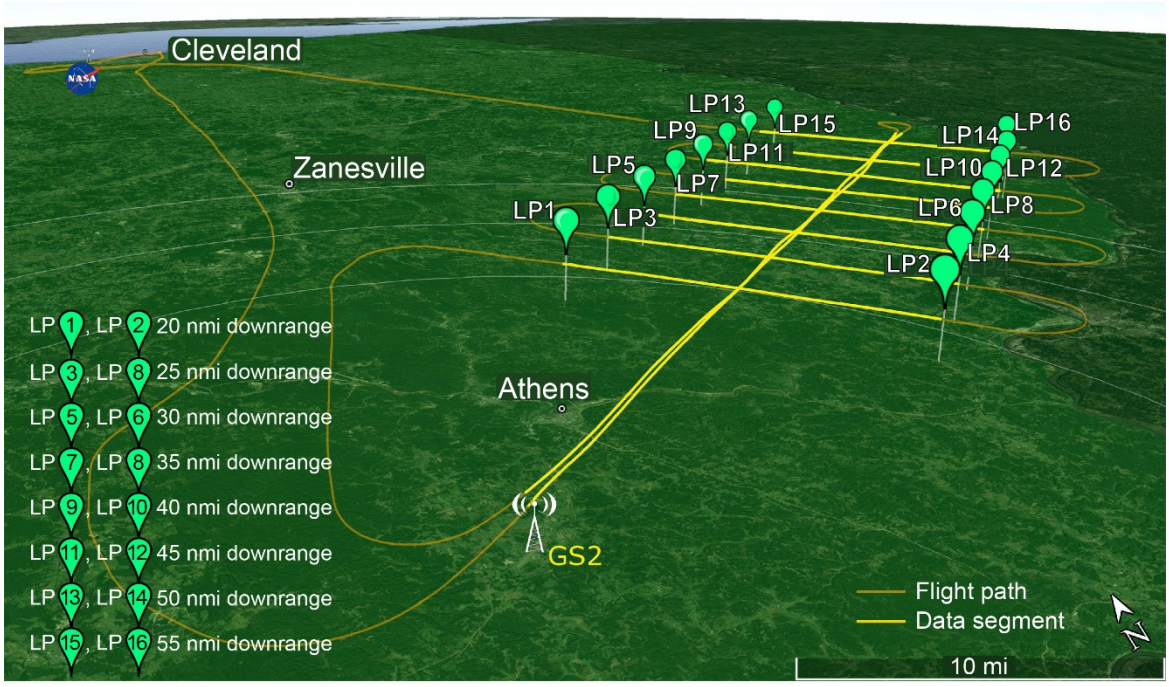

Figure 39.—Perspective view of flight path over hilly terrain for 10-mW radio test, highlighting data capture segments, April 28, 2016. Image ©2016 GoogleEarth (Ref. 5).

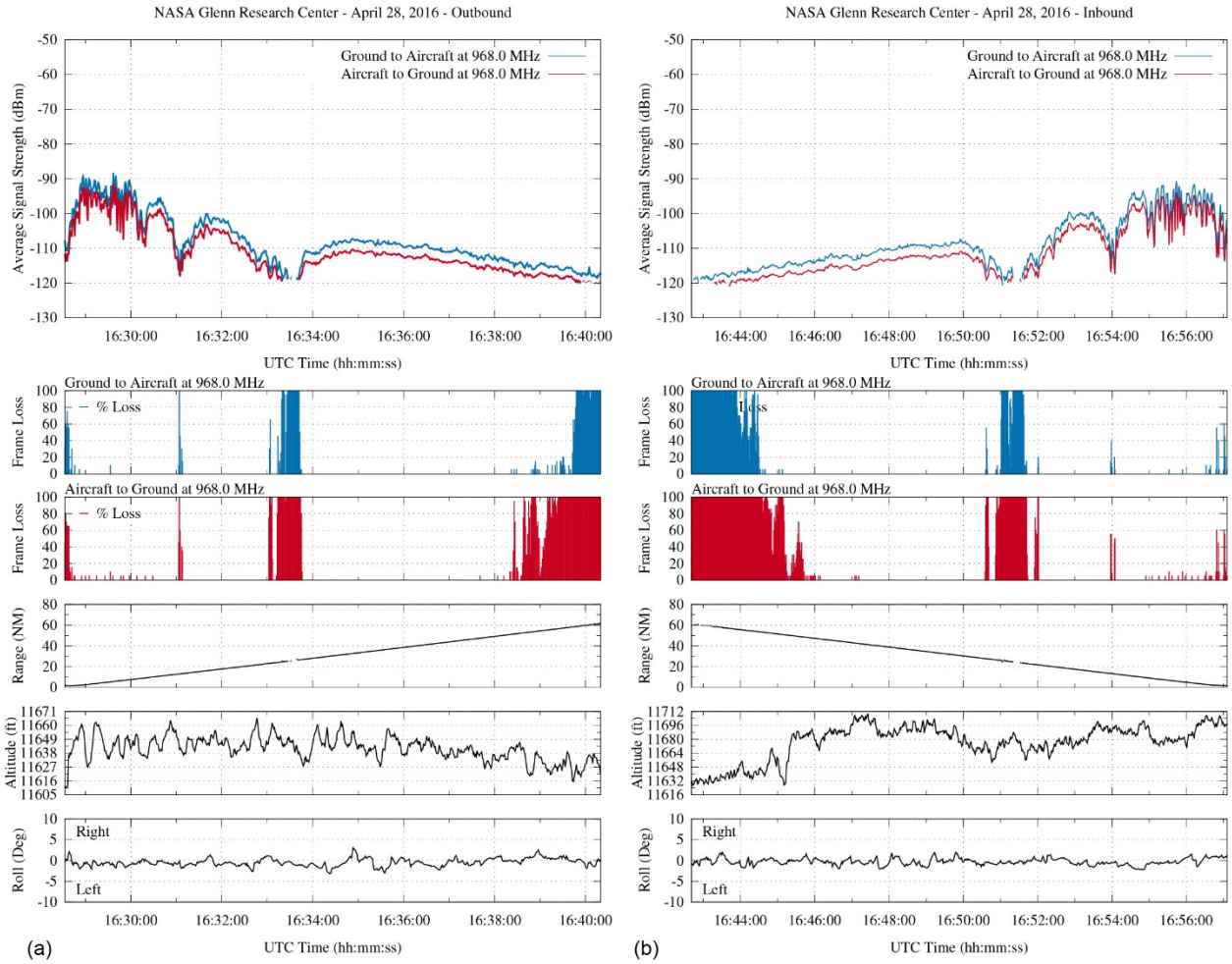

Figure 40.—L-band signal strength and frame loss over hilly terrain during outbound track. (a) From ground station 2 (GS2). (b) Toward GS2.

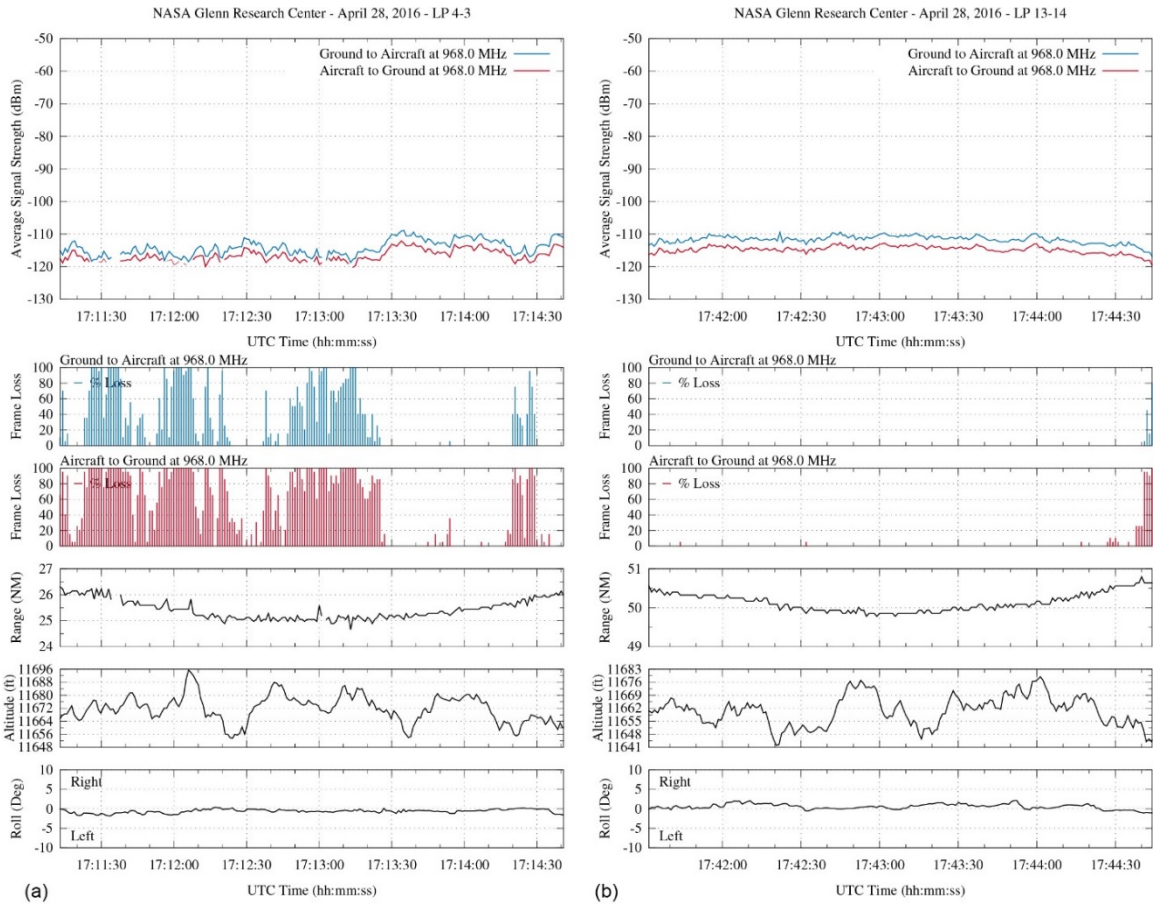

Figure 41.—L-band signal strength and frame loss over hilly terrain. (a) At 25-nmi range and 11,600-ft altitude. (b) At 50-nmi range and 11,600-ft altitude.

4.3 Network/Multiuser Testing and Analysis

On March 8, 2016, a flight was performed to test the transmission of user data over the network architecture detailed in Section 3.3. This architecture provided a scalable and secure solution that allowed the aircraft to remain directly addressable and the contents of messages encrypted. Because ranging was not the focus of this test, the flight path was a simple 25-nmi orbit around GS1 at Glenn's Lewis Field campus (Fig. 42).

These tests were intended to mimic the actual data message formats being sent over both the air-to-ground (downlink) and ground-to-air (uplink) links. The size and types of these messages are detailed in Appendix J of Reference 1 and are the basis of the Gen 4/5 waveform sizes described in Section 2.1 of this report. The message sizes represent the amount of data transmitted without any network header information.

For proper replication of the data flow, a software script was created to generate IPv6 User Datagram Protocol (UDP) packets at the precise intervals for each of the different modes and phases of flight. Figure 43 provides an example breakdown of the types and rates of messages sent for one configuration of "service class 4" traffic. The NATO Standardization Agreement (STANAG) C2 messages have been selectively combined to ensure that each message type is transmitted with the required frequencies (Ref. 6). Figure 43(b) shows the final distribution of data over a single second for the "Arrival Manual Mode Downlink" breakdown shown in Figure 43(a). This example utilizes waveform mode D to provide the appropriate network capacity to support this service class.

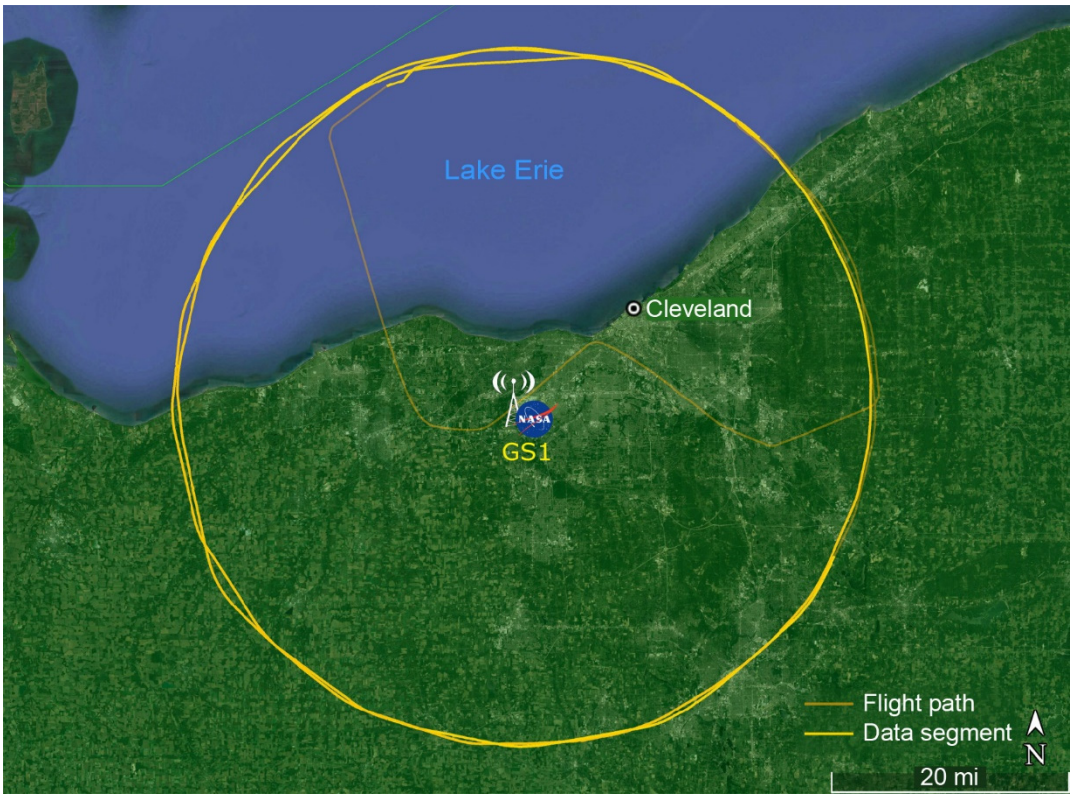

Figure 42.—Flight path for networking tests. Image ©2016 GoogleEarth (Ref. 5).

Category	Symbol	Rate (Hz)	Message Content Size (bytes)	Message Content Details
C2	■	14	27	STANAG 4586: Types 4000
	♦	4	50	STANAG 4586: Types 4000, 9001
	▼	1	42	STANAG 4586: Types 4000, 3009
	▲	1	143	STANAG 4586: Types 4000, 3009, 3002, 3006, 3007, 3015, 9001, 50001
Voice	●	10	60	ATC Voice Relay (Using 5, 20ms samples)
Targets	►	2	485	Target Data (30 Targets per message) 60 Targets per second
Weather	◄	1	60	Weather Data

Figure 43.—Example rate and size of data to be generated. (a) Service class 4 air-to-ground (downlink) traffic in manual mode during arrival. (b) User data 1-s sequence, in bytes. ATC, air traffic control; C2, command and control; STANAG, NATO Standardization Agreement.

TABLE IX.—PRIORITY MAPPINGS, HIGHEST (7) TO LOWEST (0)

Priority	IPv6[a] traffic class	Message type
7	0x7c	Reserved
6	0x6c	STANAG[b]—C2[c]; NAVAID[d]
5	0x5c	ATC[e] voice
4	0x4c	Target data
3	0x3c	Weather data
2	0x2c	Reserved
1	0x1c	Reserved
0	0x00 or 0x0c	Unclassified

[a]Internet Protocol version 6.
[b]NATO Standardization Agreement.
[c]Command and control.
[d]Navigational aid.
[e]Air traffic control.

The software program (Ref. 7) generates messages at the correct size and rate but does not fill the messages with real user data. Instead, the messages all contain sequence and time stamp information, which aid in calculating performance metrics when they are received. A data collector program was also created that would receive these messages and log the results. All of the packets were UDP except for the ATC voice traffic, which is expected to use Real-time Transport Protocol (RTP). Because the traffic generator program is not designed to process RTP, the software compensates for the missing RTP header by adding 12 bytes to the 60 bytes of application data, bringing the total for each voice packet to 72 bytes. A copy of the traffic generator program is run on the aircraft system to generate downlink traffic, while another copy of the generator program is run on a ground-based system acting as the pilot station to simulate uplink traffic. It is important to note that in this network architecture, the ground station is not a data endpoint but rather data are routed through a ground station.

Each of the message groups is also classified at one of seven available priorities. Table IX shows the priority mappings used for the different message types. In addition to setting the priority, IPv6 flow labels are enabled in order to preserve each flow through the header compressor. A separate traffic generator program is activated for each type of data to reflect the behavior of a real system. In this example, transmission of C2 and other message types are initiated simultaneously, which imposes heavy data loading at the beginning of each 1-s transmission interval. Staggering the start times for the message types would distribute the data load over time, possibly improving the data latency and efficiency for lower priority messages over the CNPC radio link.

4.3.1 Test Procedure

The networking/multiuser test procedure was created to exercise service classes for which waveforms exist. As noted in Table V, the prototype radio only supports a subset of the waveforms. So that the number of test cases would be more reasonable for a single flight, only the manual modes of flight were tested.

The tests were performed in two sets of six tests each for service classes 2 and 4. Given the time-sensitive nature of these results, all systems were time synchronized prior to takeoff. In coordination with the aircraft, the test script was executed manually on both the aircraft and the ground pilot systems, enabling data flow for a 10-min period for each specified service class, mode, phase, and direction. First, the departure phase was tested; then the arrival phase was tested. Prior to testing the en route phase, the radio configuration was modified from 20 to 15 Hz to accurately reflect the reduced resources that the phase of flight would have. Completion of all three phases of flight required 30 min. After the tests for service class 4 were completed, data collection was terminated and the data was stored. The radio was then reconfigured for service class 2 tests, and the test procedure was repeated.

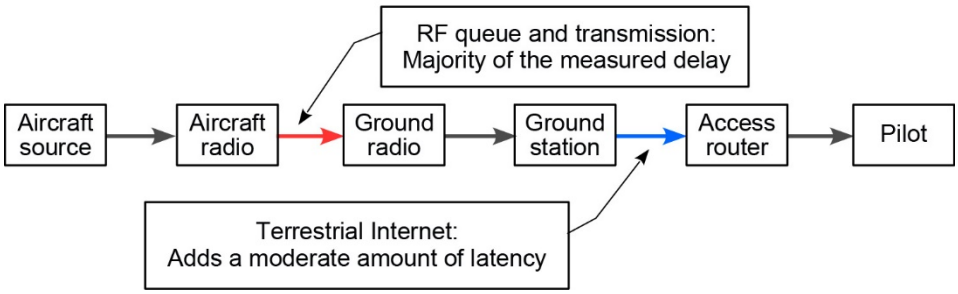

Figure 44.—Latency factors. RF, radiofrequency.

4.3.2 Test Results

The primary metric of importance for these experiments was the total, one-way latency of the messages between the aircraft and the ground-based pilot. This latency included not only the communication latency of the prototype radios but also the latency of the ground support network. A breakdown of the different latency factors is shown in Figure 44. By design, the radio will always favor higher priority traffic and so the latency could include a significant amount of time where the data are being held in a queue. Because these data are only a placeholder meant to represent the worst case in terms of size and frequency of real messages, the processing delay could be significantly higher both in terms of collecting and generating the messages and also in processing, disseminating, and displaying the messages to the pilot. These test results capture the worst-case delays for data transmission while assuming the best-case delays for data processing. The desired result is that the total latency for a particular message type be less than the frequency at which those messages are generated.

Figures 45 and 46 show the complete results of all 12 tests. Each graph captures a single test configuration of service class, waveform mode, phase of flight, and propagation direction. Traces display a cumulative distribution function (CDF) of delays for each message type present in each configuration. Not all configurations generate the same amount or types of data. The CDFs show the percentage of messages that arrived at or before a given amount of time. Each plot also has statistics for each data type, including the number of messages that arrived within the 10-min test period. Table X shows a breakdown of the metrics for each data type. For example, Figure 45 shows that roughly 35 percent of C2 messages arrived in 60 ms, roughly 65 percent by 80 ms, and 100 percent within 105.7 ms, confirmed by looking at the statistics for C2, which list the maximum latency at 105.7 ms.

A majority of the test results confirm that the links are sized appropriately, with the CDF curves showing sharp vertical lines, indicating that nearly all samples incurred the same amount of delay and that very little variation, or jitter, was present in the data flow. The uplink flows for arrival and departure phases for both service classes 2 and 4 show this behavior, with C2 flows sharply on 50-ms latencies and voice flows on 100-ms latencies.

Figure 46(a) shows a downlink service class 4 plot with all four types of traffic. The figure shows that a majority of C2 data arrived within 54 ms and that voice data arrived within 105 ms. Target and weather data also with a majority of samples were received near 455 ms and 505 ms, respectively. The target and weather data traces have larger “tails” on both ends of the CDF, indicating that some samples can take significantly less or more time than the average. Even so, both tails only account for about 5 percent of the samples. Even a smaller subset, less than 1 percent, is extremely large, with latencies near 1 s. However, some of these results were expected because of several factors.

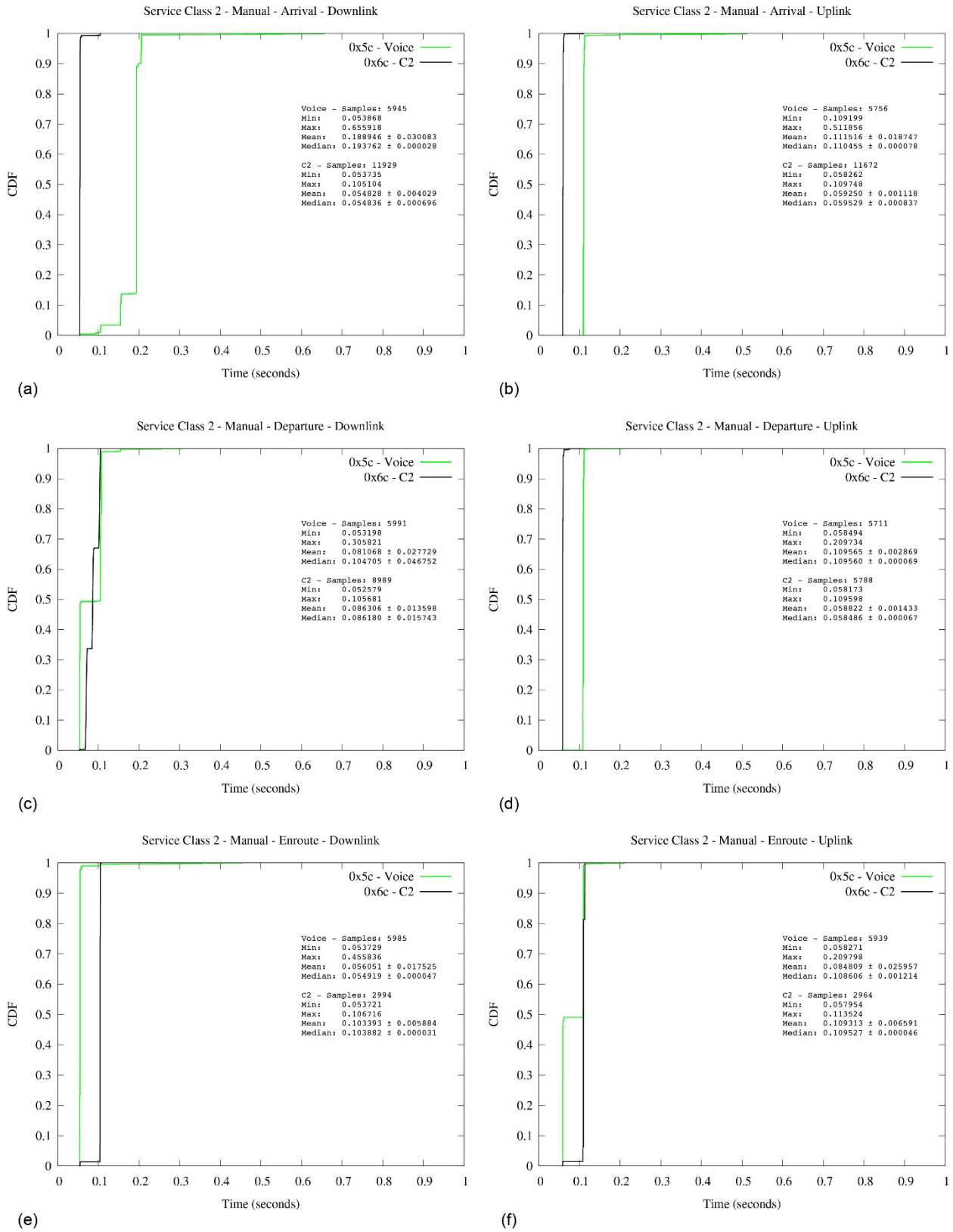

Figure 45.—Service class 2 flight test latency results.

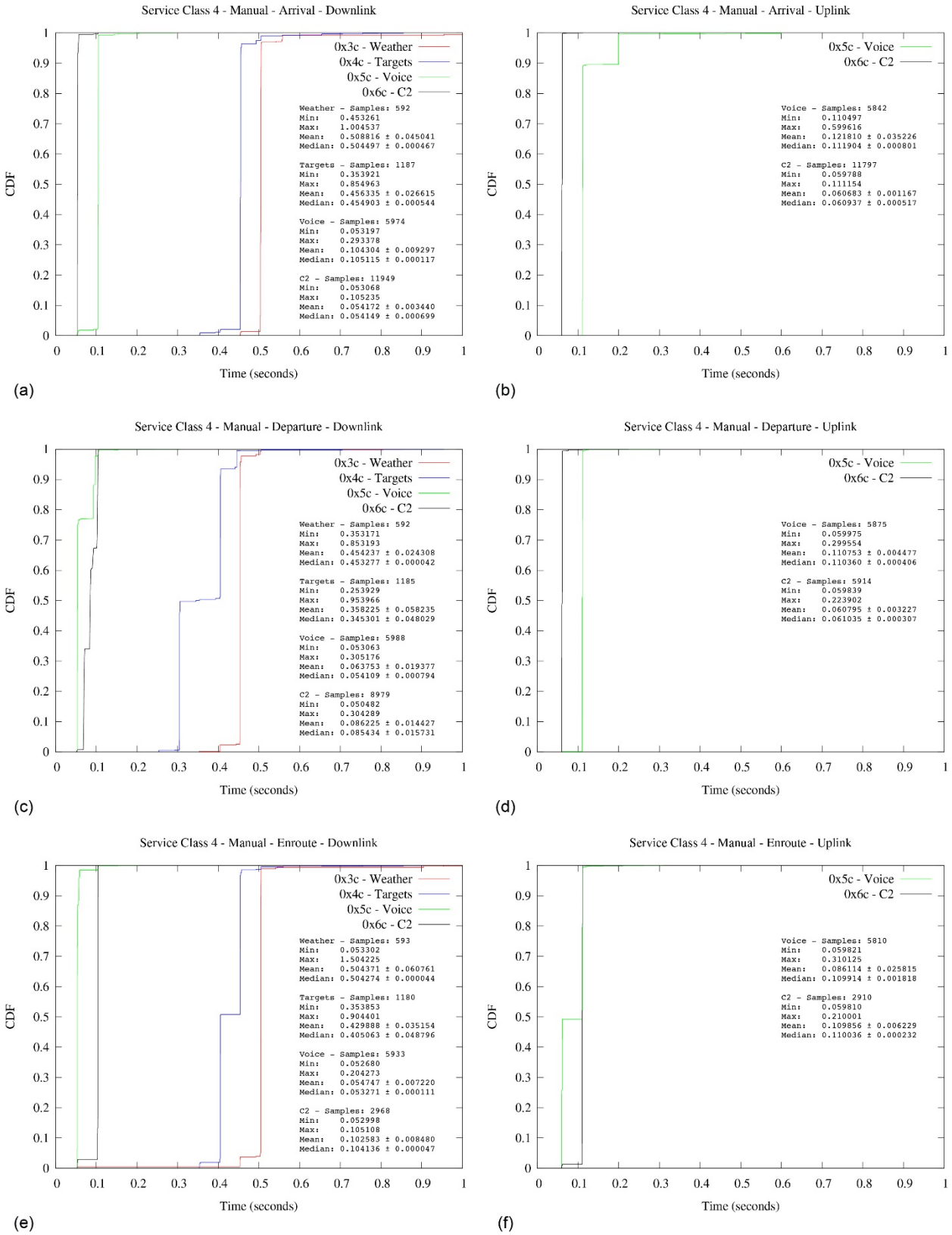

Figure 46.—Service class 4 flight test latency results.

TABLE X.—DATA TYPE METRICS

Metric	Description
Samples	Number of messages that were successfully received
Min.	Minimum latency observed
Max.	Maximum latency observed
Mean±StdDev	Mean or average of all samples and their standard deviation
Median±MAD	Median or midpoint of all samples and their median absolute deviation

When any data stream begins, it does not immediately benefit from header compression. The header compressor must first establish a "context" for each data flow, which takes three or more messages. This impacts all new data flows, but the lower priority flows suffer the most because the larger messages coupled with the lower priority make it more difficult to transmit the message quickly. This is due to the prototype radio starving lower priority data from any resources as part of an important design goal to ensure that high-priority messages always have the lowest latency. Because all flows started around the same time during these tests, the problem is further compounded. Fortunately, the link was sized correctly to tolerate the burst of data; however, it required more time to recover. If the large latency on the initial low-priority data is an issue, one solution to consider would be delaying the start of the low-priority traffic slightly when a new mode of flight is entered. Even though the header compression fully compressed all data traffic, there were periods where the queue for lower priority data built slightly. This resulted in the tails toward the top of the plots and other steps seen in some of the figures. The tails seen near the bottoms of the plots are the exact opposite situation, where a low-priority message came in at a time when the queues were empty and no higher priority message was blocking its immediate transmission.

Although the shapes of the plots align with expectations, not all of the CDF curves align with the expected values for the different message types. Figure 46(e) shows this clearly. Even though the shapes of the figures make sense, it is observed that the C2 data have an overall longer latency than the voice data have, contradicting their priorities. The issue is consistent for over 95 percent of the samples, indicating that it is not a small portion of voice messages that are "beating out" higher priority traffic. Similar behavior can be seen in some of the other results, which prompted further analysis. Ground testing was able to replicate the issue, and detailed analysis found that the additional latency was being generated by the receiving radio. It was discovered that the issue lay in the means with which the prototype CNPC radio communicated with the NASA systems. The prototype radio interfaced with the NASA systems over Transmission Control Protocol (TCP) and had not been using the TCP NODELAY option. Without the option enabled, the prototype radio was essentially waiting for more data to arrive. Such behavior is acceptable in most systems, but it causes problems in time-critical messages, especially when they are small in size like many of the C2 messages.

To confirm the impact of this option, the radio manufacturer released a new version of prototype radio firmware with the TCP NODELAY option enabled. A bench test was then performed with the same configuration as for the flight tests, and data were transmitted for 5 min using the new firmware. Figure 47 shows a comparison of the results shown in Figure 46(e) with those of the ground tests. The results confirm that the option was indeed playing a major role in the results.

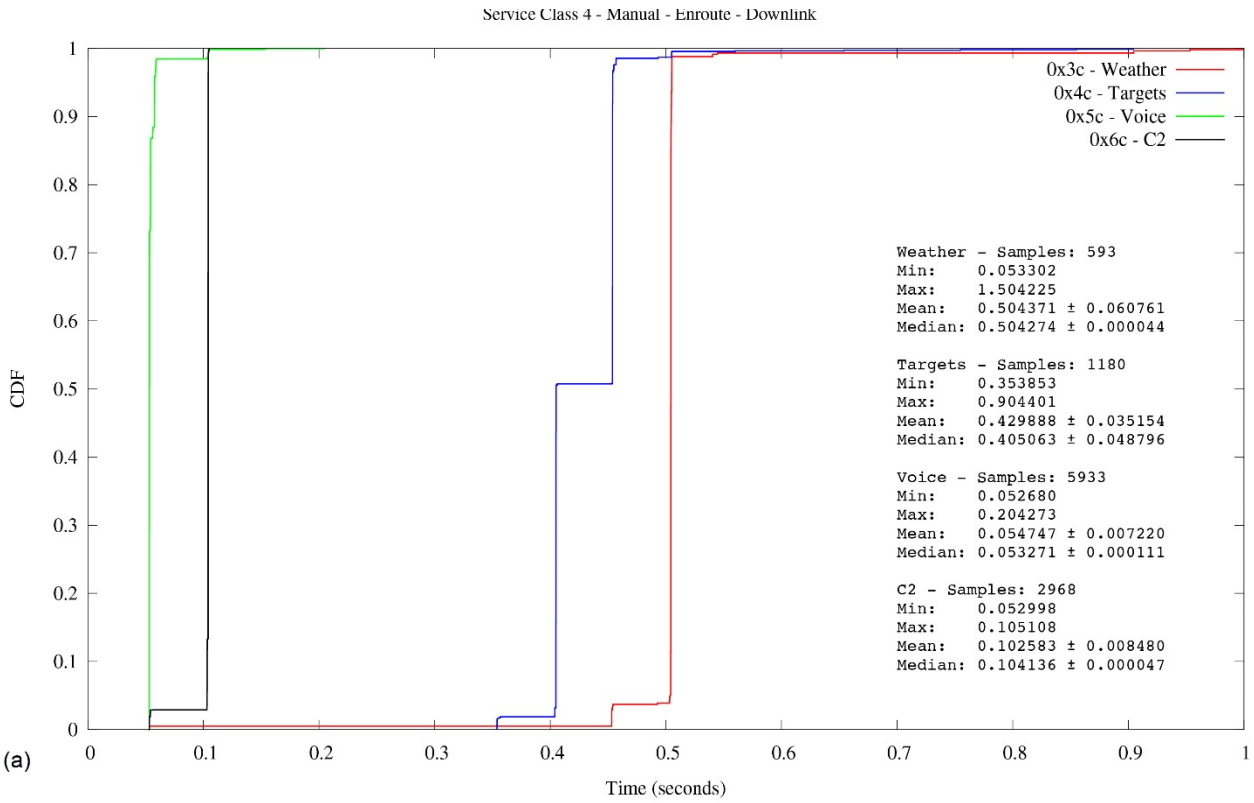

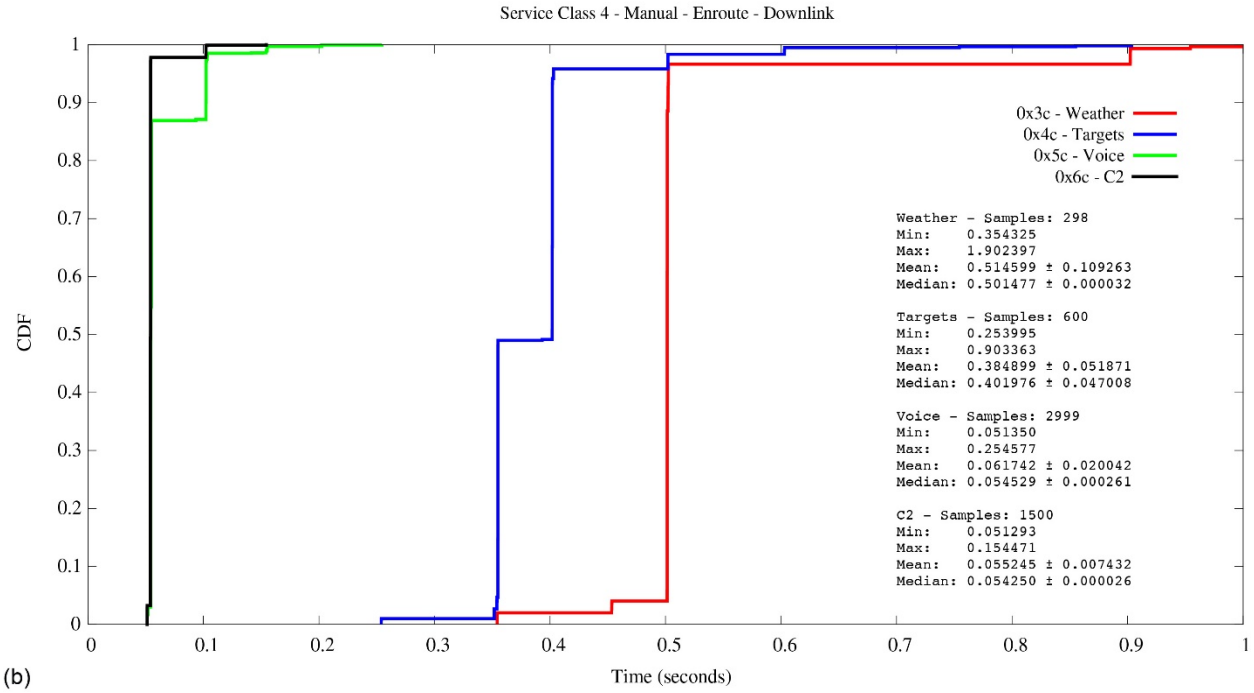

Figure 47.—Impact of the Transmission Control Protocol (TCP) NODELAY option. (a) NODELAY Off. (b) NODELAY On.

5.0 Conclusions

The Unmanned Aircraft Systems (UAS) Integration in the National Airspace System (NAS) communications flight test campaign produced a significant amount of empirical data for validating Control and Non-Payload Communications (CNPC) radios in relevant flight environments. The primary goals of demonstrating radio-to-radio connectivity, acquiring performance data for system analysis, and supplying the RTCA Special Committee, Inc., SC–228 working group with validation data were all achieved.

This report provides only a preliminary analysis of the flight test data and was intended to validate that radio electronics of this type could successfully communicate command and control (C2) information with an aircraft in flight. Efforts are underway to study the radio performance in greater detail and to refine the understanding of performance capabilities to assist in applying CNPC radios in future systems. The flight test campaign yielded several important findings:

Radio Hardware Development Process.—The iterative approach to developing the prototype CNPC radios was highly effective, allowing evolutionary improvements to be incorporated into the radio as each new set of test results was received. These progressive changes, spanning five "generations," or change cycles, allowed NASA to sequentially add new operating frequencies, waveform modes, and test capabilities over the course of the flight test program. The decision to utilize a software defined radio allowed rapid upgrades and test trials without hardware changes.

Terrain Obstructions and Multipath Interference.—The diverse set of flight test environments offered in the Ohio test areas provided researchers excellent opportunities to investigate multiple radiofrequency (RF) propagation characteristics. The relatively flat terrain in the northern Ohio flight test area, for example, afforded a significant unobstructed line-of-sight distance to provide valuable data on the maximum RF range of the CNPC radios. Similarly, the hilly terrain in the southern Ohio region allowed a thorough investigation of the line-of-sight obstruction issues by flying the test aircraft at specific planned altitudes near known terrain features. In addition, test flights over the open, fresh water of Lake Erie provided excellent information on multipath interference and signal dispersion from the water surface. All three of these test environments were readily accessible by aircraft from the NASA Glenn Research Center and are recommended as candidates for future test operations as part of a comprehensive flight test campaign.

Evidence of multipath interference and terrain obstruction seem to appear in many of the flight test data sets included in this report. Flight test data also indicates that manmade structures had adverse effects on CNPC signal propagation. This report provides a substantial amount of flight test data that can, when used in conjunction with the comprehensive L-band and C-band channel models, yield valuable propagation information. Further analysis and possibly additional flight tests are recommended.

Data Latency.—Testing demonstrated that the message prioritization scheme designed into the CNPC prototype radios works well with IP network traffic classes. For service classes 2 and 4, the prototype radios transferred the higher priority C2 and voice data with nominally 50 to 100 ms of transit delay (latency) with very little latency jitter. In service class 4, the lower priority weather and target data messages incurred the expected larger transit delays, but average latency still fell below 500 ms. Flight testing confirmed that header compression techniques utilized in the NASA system architecture worked effectively to reduce delays and keep latency variation low. These techniques proved to be essential and are planned to be detailed in a future NASA publication.

Communications Capability.—The prototype radios used in this test campaign demonstrated reliable C-band and L-band connectivity at a range up to 100 nmi using only the internal transmitters. This operating range is well in excess of the 69-nmi target range established in early UAS architecture studies. Additional analysis remains to be performed as these systems move from the prototype stage to deployment, but these preliminary results are very encouraging.

One of the primary goals of the CNPC flight test campaign was to validate the requirements of the RTCA, Inc., C2 Minimum Operational Performance Standards (RTCA Paper No. DO–362, Command and Control (C2) Data Link Minimum Operational Performance Standards (MOPS) (Terrestrial), 2016, Ref. 1), to prove that the prototype radios can support the operation of unmanned aircraft (UA) at the ranges and altitudes of interest to UAS designers and operators. The NASA in-flight test data clearly show that the prototype CNPC radios are capable of these operations, in either a point-to-point or multiuser network configuration. The flight tests demonstrated that UA can be provided with long-range, reliable RF channels and low user data error rates that can ultimately allow for safe and efficient UAS operation.

Appendix A.—Flight Test Data

This appendix presents data recorded during flight tests of the Rockwell Collins Generation 5 prototype Control and Non-Payload Communications (CNPC) radios. Data collected during the flight test campaign were used to validate the technical requirements in Section 2.2.2 of the Minimum Operational Performance Standards (MOPS, Ref. 1) and serve as the basis for the analysis in Appendix K, Section K.4.4.1.6.2 of the MOPS.

The validation flight tests were conducted from February to April 2016 in the airspace above Ohio, U.S.A.

A.1 Test Data for Validation Flight Over Hilly Terrain, February 19, 2016

C-band validation flight test data over hilly terrain are presented in Figures A.1. to A.11., and corresponding L-band flight test data are presented in Figures A.12. to A.22.

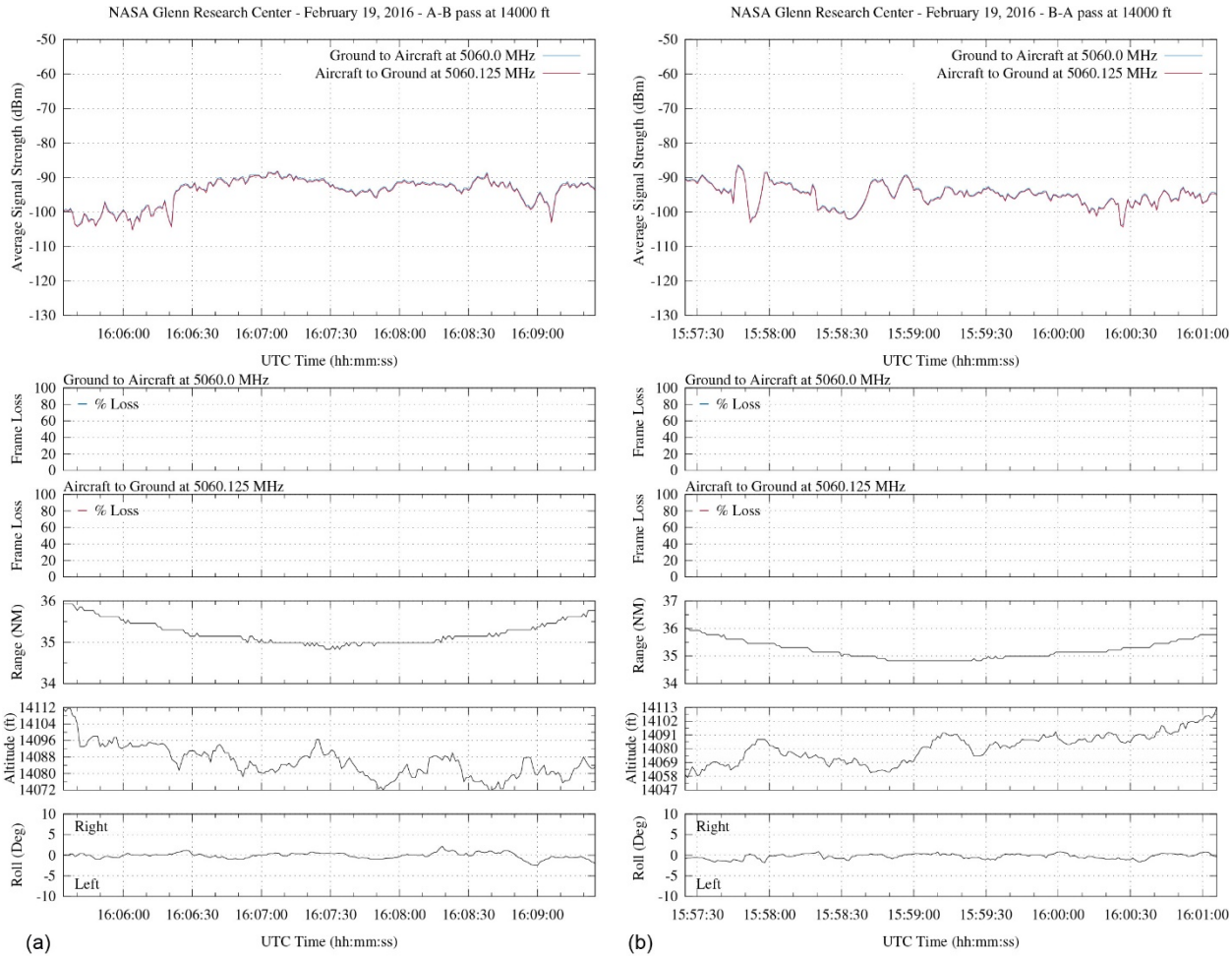

Figure A.1.—C-band signal strength and frame loss over hilly terrain at 35-nmi range and 14,000-ft altitude. (a) Traveling from waypoint A to B. (b) Traveling from waypoint B to A.

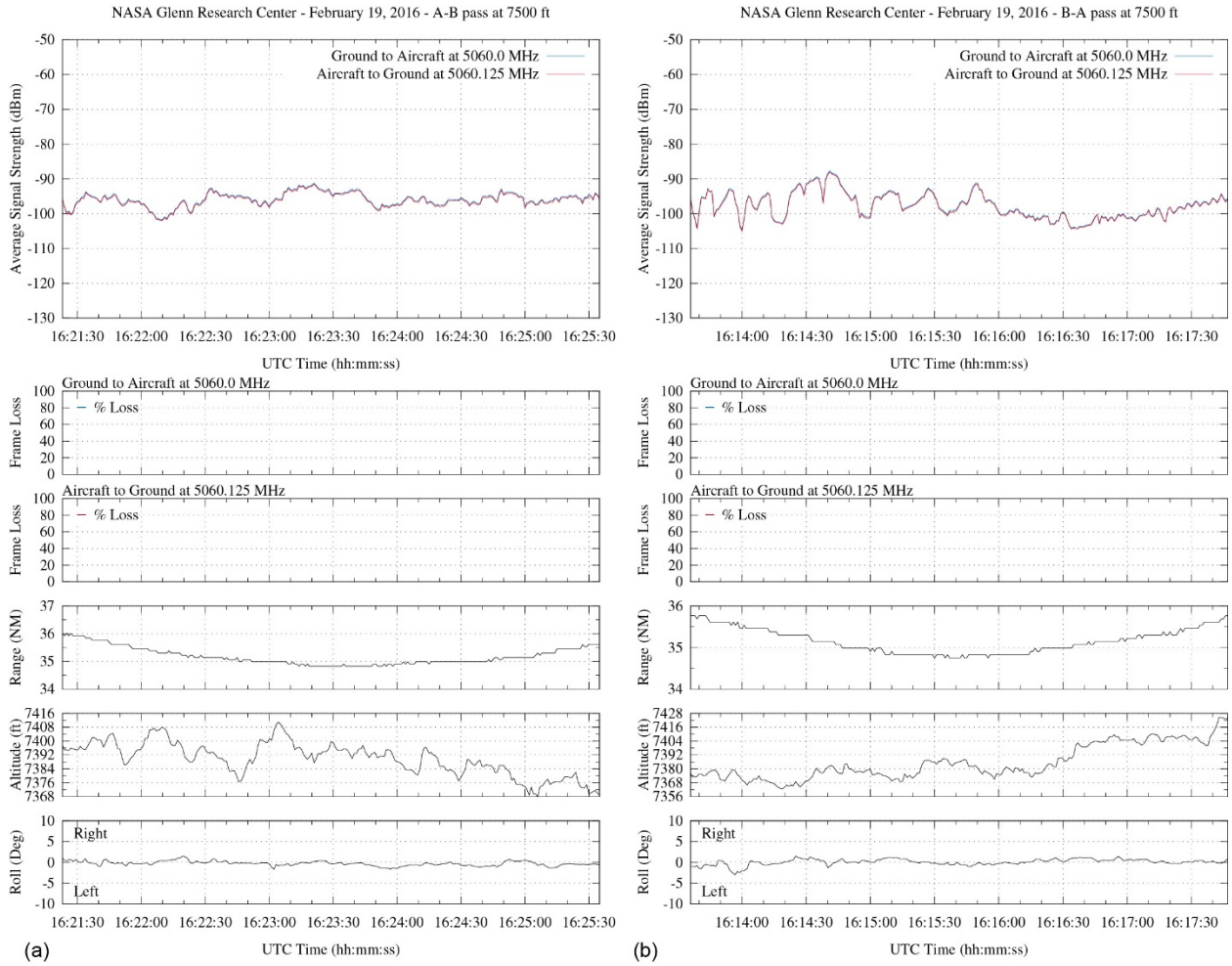

Figure A.2.—C-band signal strength and frame loss over hilly terrain at 35-nmi range and 7500-ft altitude. (a) Traveling from waypoint A to B. (b) Traveling from waypoint B to A.

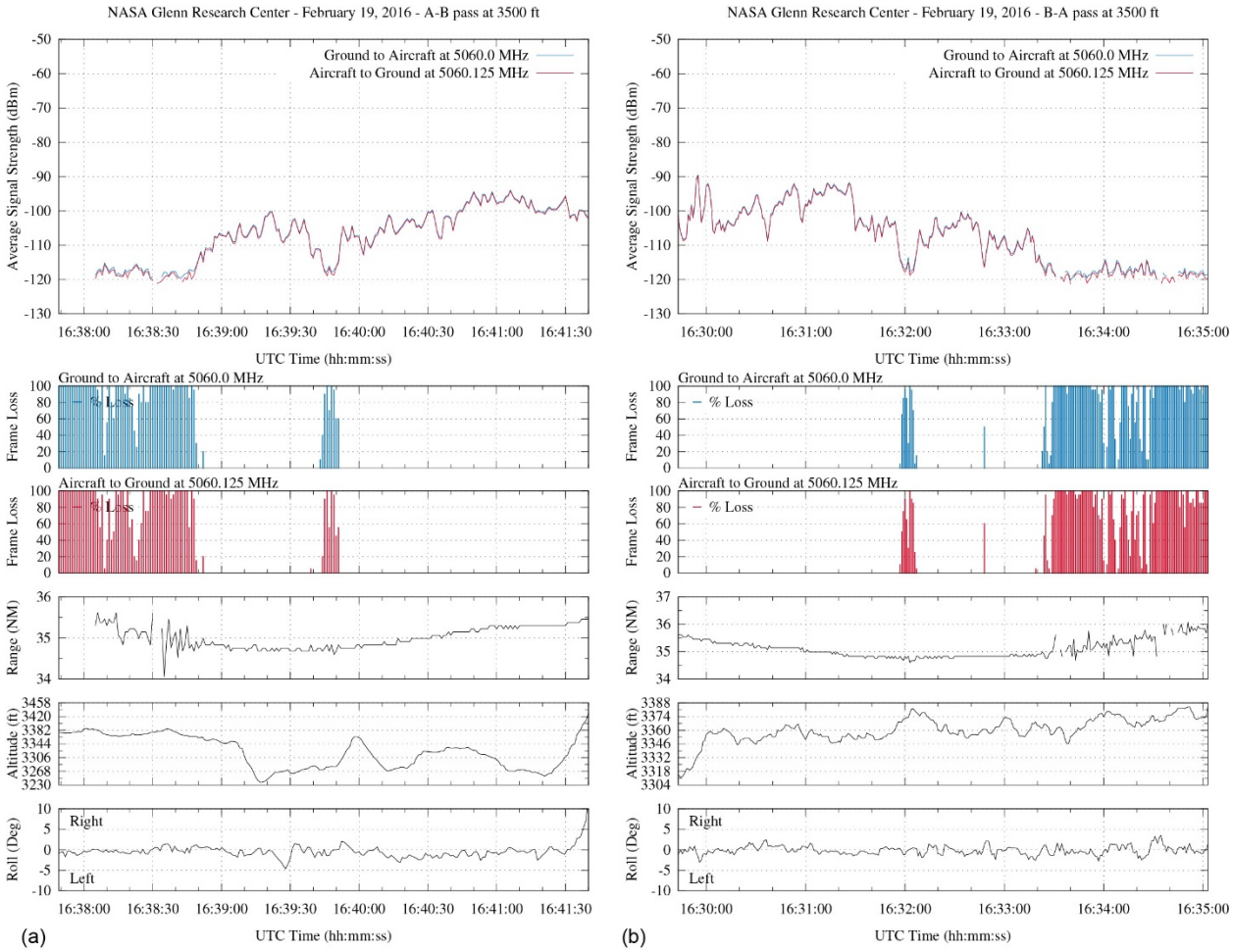

Figure A.3.—C-band signal strength and frame loss over hilly terrain at 35-nmi range and 3500-ft altitude. (a) Traveling from waypoint A to B. (b) Traveling from waypoint B to A.

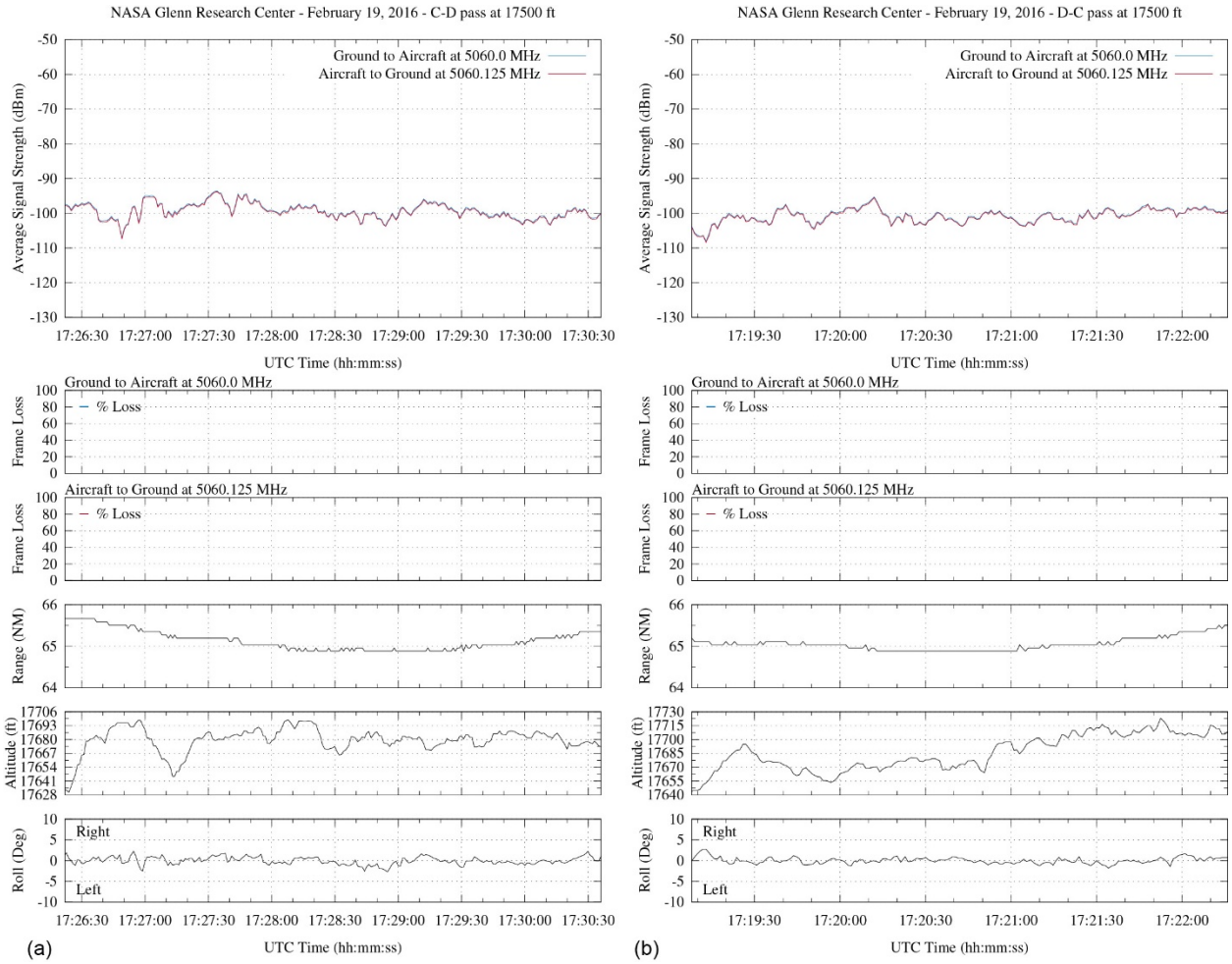

Figure A.4.—C-band signal strength and frame loss over hilly terrain at 65-nmi range and 17,500-ft altitude. (a) Traveling from waypoint C to D. (b) Traveling from waypoint D to C.

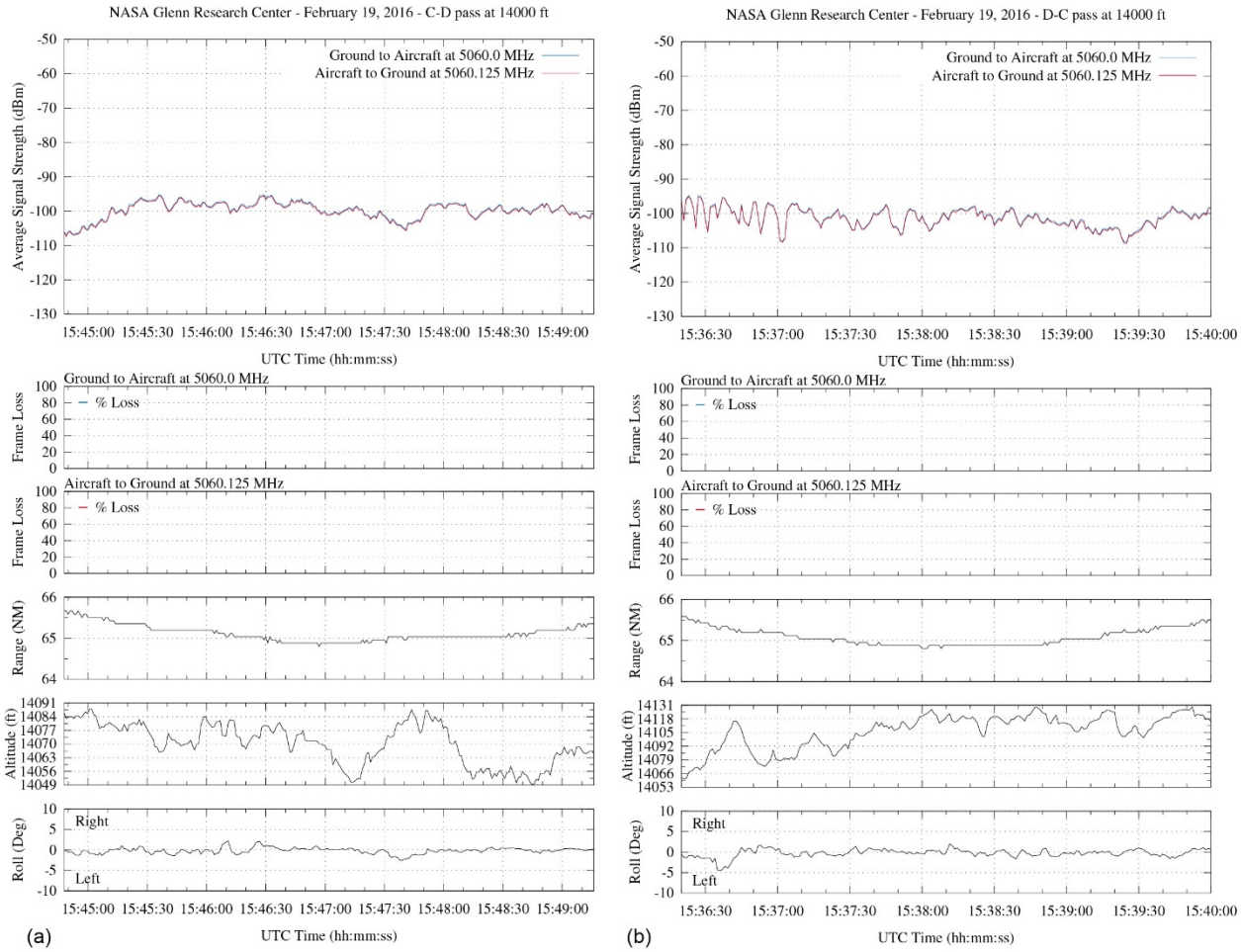

Figure A.5.—C-band signal strength and frame loss over hilly terrain at 65-nmi range and 14,000-ft altitude. (a) Traveling from waypoint C to D. (b) Traveling from waypoint D to C.

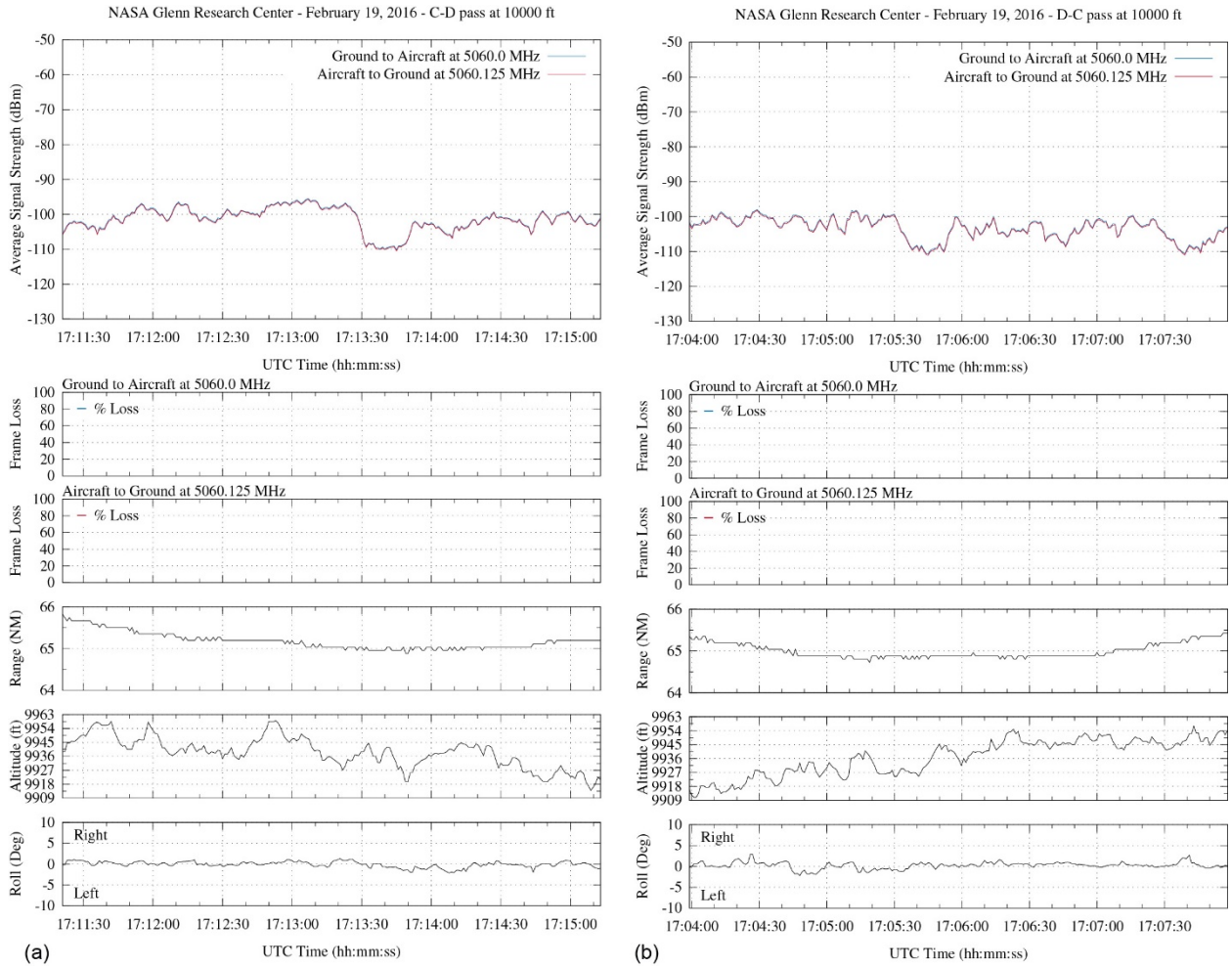

Figure A.6.—C-band signal strength and frame loss over hilly terrain at 65-nmi range and 10,000-ft altitude. (a) Traveling from waypoint C to D. (b) Traveling from waypoint D to C.

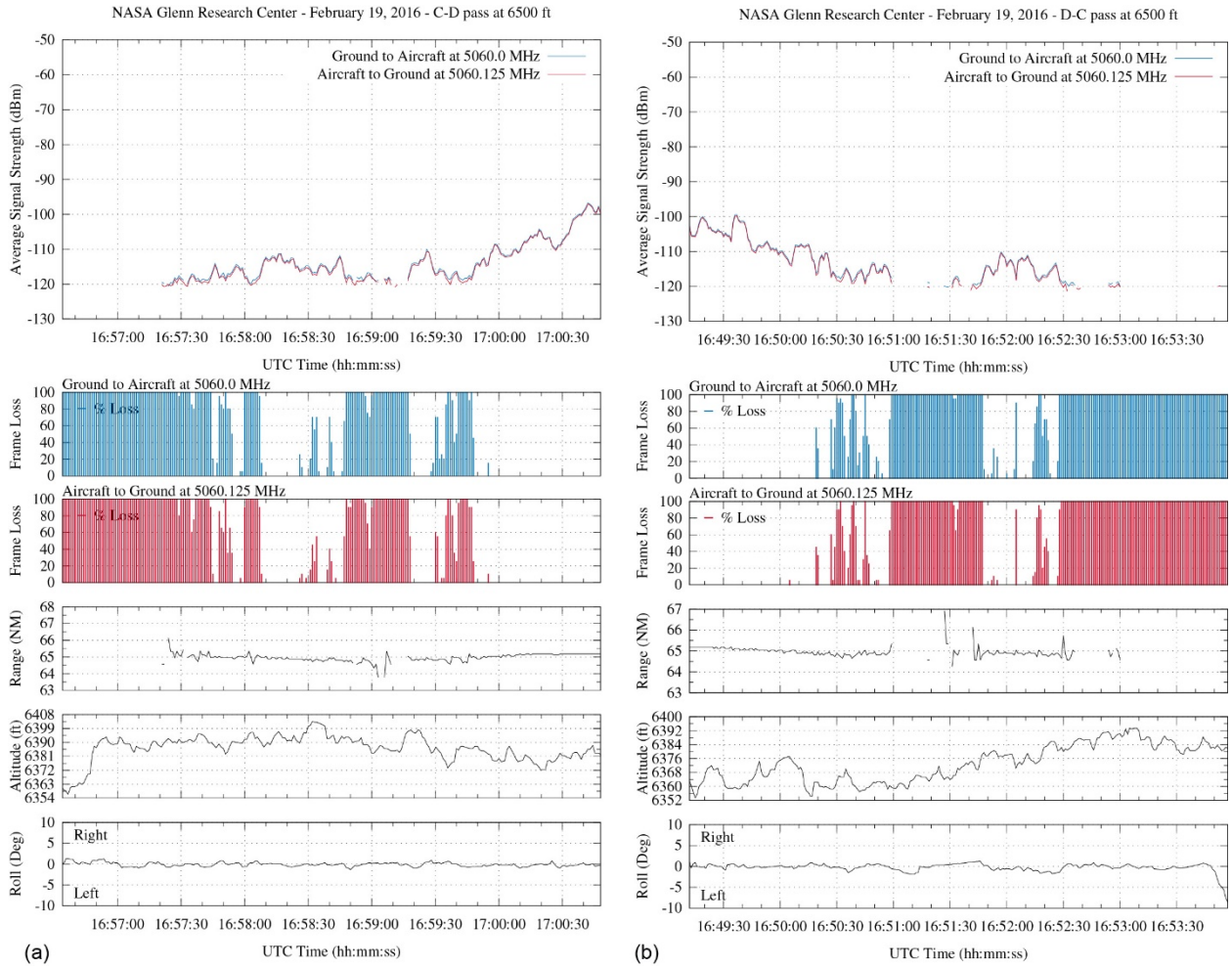

Figure A.7.—C-band signal strength and frame loss over hilly terrain at 65-nmi range and 6500-ft altitude. (a) Traveling from waypoint C to D. (b) Traveling from waypoint D to C.

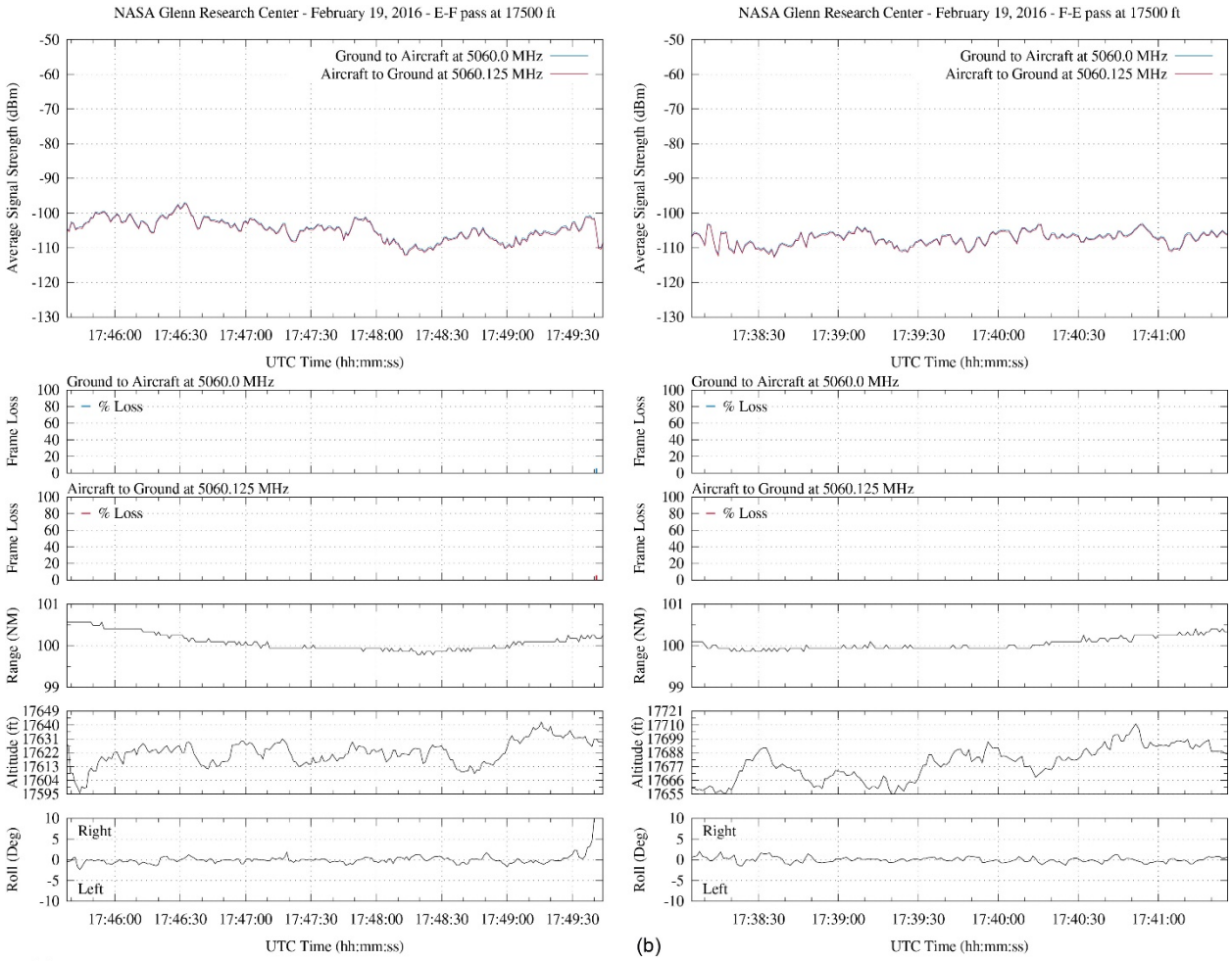

Figure A.8.—C-band signal strength and frame loss over hilly terrain at 100-nmi range and 17,500-ft altitude. (a) Traveling from waypoint E to F. (b) Traveling from waypoint F to E.

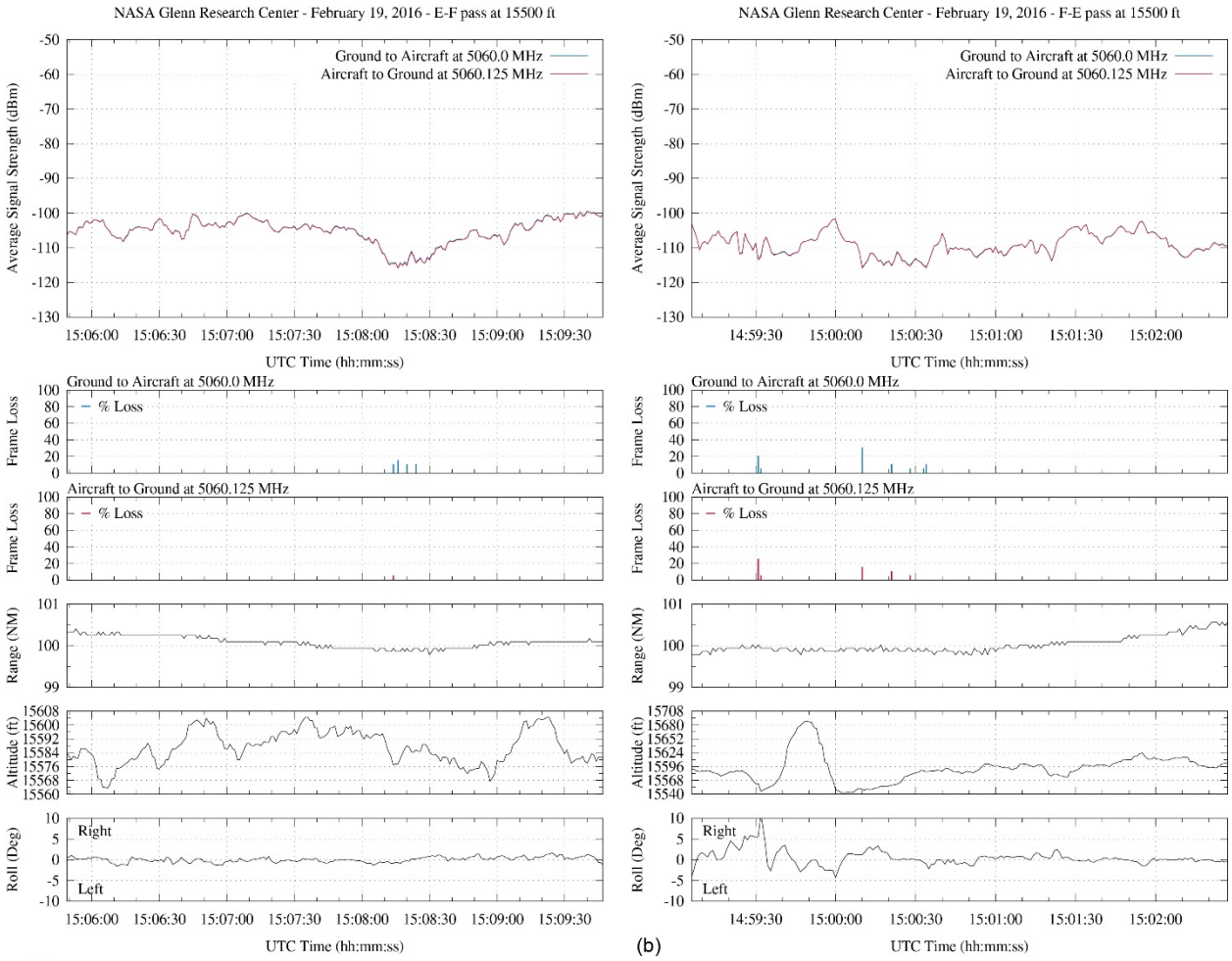

Figure A.9.—C-band signal strength and frame loss over hilly terrain at 100-nmi range and 15,500-ft altitude. (a) Traveling from waypoint E to F. (b) Traveling from waypoint F to E.

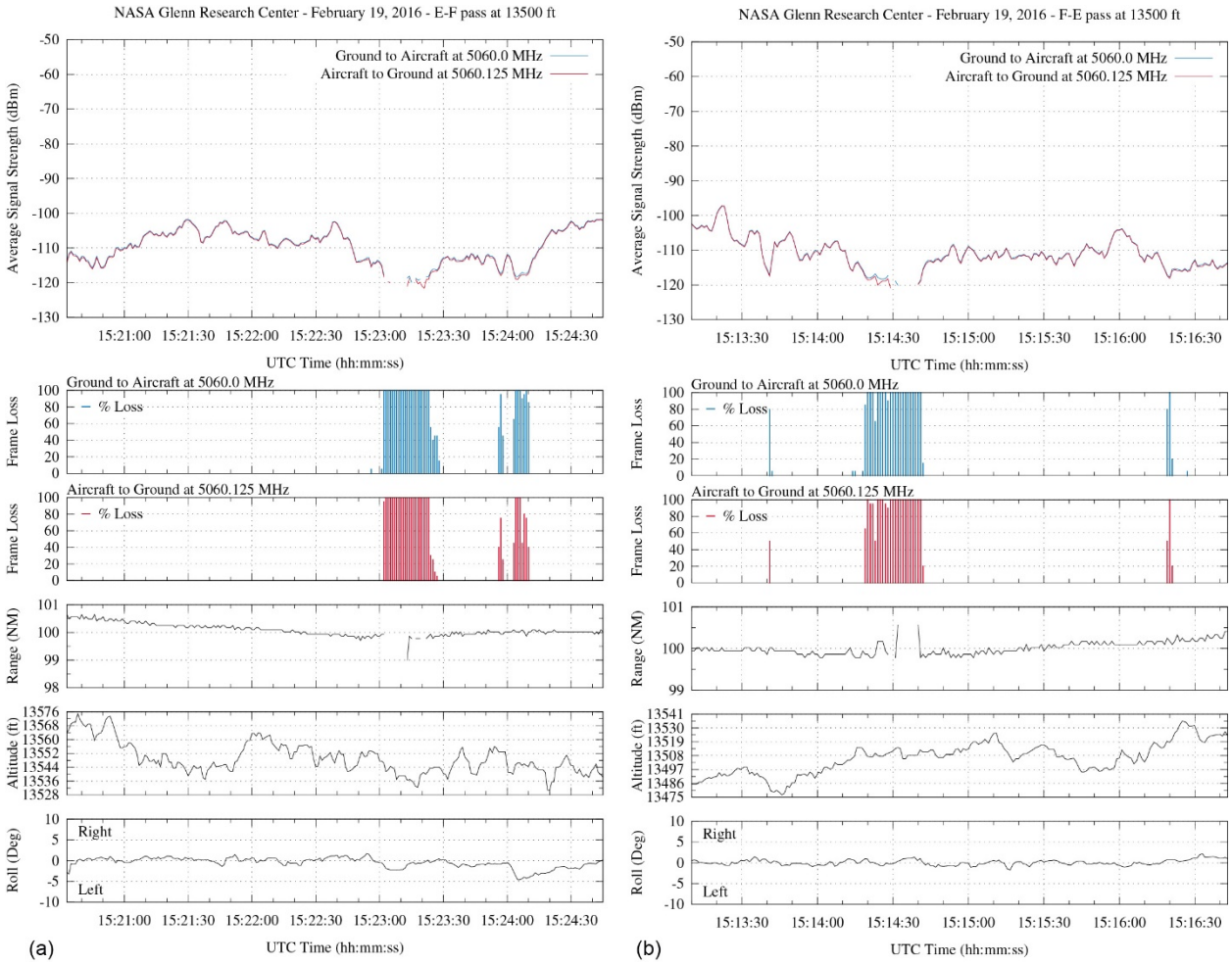

Figure A.10.—C-band signal strength and frame loss over hilly terrain at 100-nmi range and 13,500-ft altitude. (a) Traveling from waypoint E to F. (b) Traveling from waypoint F to E.

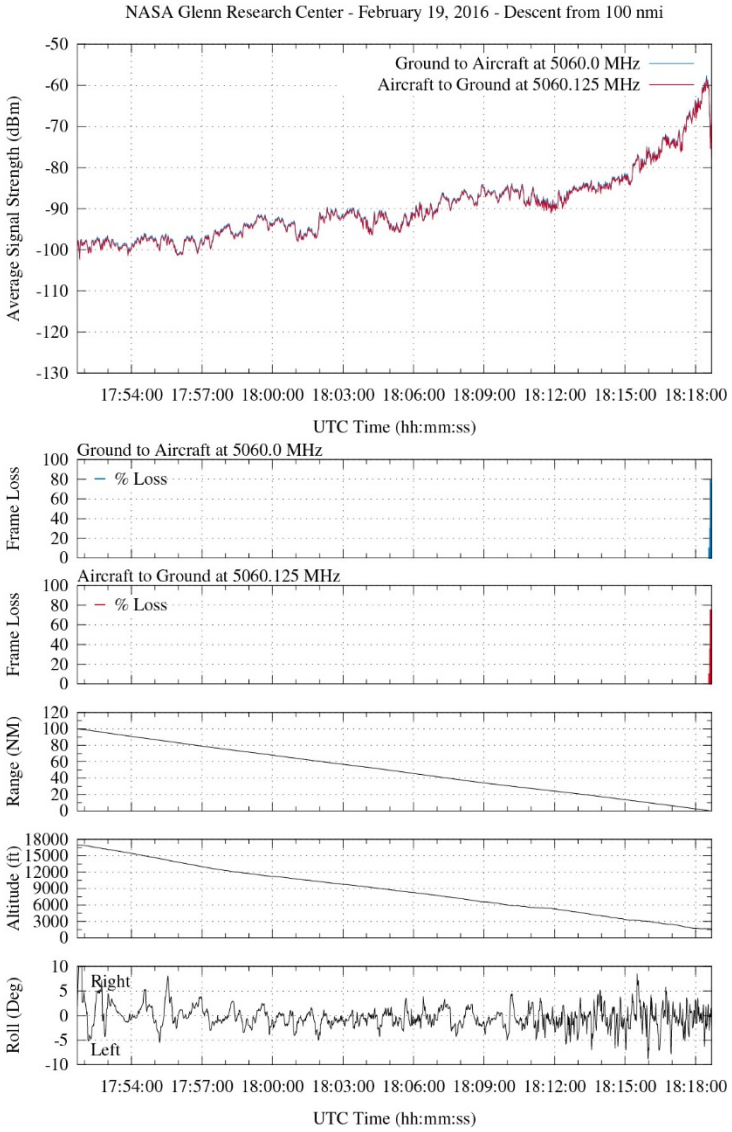

Figure A.11.—C-band signal strength and frame loss over hilly terrain during inbound, descending track from 100-nmi range and 17,000-ft altitude, traveling toward ground station 2 (GS2).

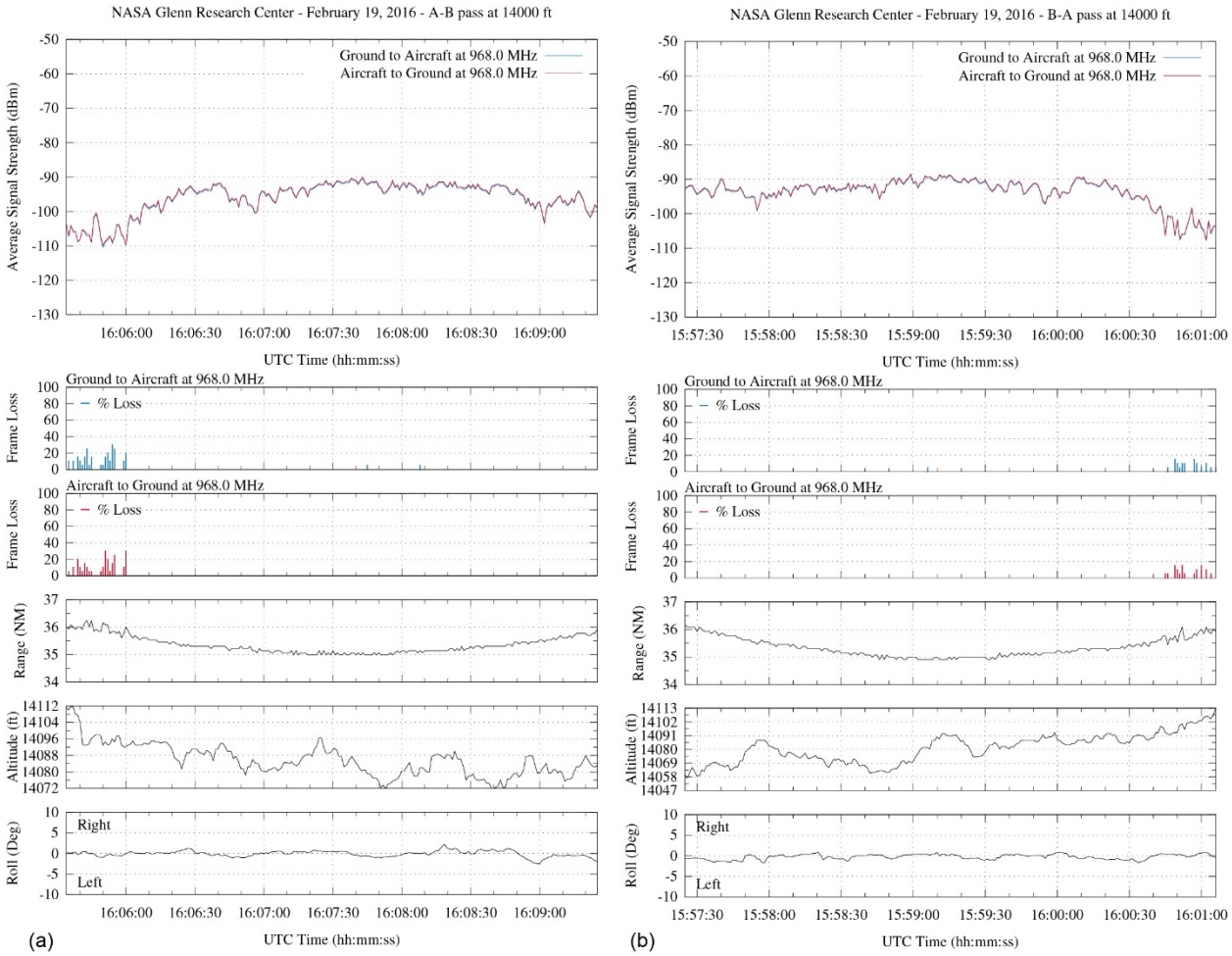

Figure A.12.—L-band signal strength and frame loss over hilly terrain at 35-nmi range and 14,000-ft altitude. (a) Traveling from waypoint A to B. (b) Traveling from waypoint B to A.

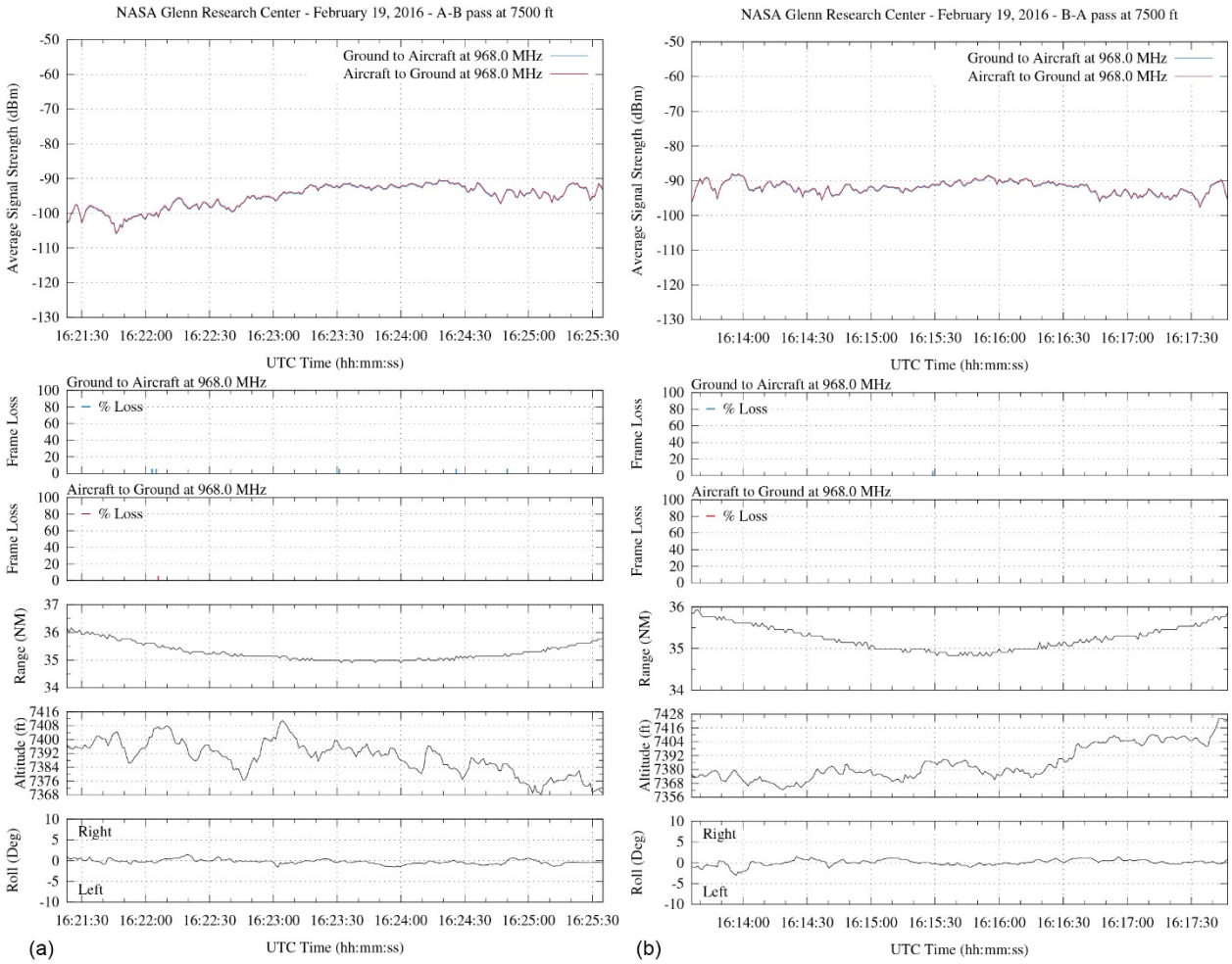

Figure A.13.—L-band signal strength and frame loss over hilly terrain at 35-nmi range and 7500-ft altitude. (a) Traveling from waypoint A to B. (b) Traveling from waypoint B to A.

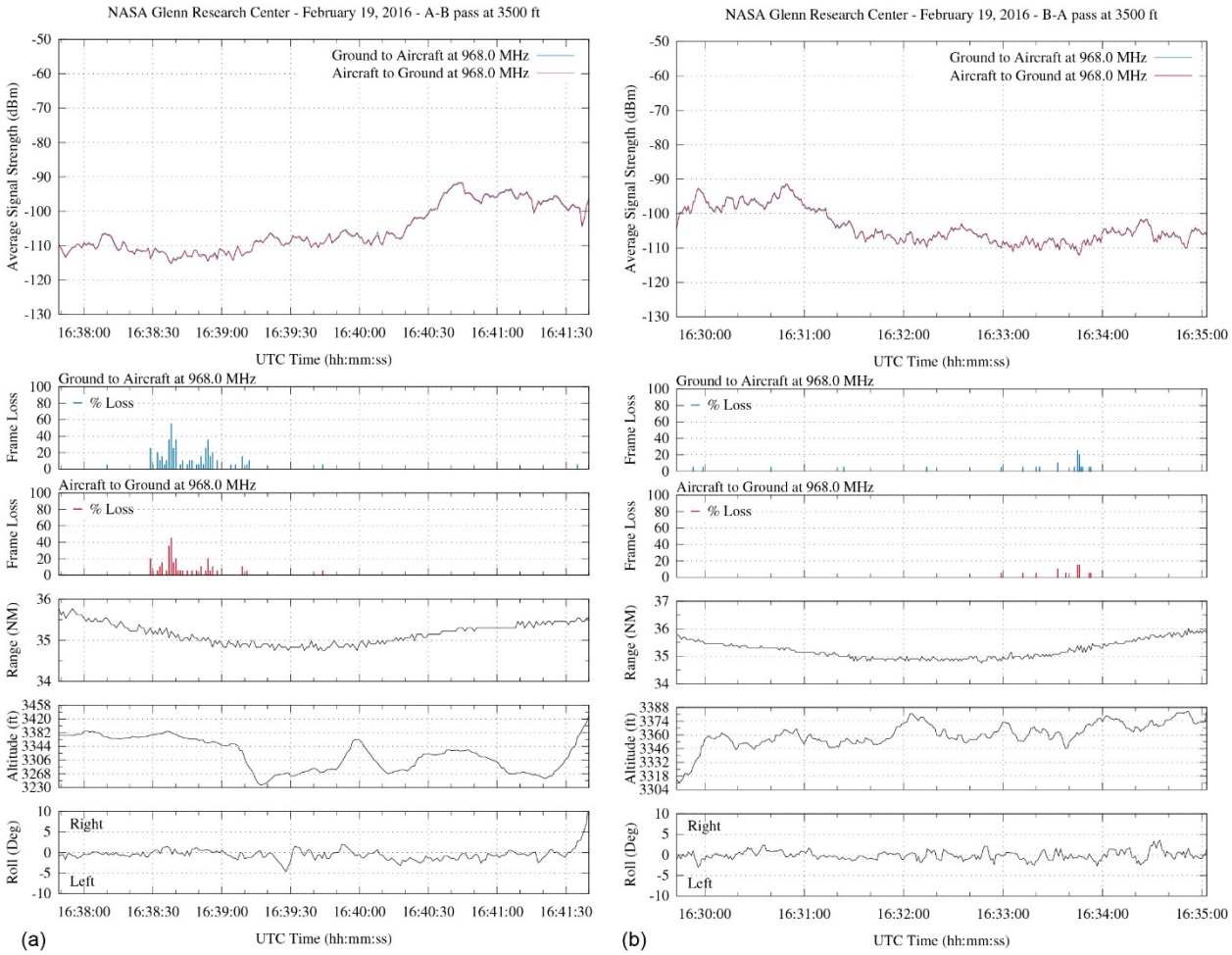

Figure A.14.—L-band signal strength and frame loss over hilly terrain at 35-nmi range and 3500-ft altitude. (a) Traveling from waypoint A to B. (b) Traveling from waypoint B to A.

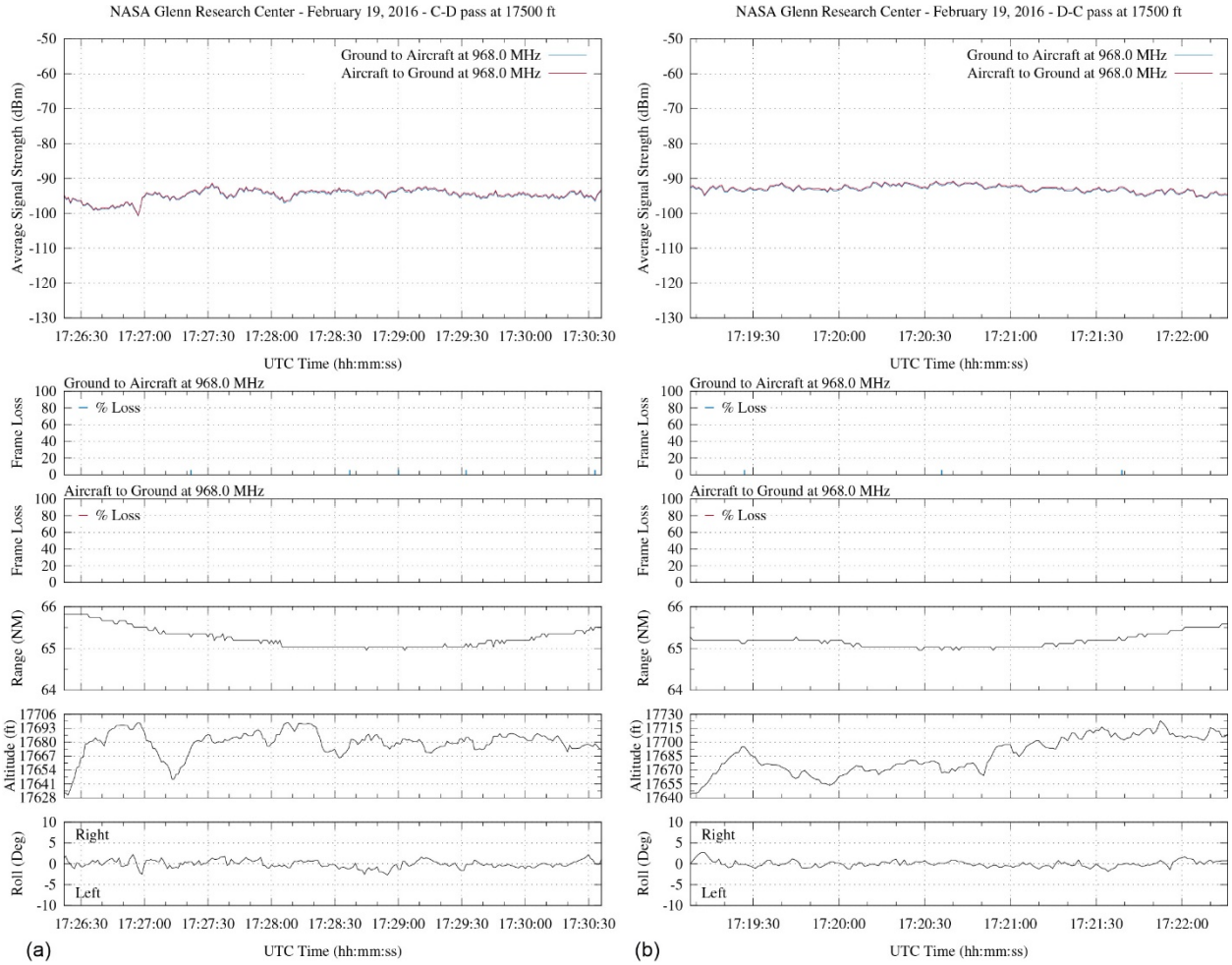

Figure A.15.—L-band signal strength and frame loss over hilly terrain at 65-nmi range and 17,500-ft altitude. (a) Traveling from waypoint C to D. (b) Traveling from waypoint D to C.

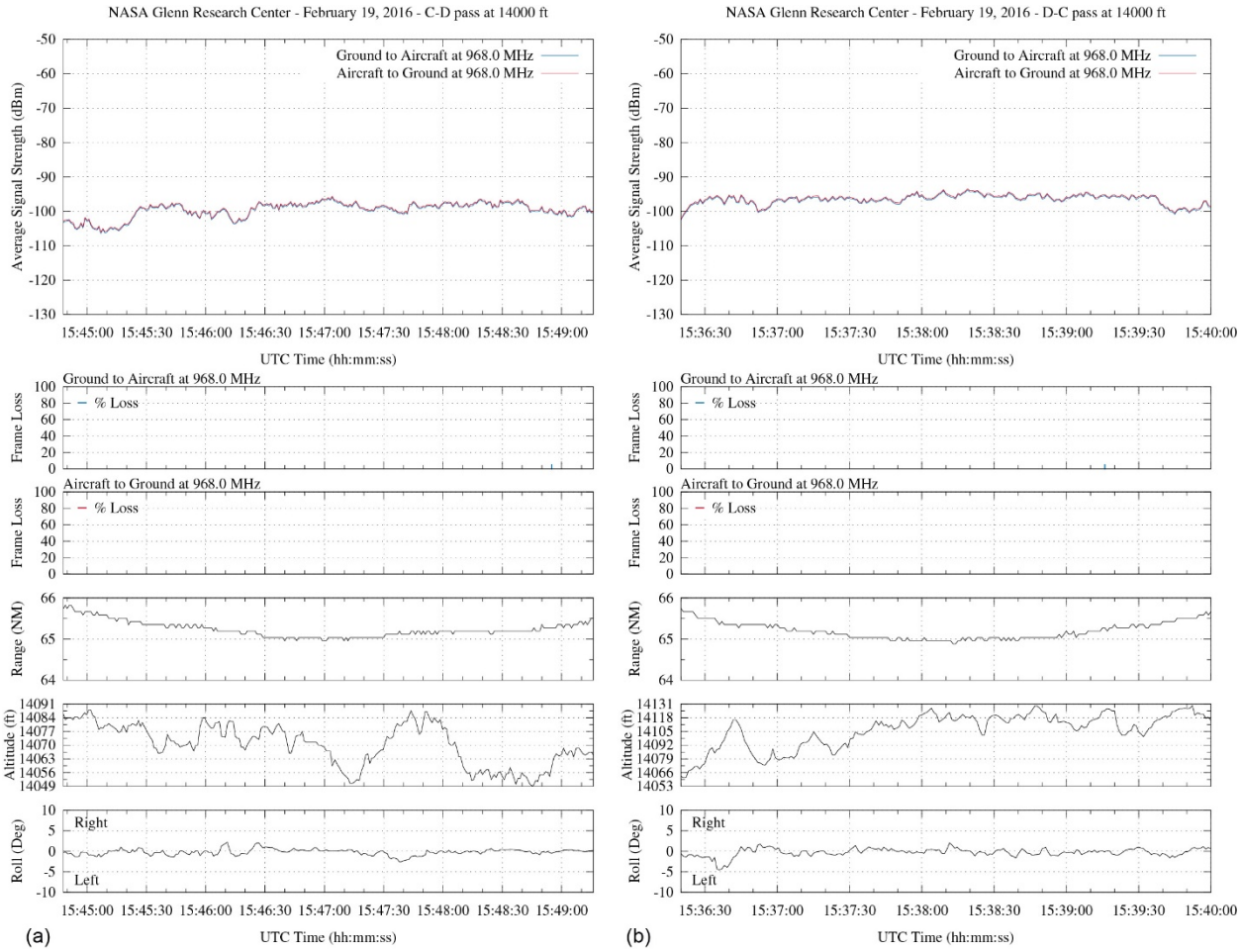

Figure A.16.—L-band signal strength and frame loss over hilly terrain at 65-nmi range and 14,000-ft altitude. (a) Traveling from waypoint C to D. (b) Traveling from waypoint D to C.

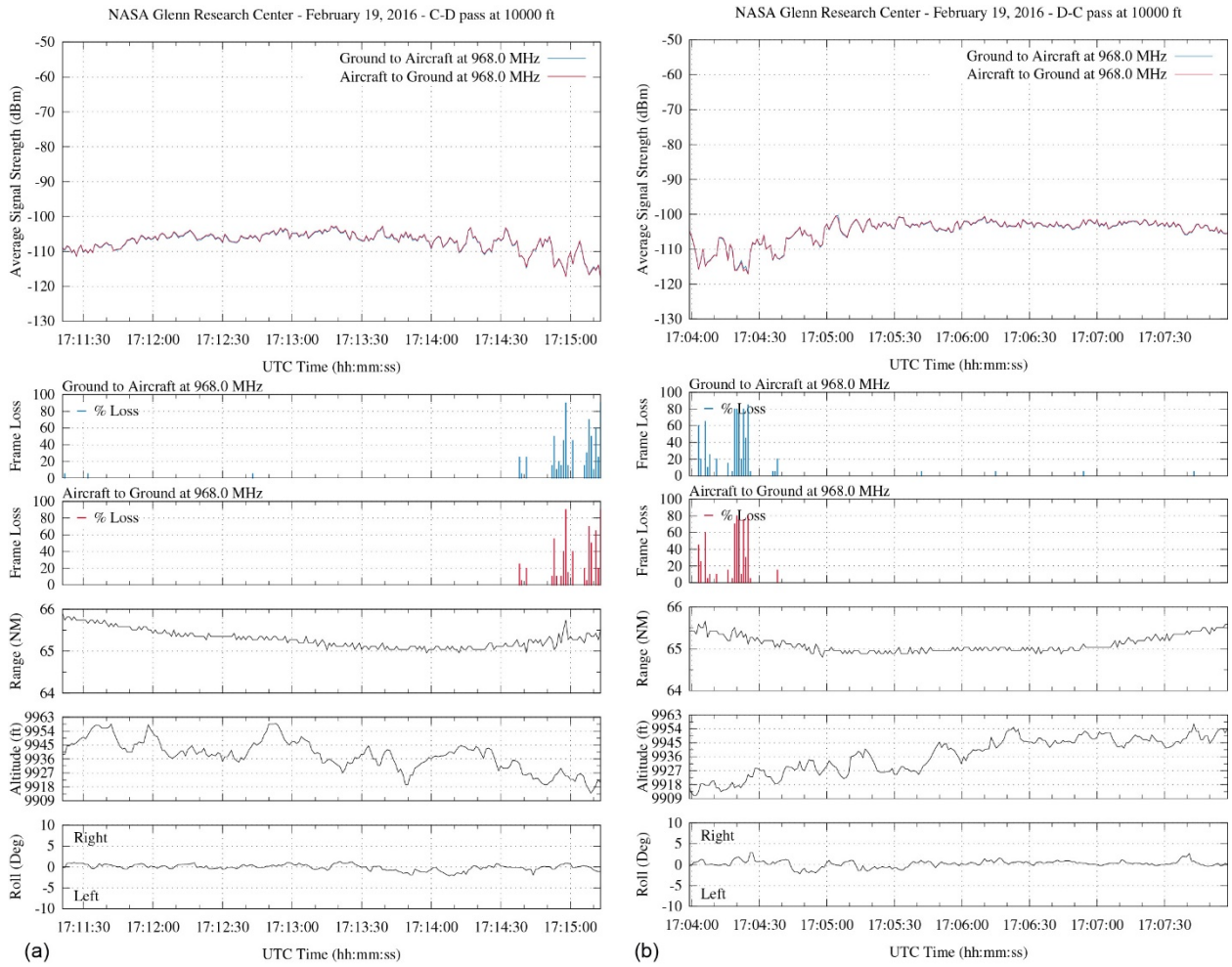

Figure A.17.—L-band signal strength and frame loss over hilly terrain at 65-nmi range and 10,000-ft altitude. (a) Traveling from waypoint C to D. (b) Traveling from waypoint D to C.

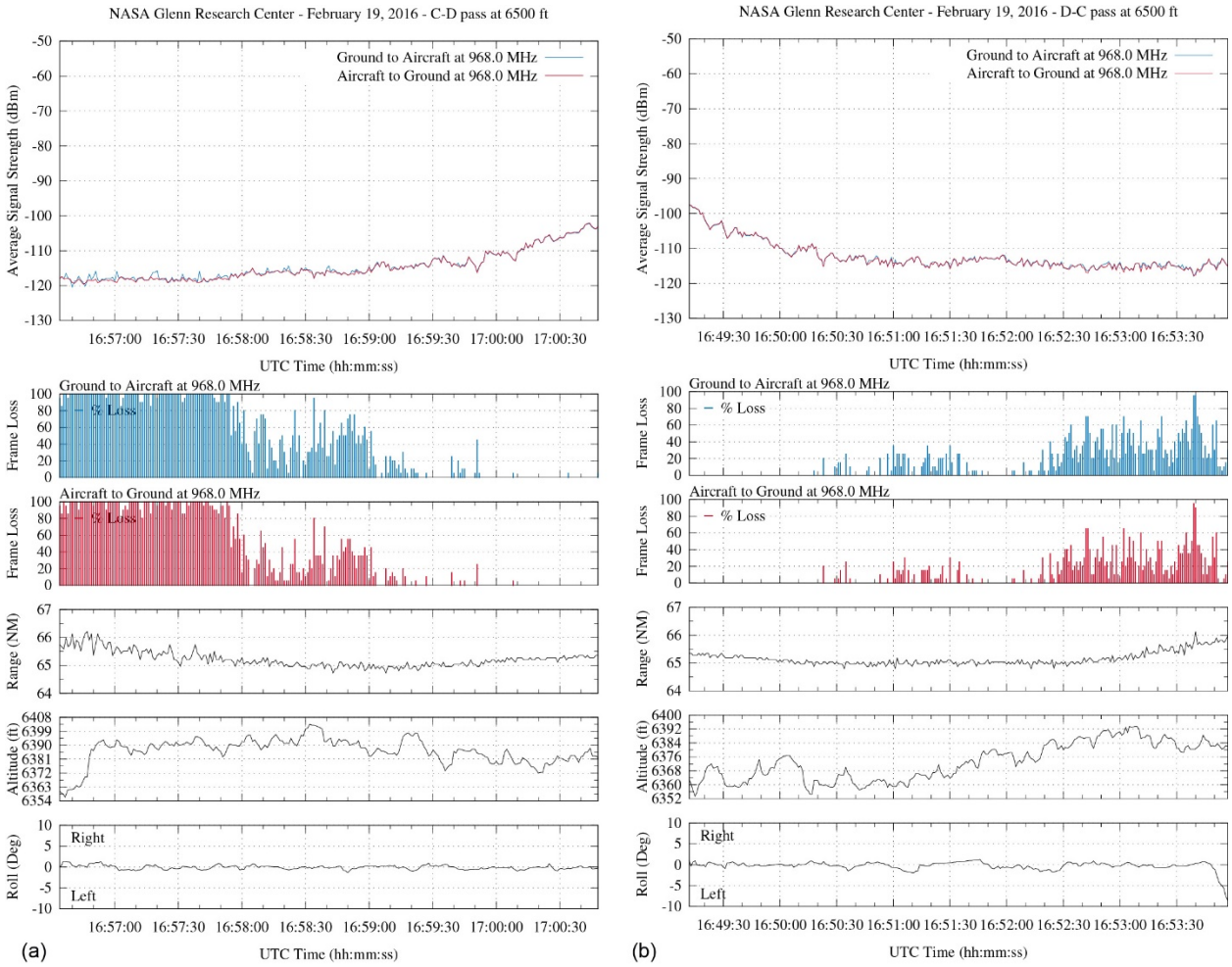

Figure A.18.—L-band signal strength and frame loss over hilly terrain at 65-nmi range and 6500-ft altitude. (a) Traveling from waypoint C to D. (b) Traveling from waypoint D to C.

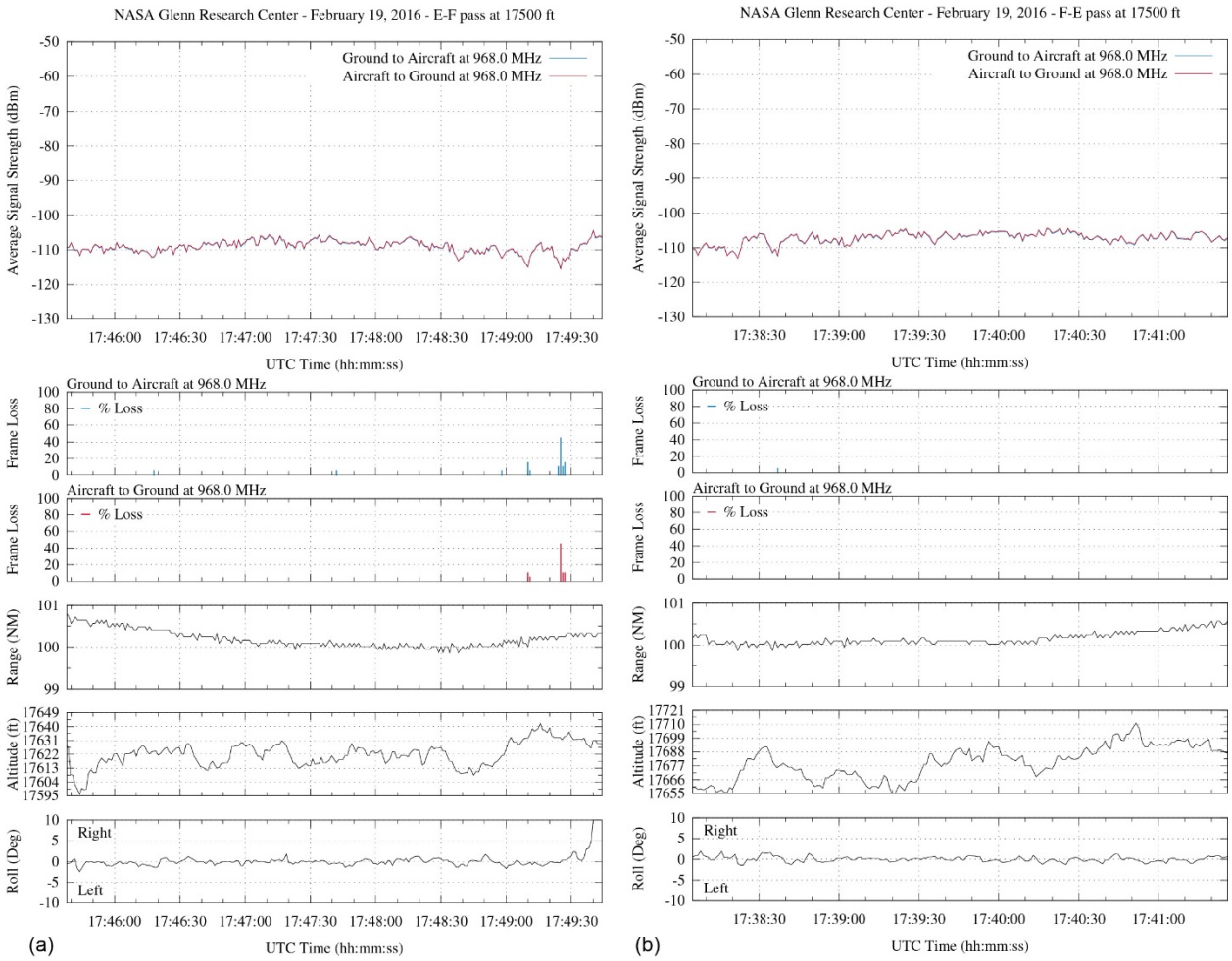

Figure A.19.—L-band signal strength and frame loss over hilly terrain at 100-nmi range and 17,500-ft altitude. (a) Traveling from waypoint E to F. (b) Traveling from waypoint F to E.

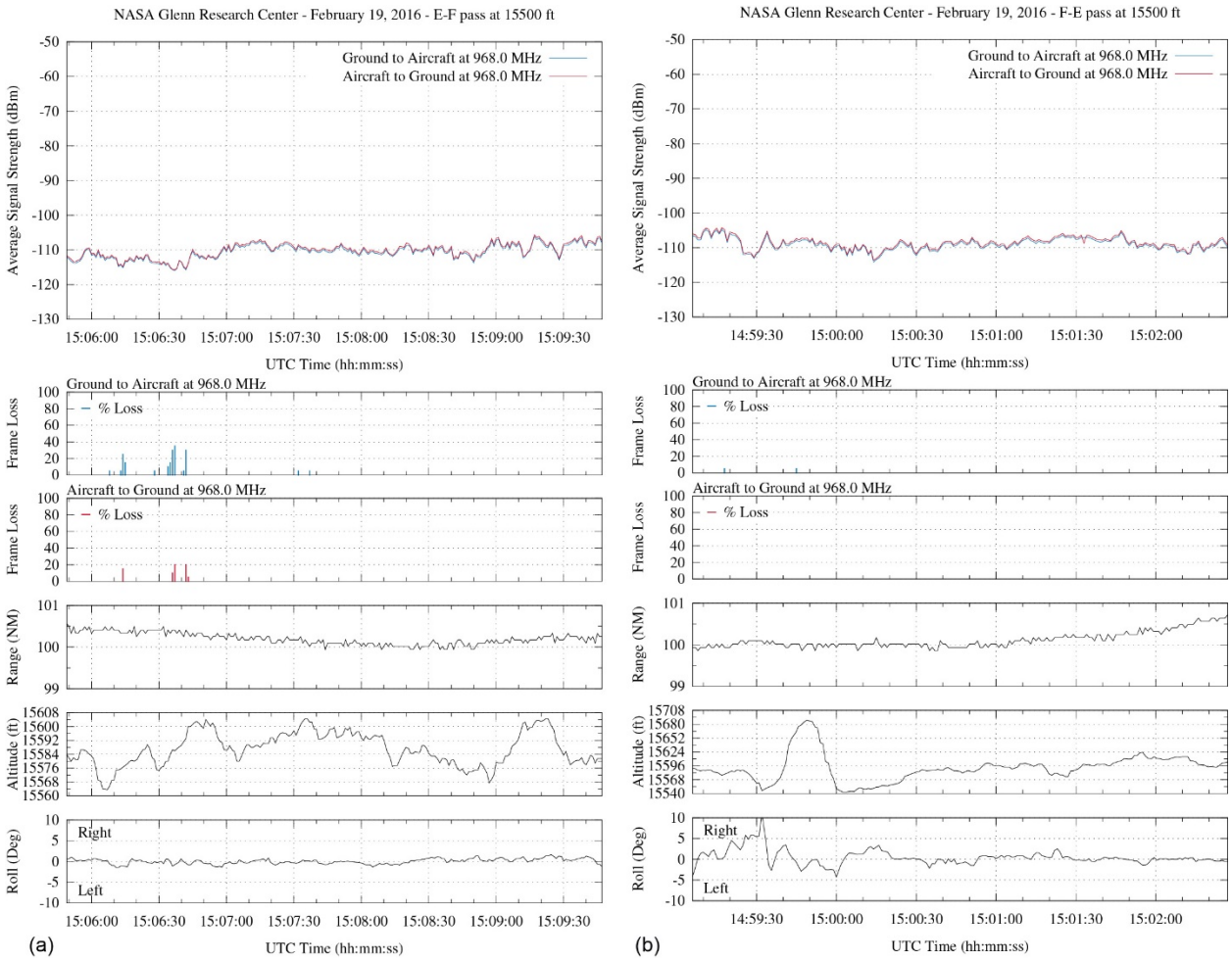

Figure A.20.—L-band signal strength and frame loss over hilly terrain at 100-nmi range and 15,500-ft altitude. (a) Traveling from waypoint E to F. (b) Traveling from waypoint F to E.

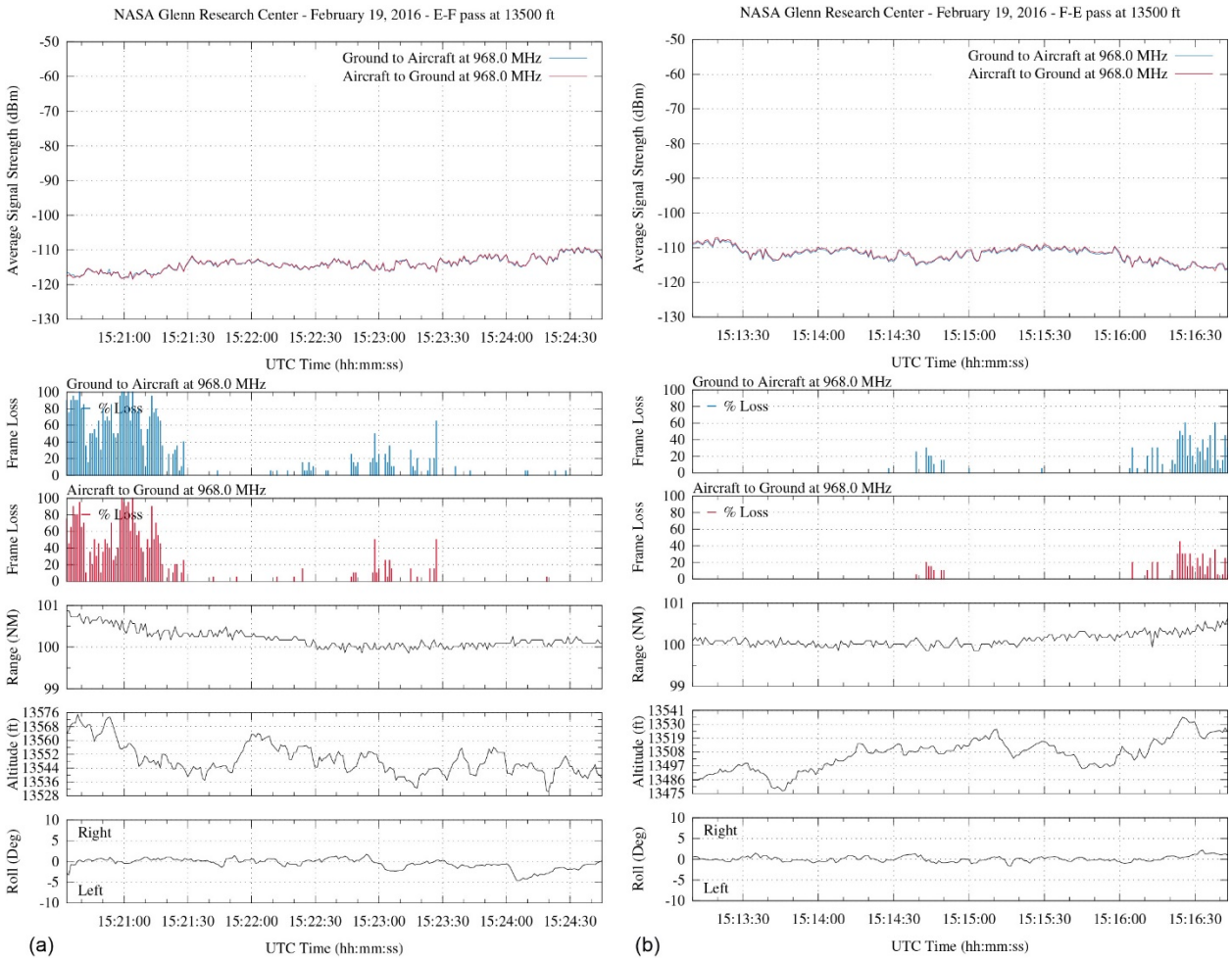

Figure A.21.—L-band signal strength and frame loss over hilly terrain at 100-nmi range and 13,500-ft altitude. (a) Traveling from waypoint E to F. (b) Traveling from waypoint F to E.

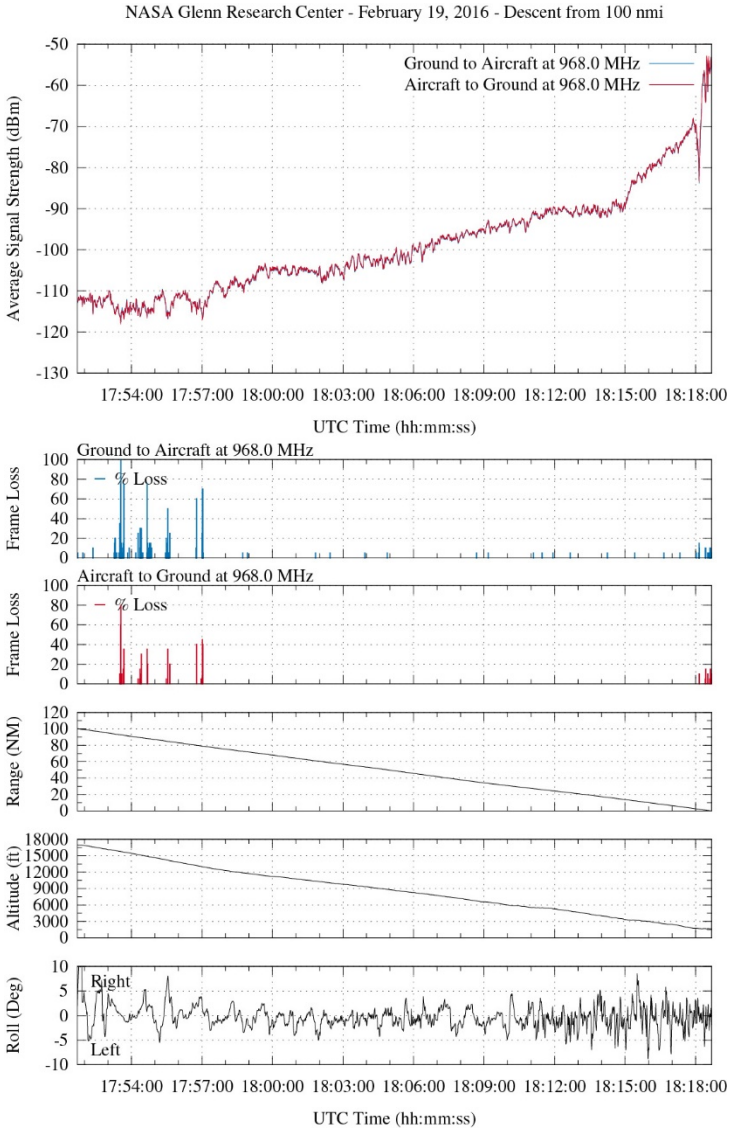

Figure A.22.—L-band signal strength and frame loss over hilly terrain during inbound, descending track from 100-nmi range and 17,000-ft altitude; traveling toward ground station 2 (GS2).

A.2 Test Data for Validation Flight Over Fresh Open Water, March 1 and 3, 2016

C-band validation flight test data over open water are presented in Figures A.23. to A.32., and corresponding L-band flight test data are presented in Figures A.33. to A.41.

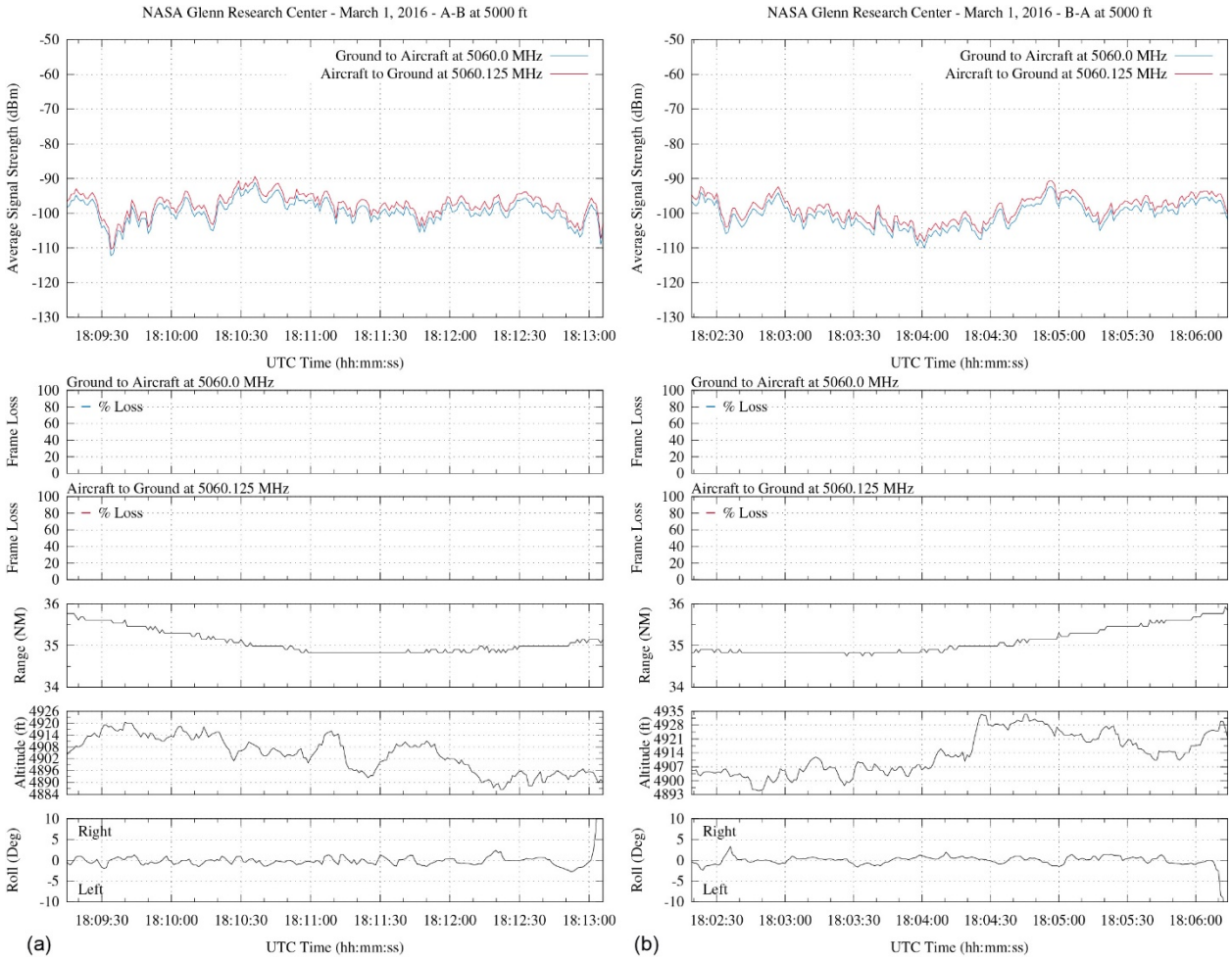

Figure A.23.—C-band signal strength and frame loss over water at 35-nmi range and 5000-ft altitude. (a) Traveling from waypoint A to B. (b) Traveling from waypoint B to A.

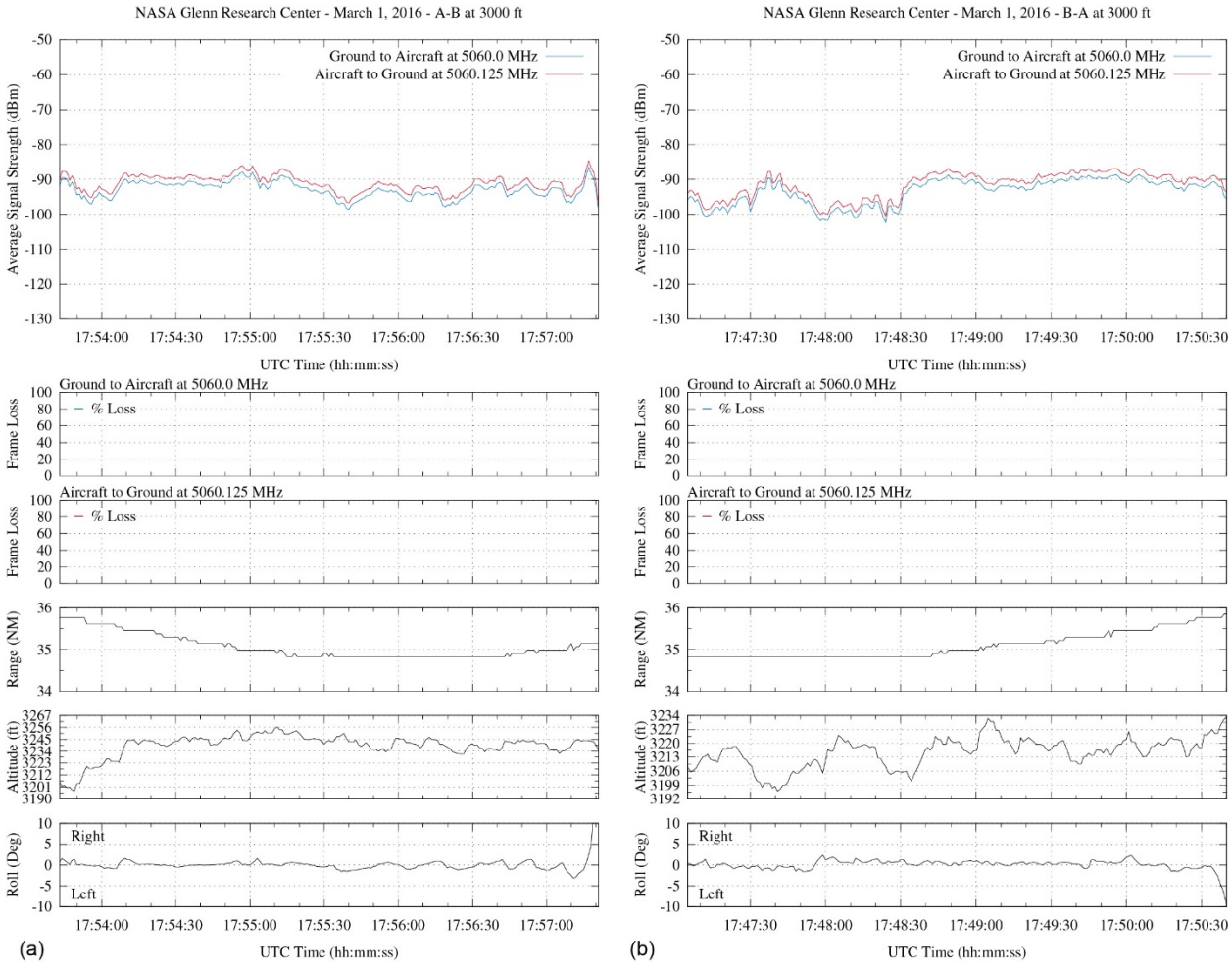

Figure A.24.—C-band signal strength and frame loss over water at 35-nmi range and 3000-ft altitude. (a) Traveling from waypoint A to B. (b) Traveling from waypoint B to A.

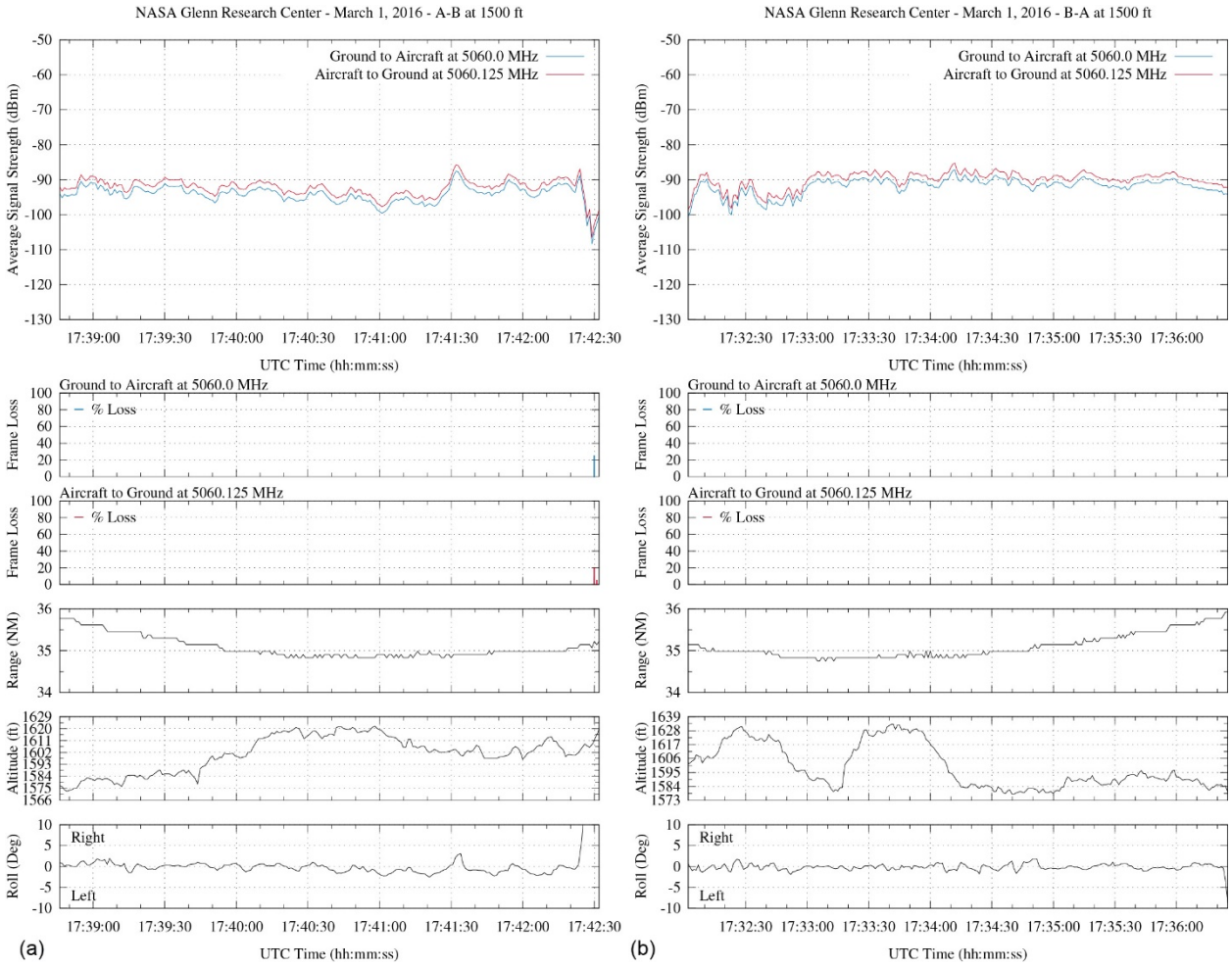

Figure A.25.—C-band signal strength and frame loss over water at 35-nmi range and 1500-ft altitude. (a) Traveling from waypoint A to B. (b) Traveling from waypoint B to A.

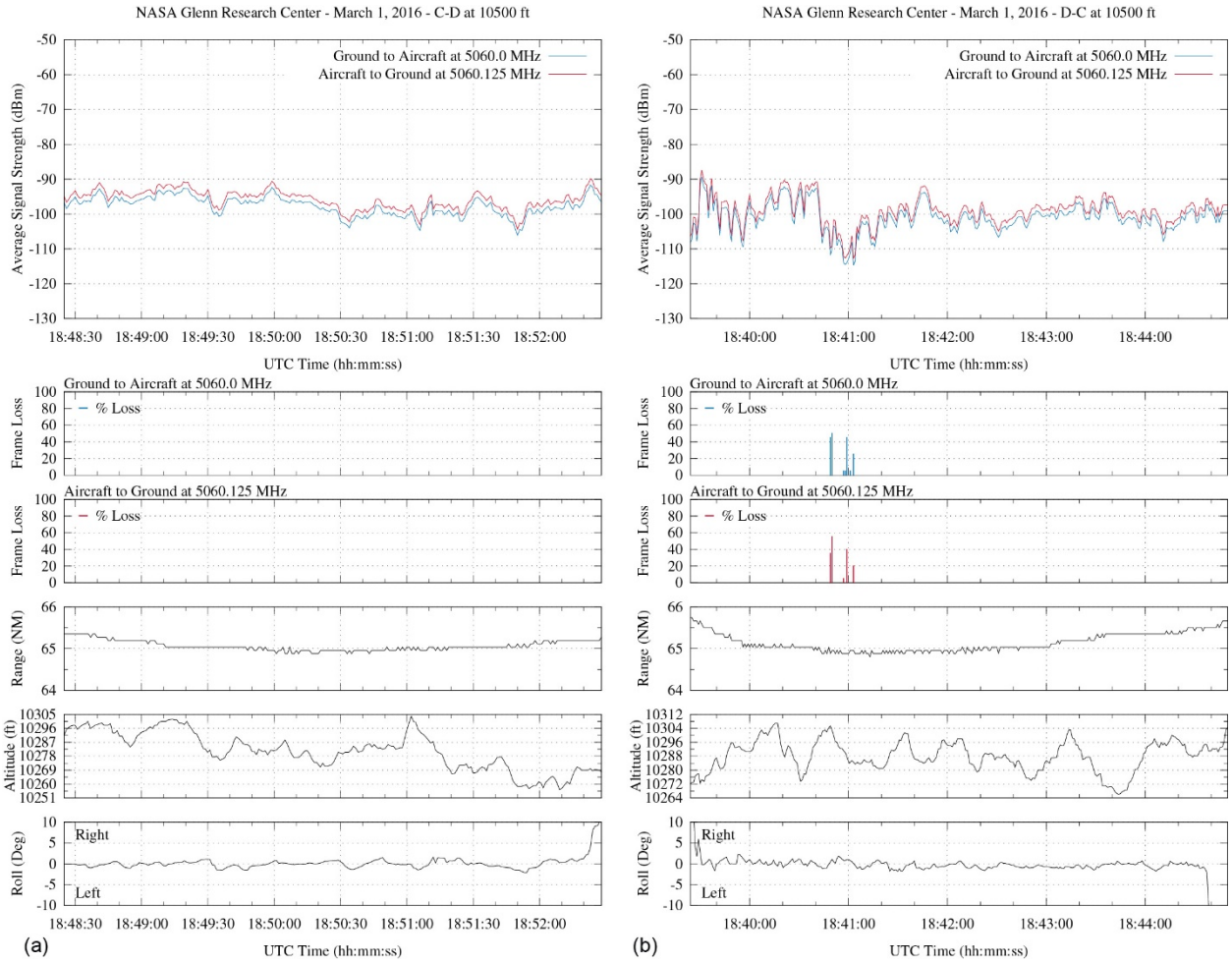

Figure A.26.—C-band signal strength and frame loss over water at 65-nmi range and 10,500-ft altitude. (a) Traveling from waypoint C to D. (b) Traveling from waypoint D to C.

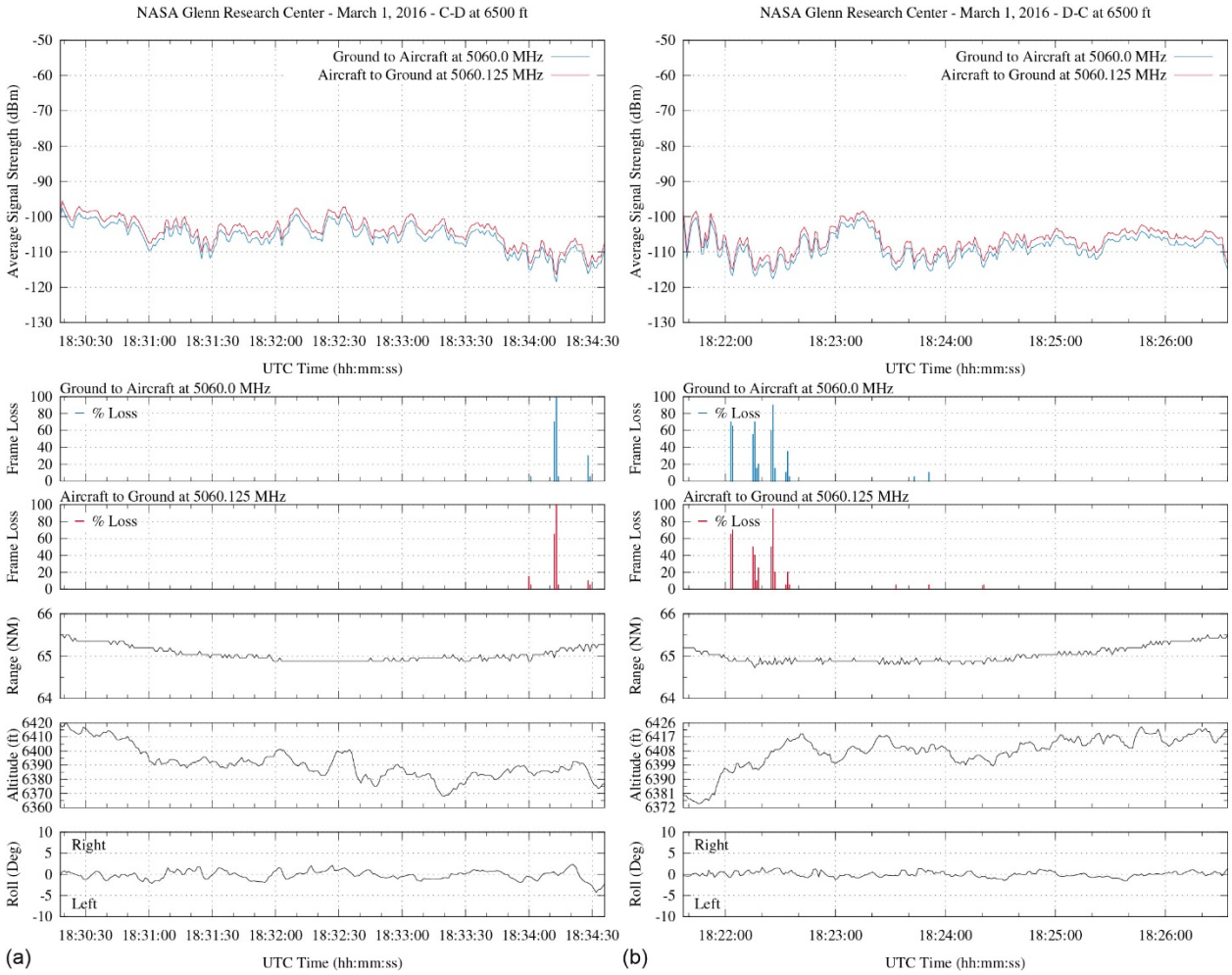

Figure A.27.—C-band signal strength and frame loss over water at 65-nmi range and 6500-ft altitude. (a) Traveling from waypoint C to D. (b) Traveling from waypoint D to C.

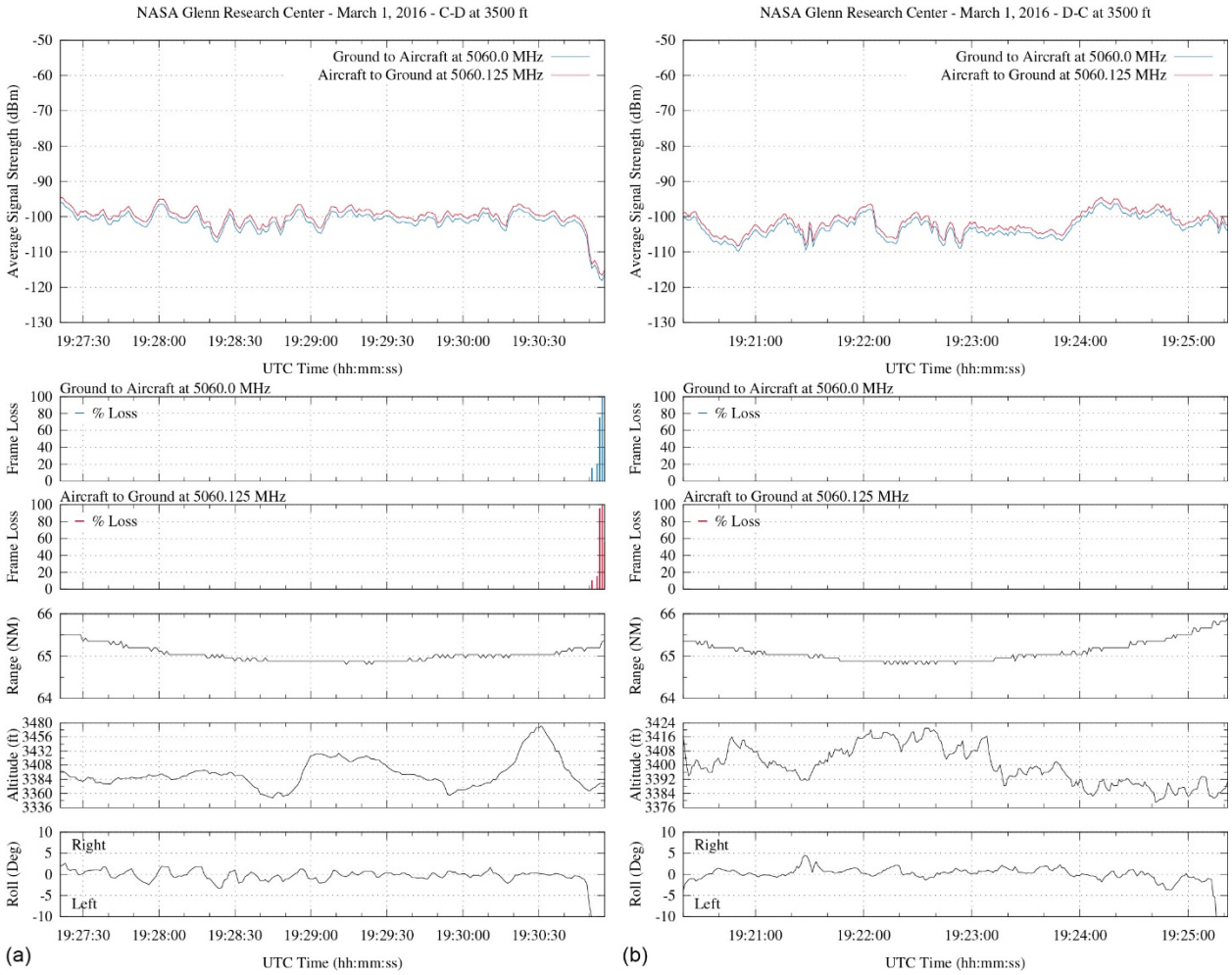

Figure A.28.—C-band signal strength and frame loss over water at 65-nmi range and 3500-ft altitude. (a) Traveling from waypoint C to D. (b) Traveling from waypoint D to C.

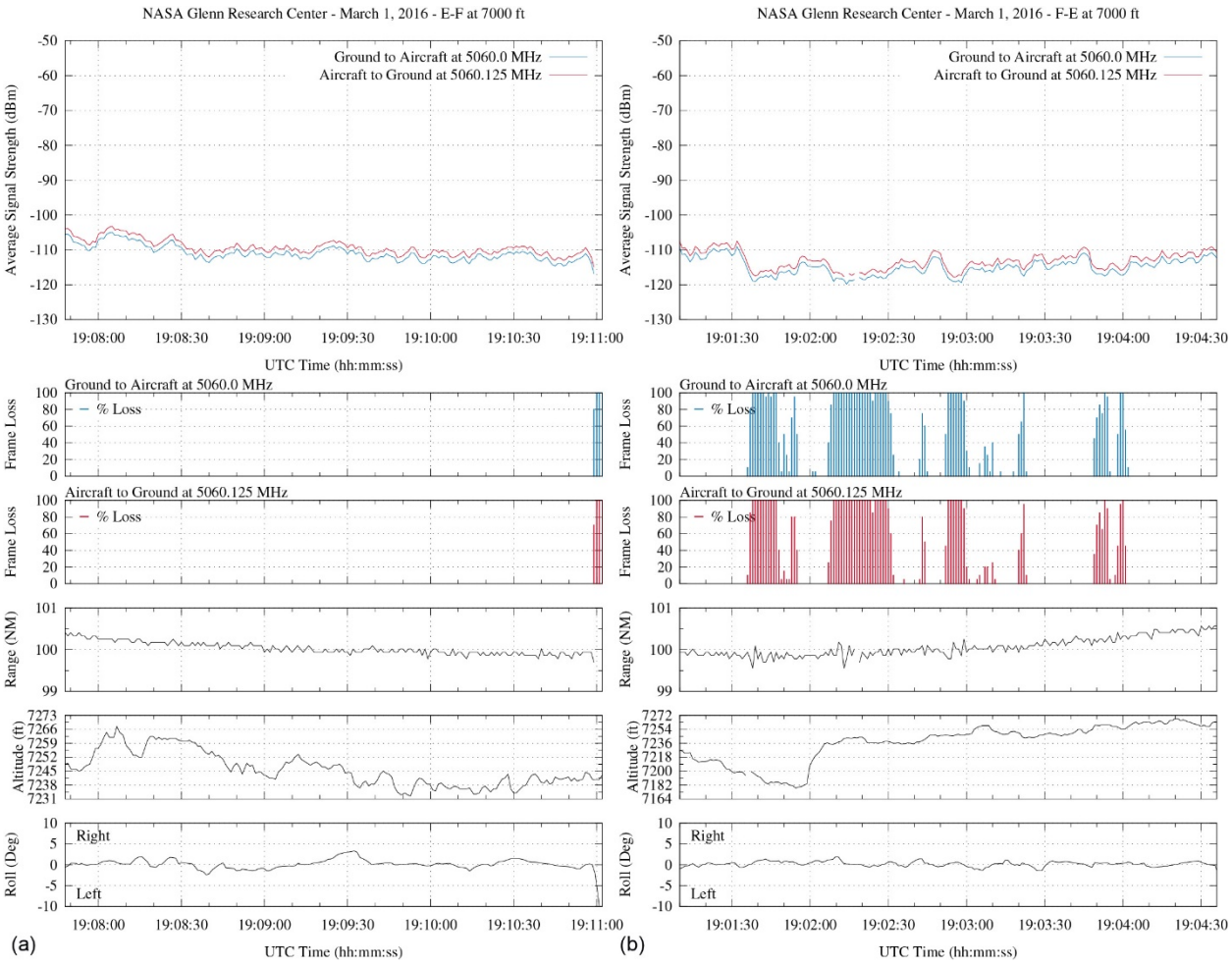

Figure A.29.—C-band signal strength and frame loss over water at 100-nmi range and 7000-ft altitude. (a) Traveling from waypoint E to F. (b) Traveling from waypoint F to E.

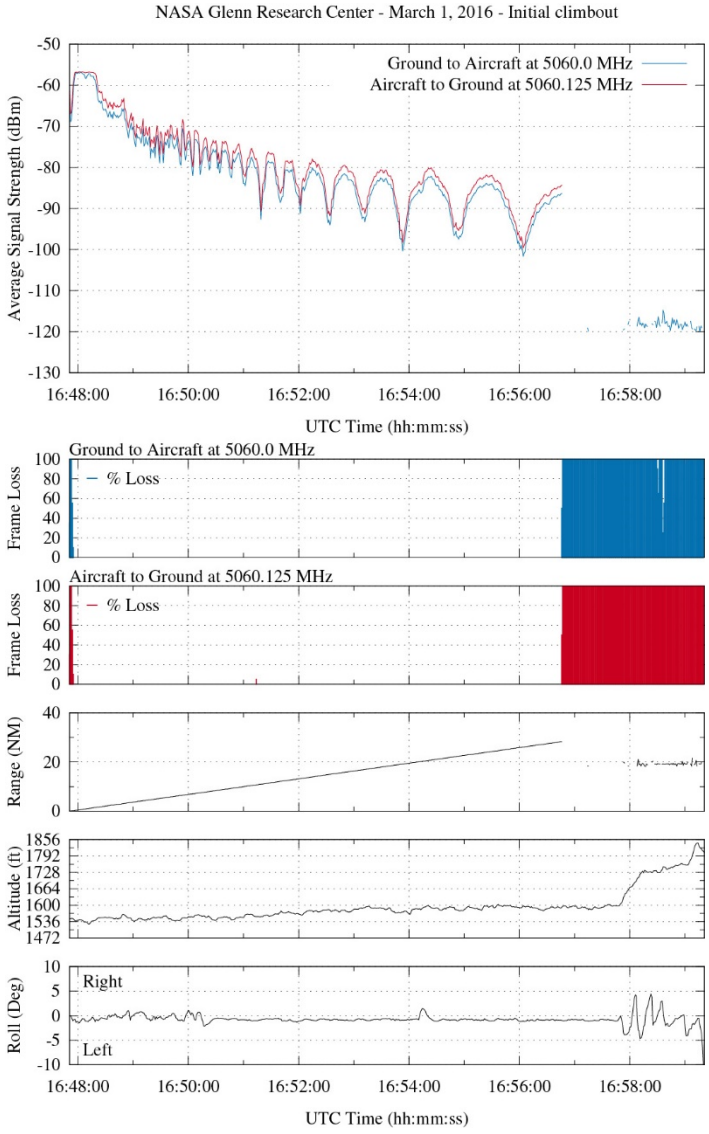

Figure A.30.—C-band signal strength and frame loss over water during outbound track traveling from ground station 3 (GS3) to 40-nmi range at 1500-ft altitude.

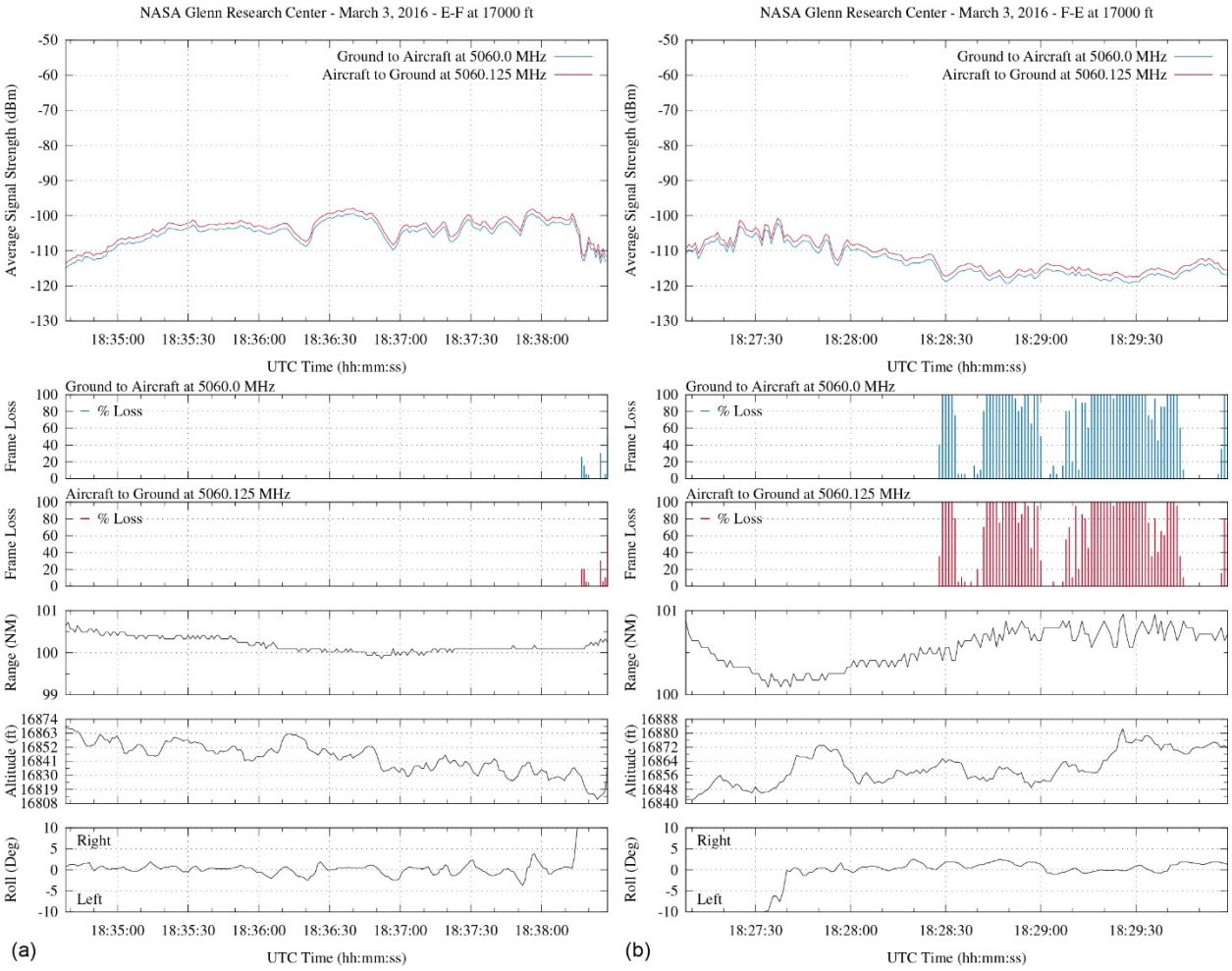

Figure A.31.—C-band signal strength and frame loss over water at 100-nmi range and 17,000-ft altitude. (a) Traveling from waypoint E to F. (b) Traveling from waypoint F to E.

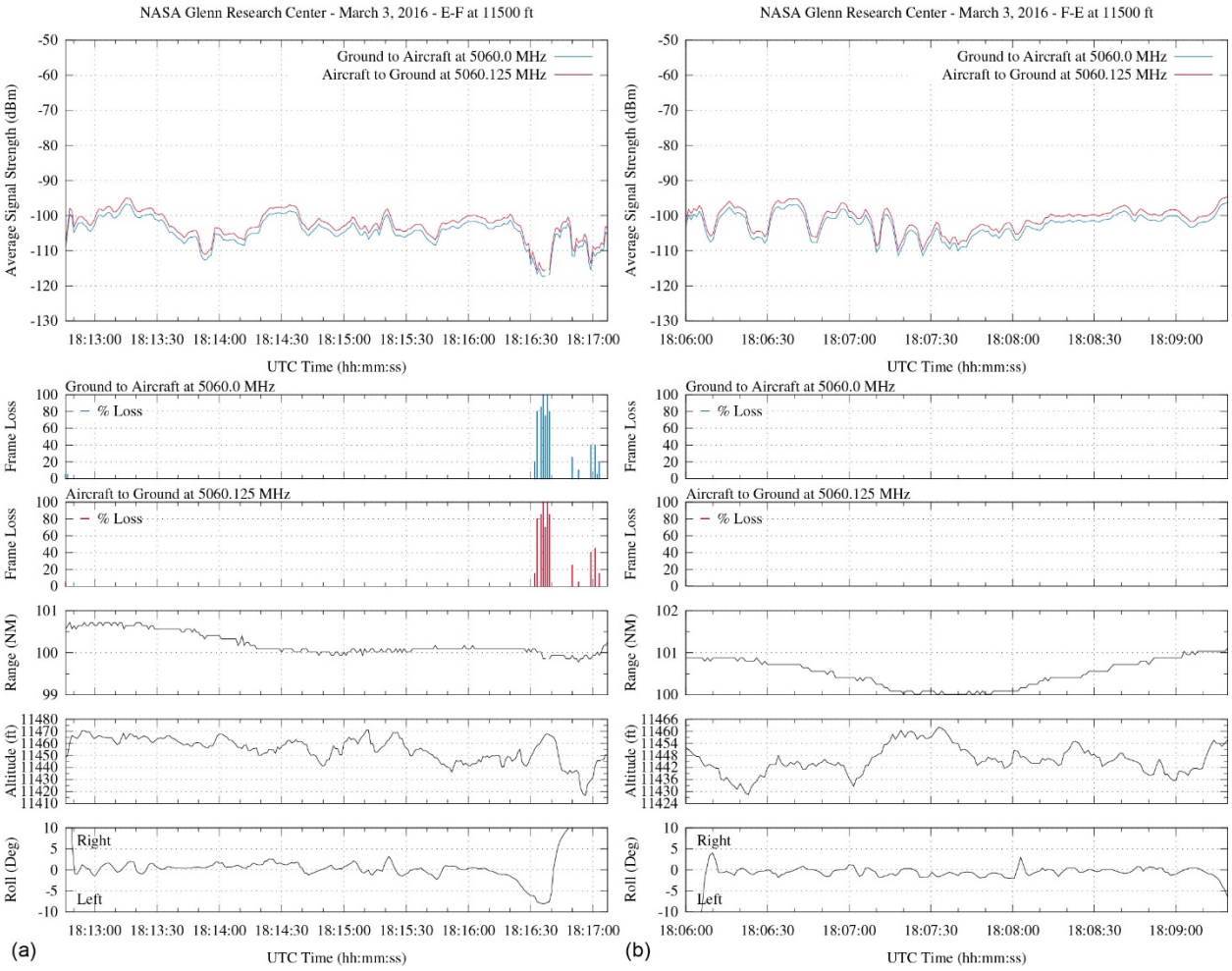

Figure A.32.—C-band signal strength and frame loss over water at 100-nmi range and 11,500-ft altitude. (a) Traveling from waypoint E to F. (b) Traveling from waypoint F to E.

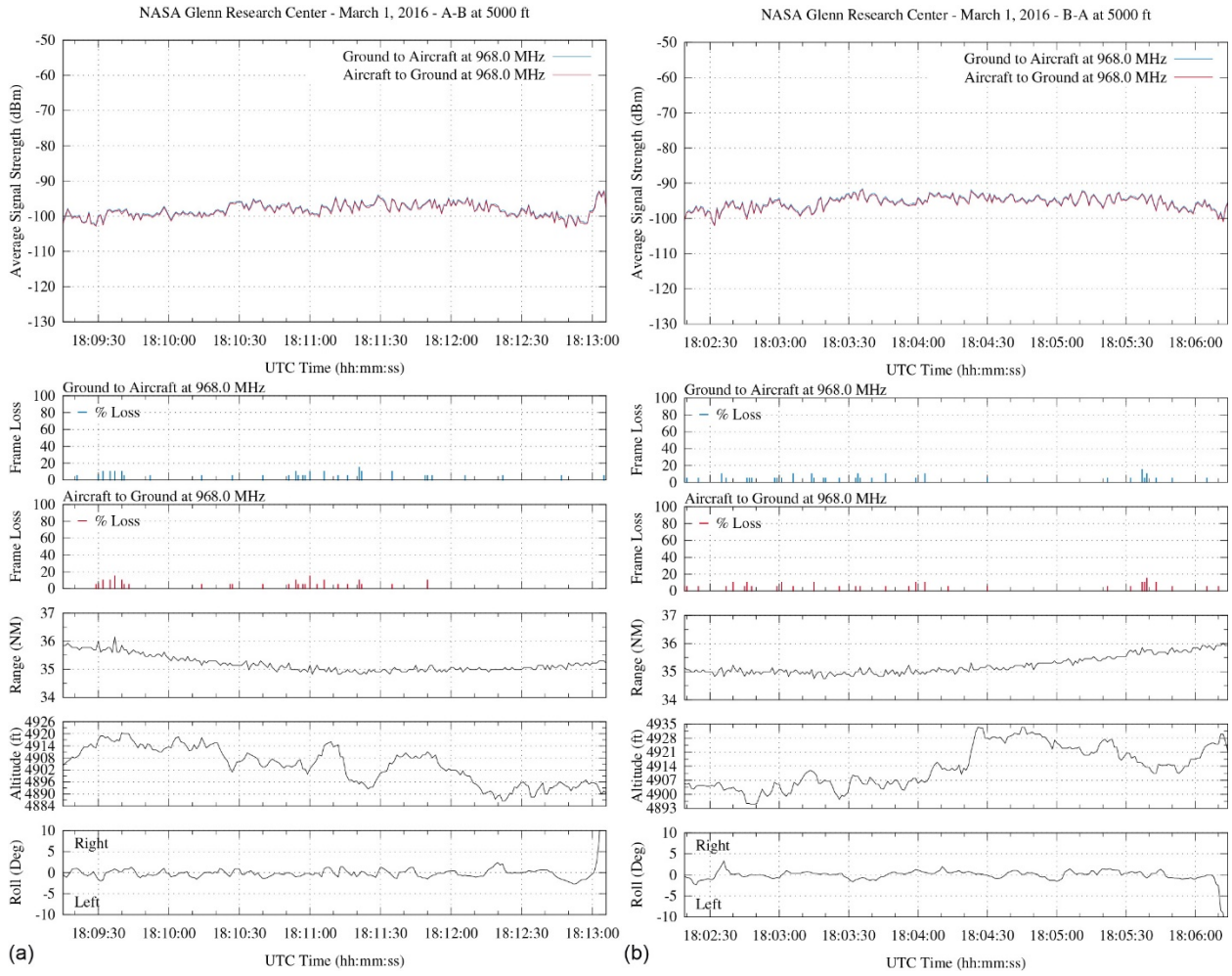

Figure A.33.—L-band signal strength and frame loss over water at 35-nmi range and 5000-ft altitude. (a) Traveling from waypoint A to B. (b) Traveling from waypoint B to A.

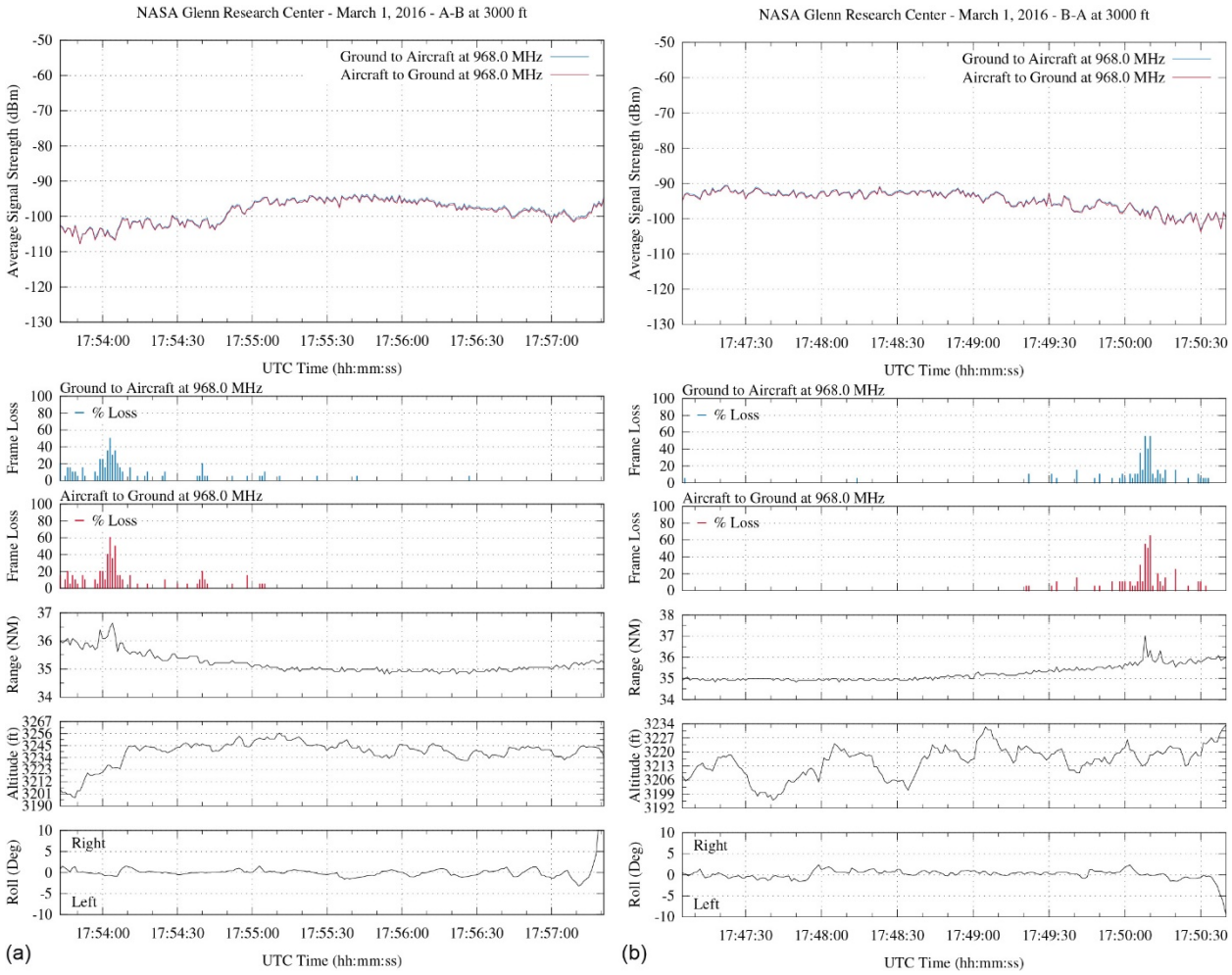

Figure A.34.—L-band signal strength and frame loss over water at 35-nmi range and 3000-ft altitude. (a) Traveling from waypoint A to B. (b) Traveling from waypoint B to A.

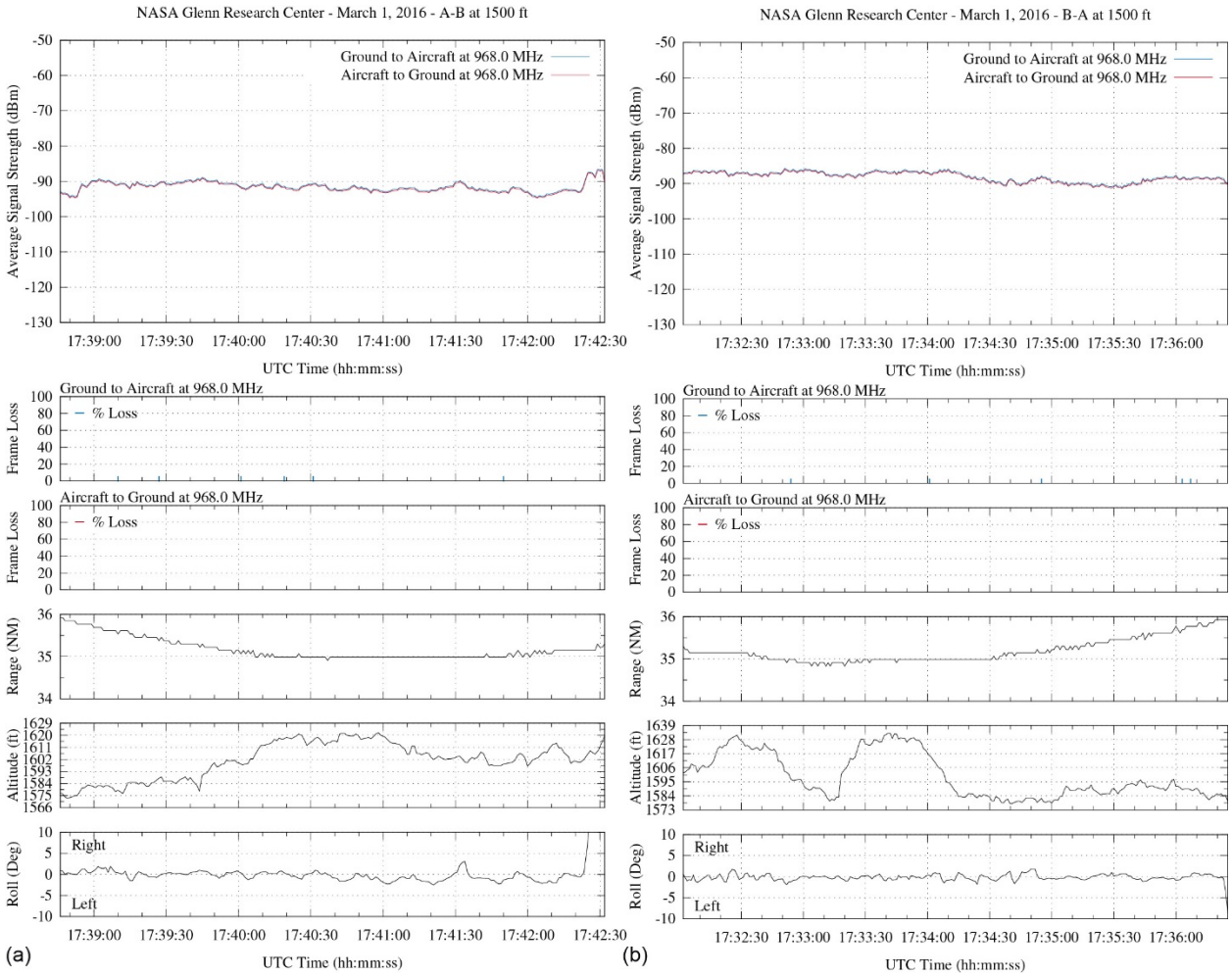

Figure A.35.—L-band signal strength and frame loss over water at 35-nmi range and 1500-ft altitude. (a) Traveling from waypoint A to B. (b) Traveling from waypoint B to A.

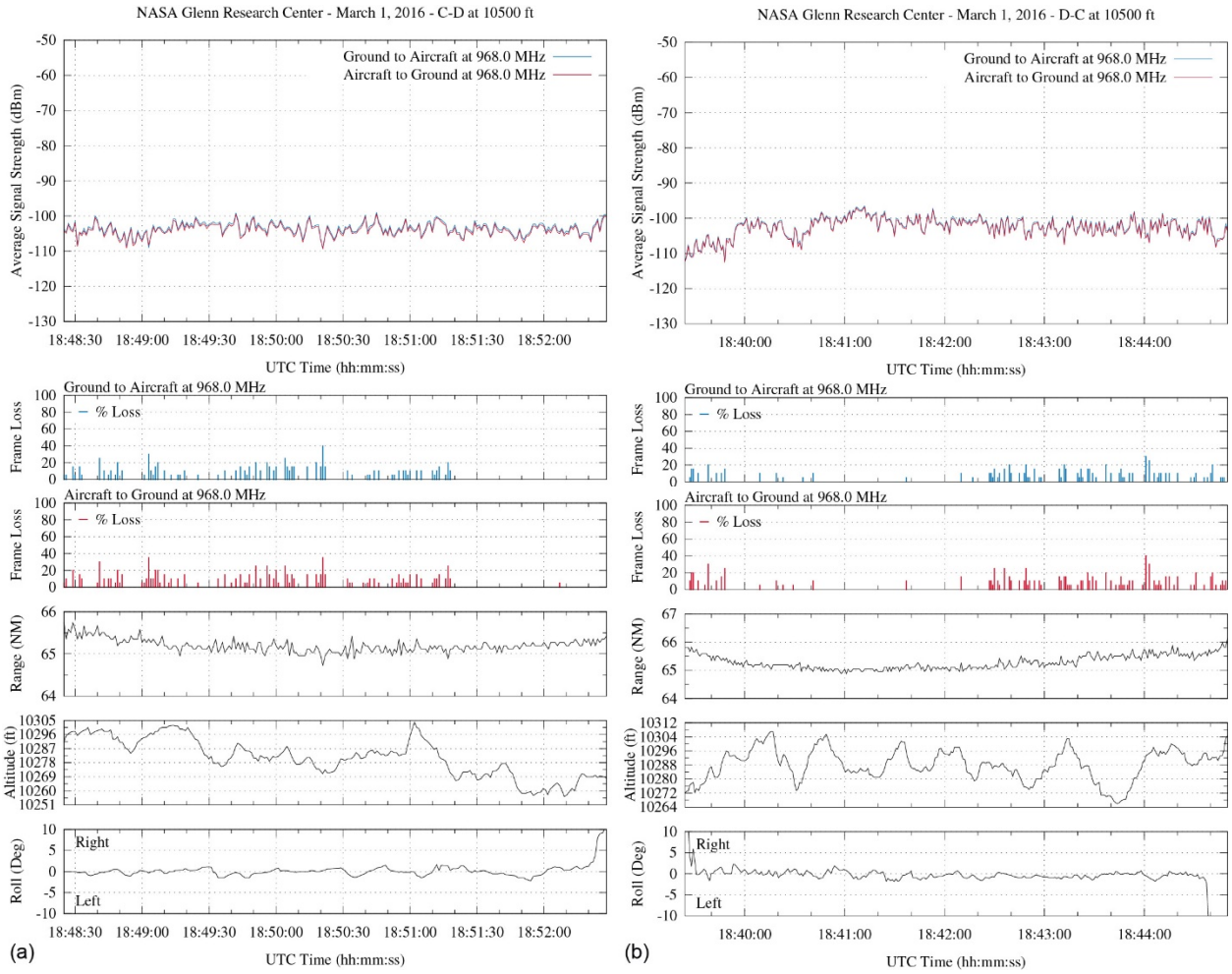

Figure A.36.—L-band signal strength and frame loss over water at 65-nmi range and 10,500-ft altitude. (a) Traveling from waypoint C to D. (b) Traveling from waypoint D to C.

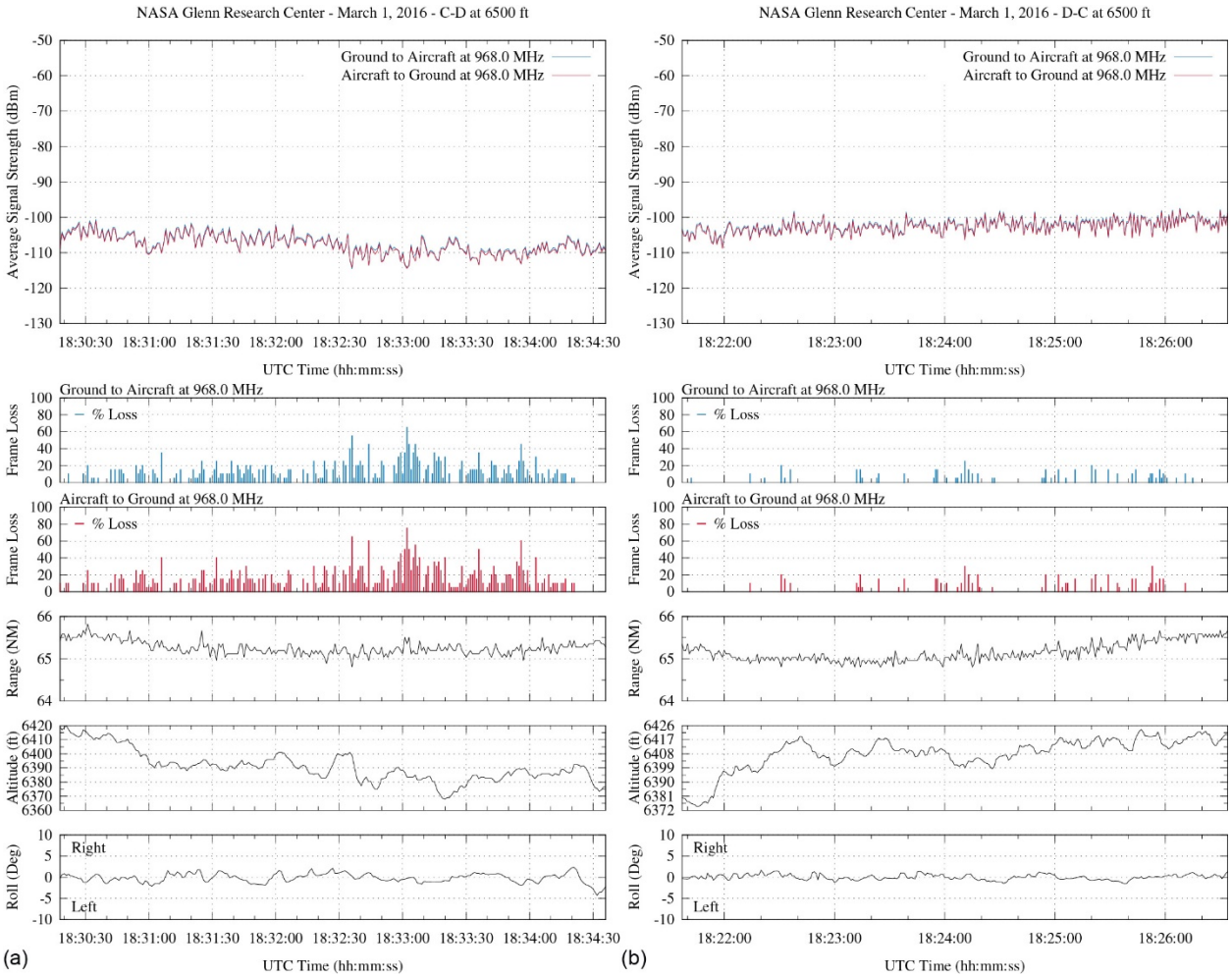

Figure A.37.—L-band signal strength and frame loss over water at 65-nmi range and 6500-ft altitude. (a) Traveling from waypoint C to D. (b) Traveling from waypoint D to C.

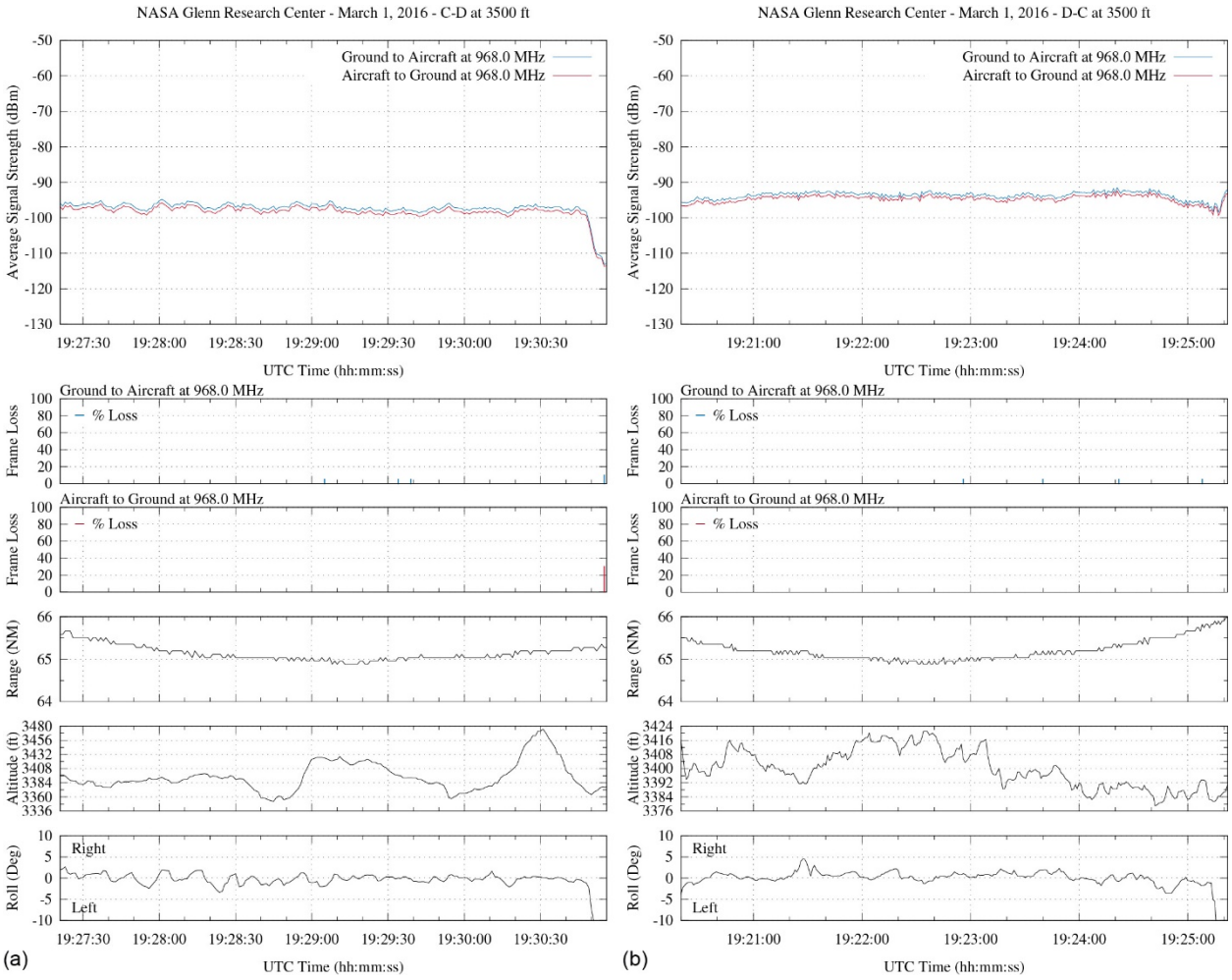

Figure A.38.—L-band signal strength and frame loss over water at 65-nmi range and 3500-ft altitude. (a) Traveling from waypoint C to D. (b) Traveling from waypoint D to C.

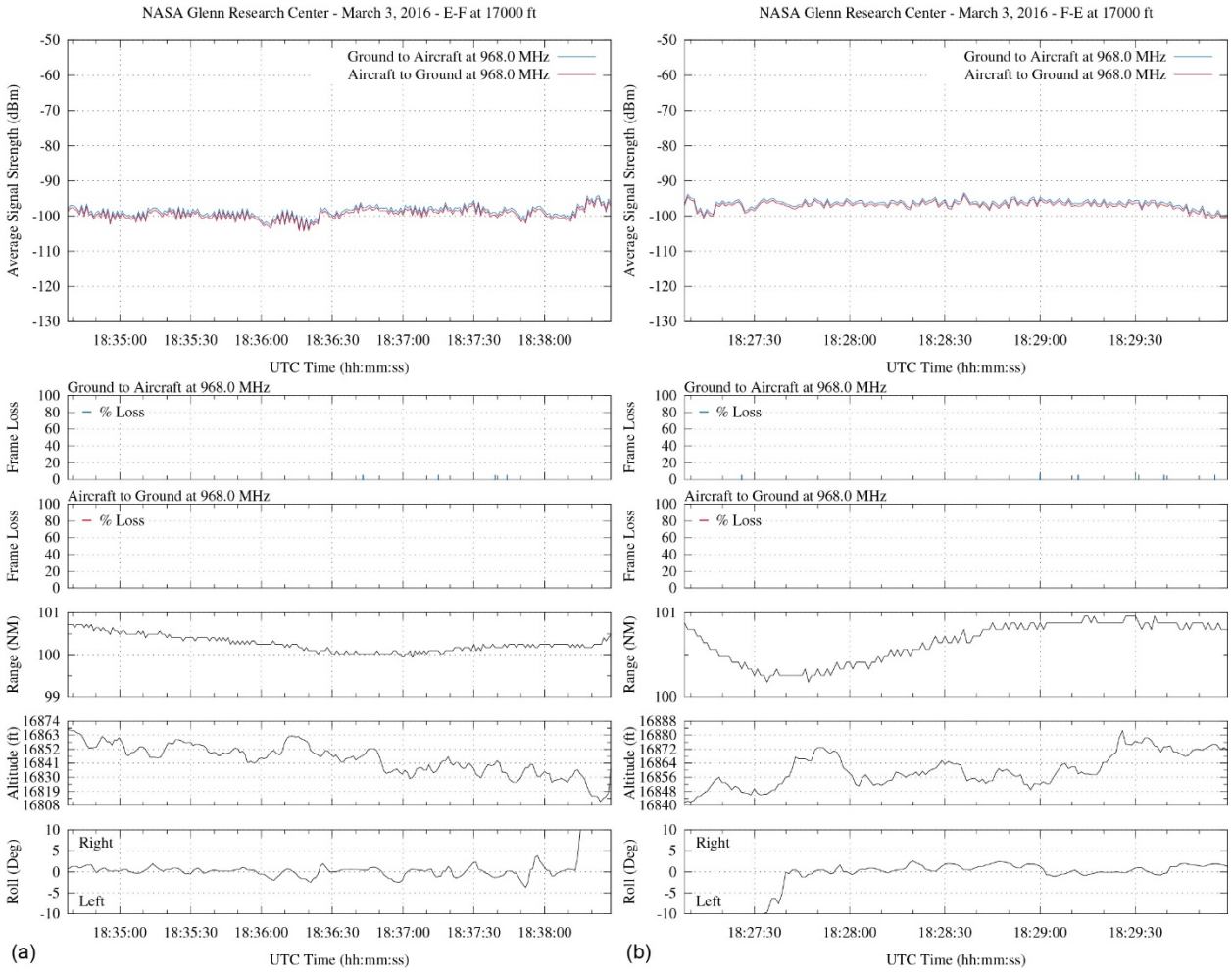

Figure A.39.—L-band signal strength and frame loss over water at 100-nmi range and 17,000-ft altitude. (a) Traveling from waypoint E to F. (b) Traveling from waypoint F to E.

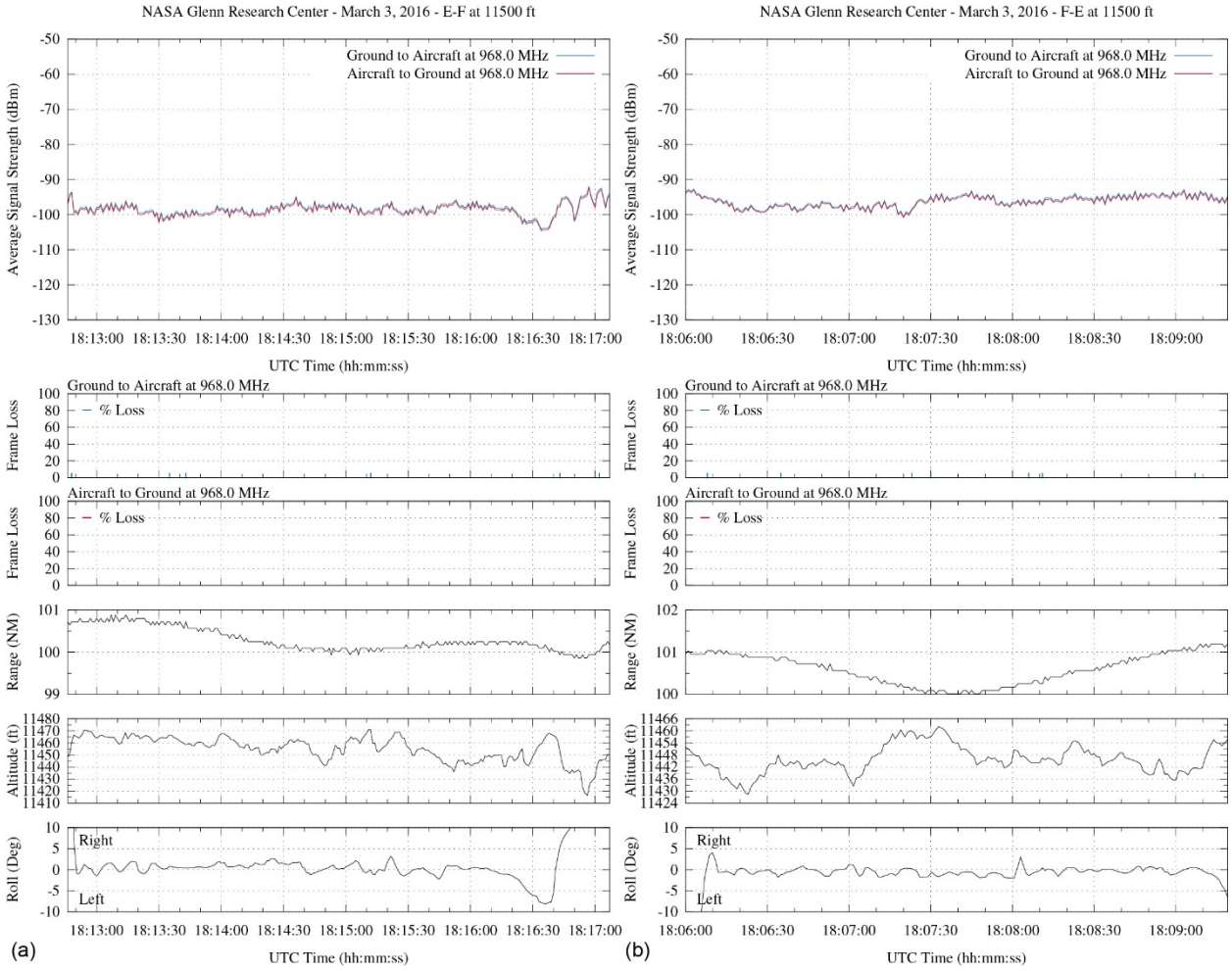

Figure A.40.—L-band signal strength and frame loss over water at 100-nmi range and 11,500-ft altitude. (a) Traveling from waypoint E to F. (b) Traveling from waypoint F to E.

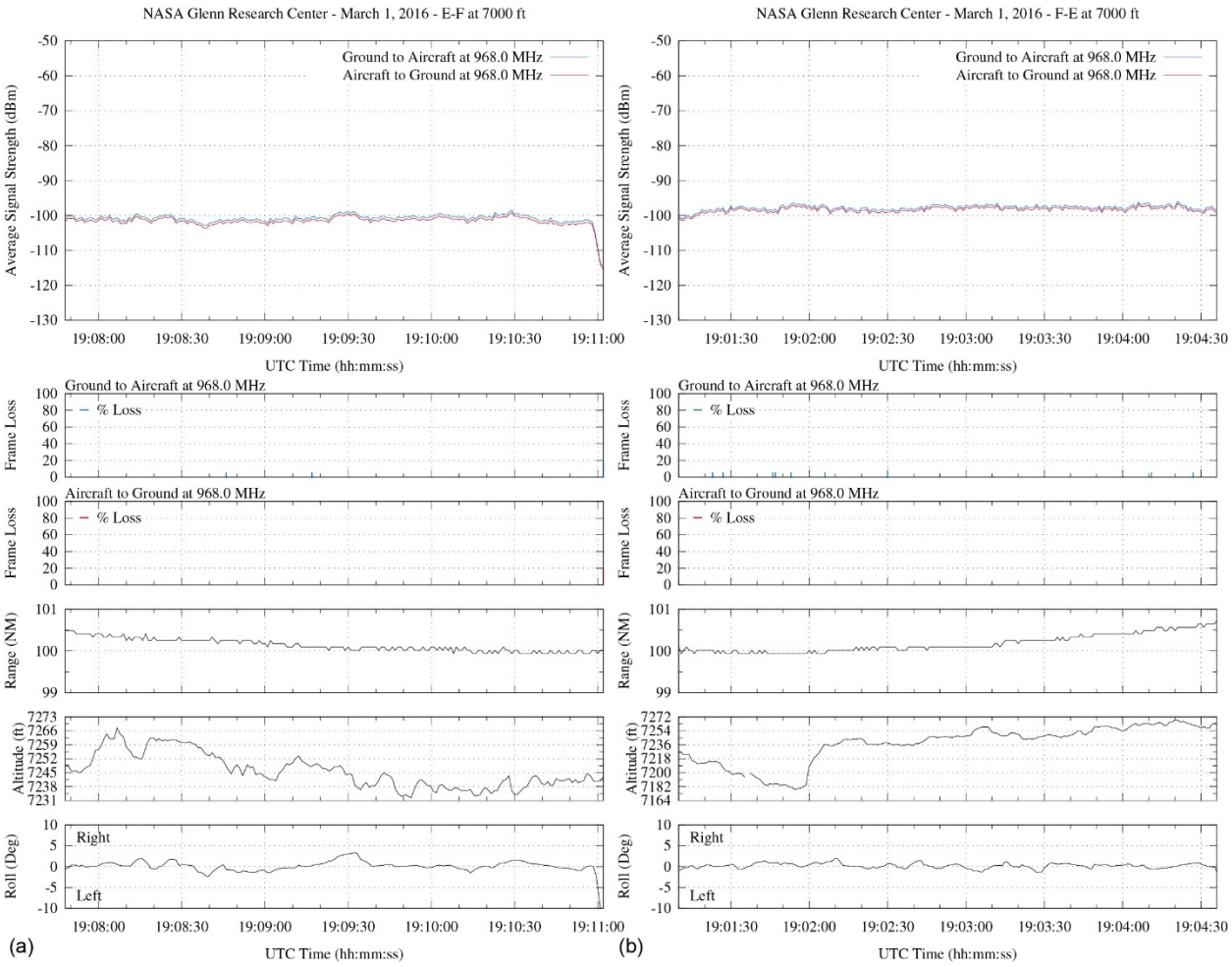

Figure A.41.—L-band signal strength and frame loss over water at 100-nmi range and 7000-ft altitude. (a) Traveling from waypoint E to F. (b) Traveling from waypoint F to E.

A.3 Test Data for Validation Flight During Standard Airport Departure and Ascent, March 7, 2016

C-band validation flight test data during airfield departure are presented in Figure A.42., and corresponding L-band flight test data are presented in Figure A.43.

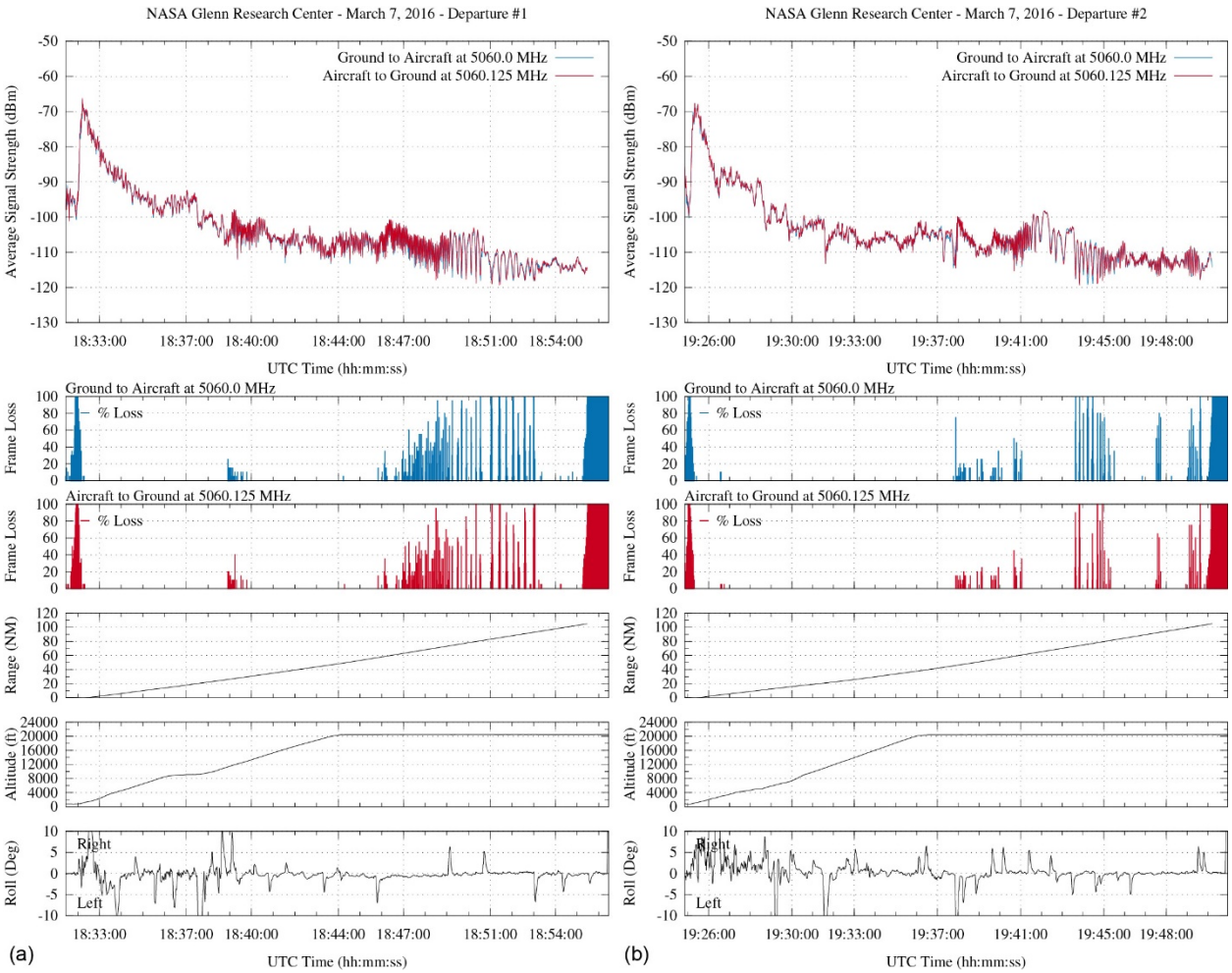

Figure A.42.—C-band signal strength and frame loss. (a) During controlled airfield standard departure 1. (b) During controlled airfield standard departure 2.

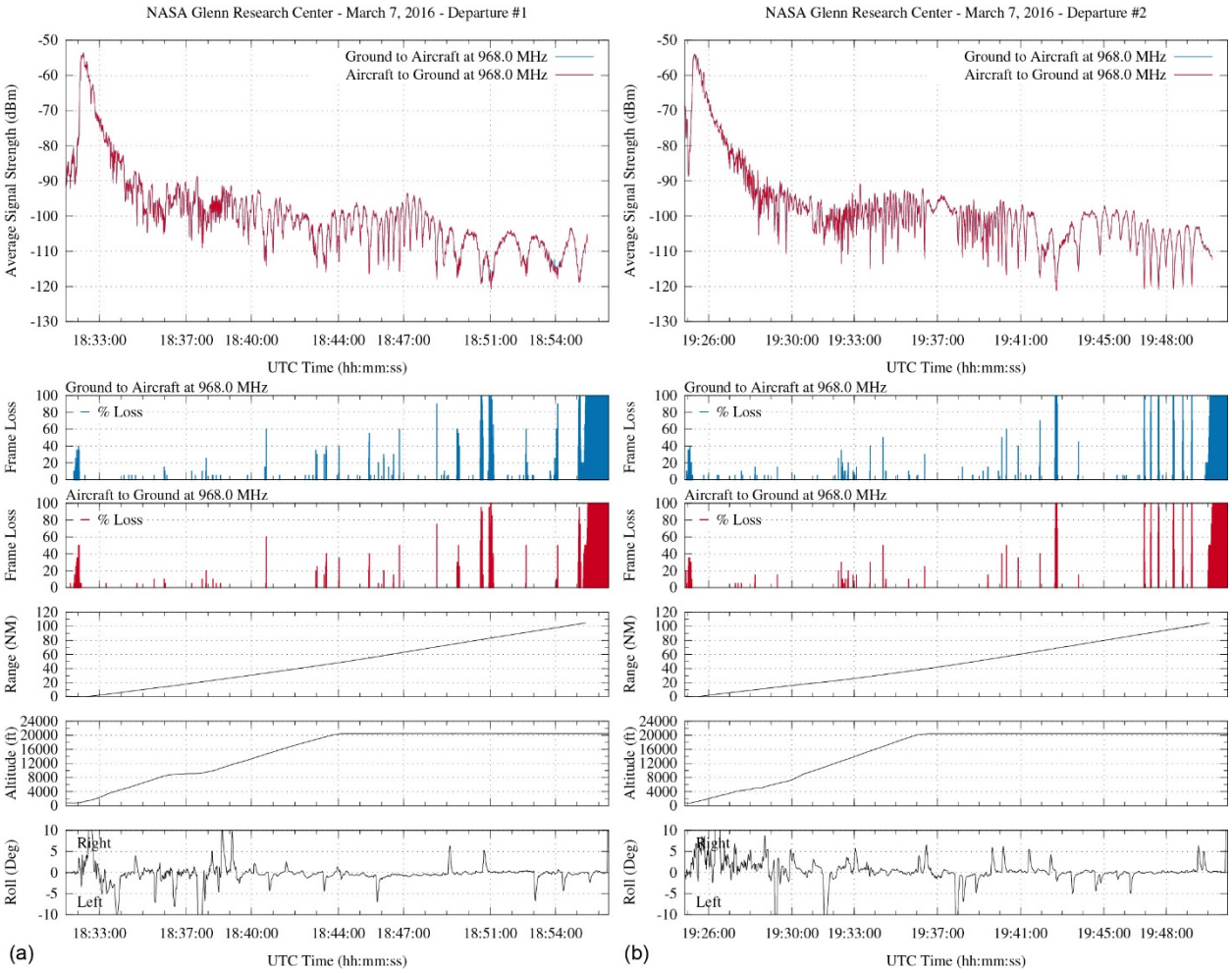

Figure A.43.—L-band signal strength and frame loss. (a) During controlled airfield standard departure 1. (b) During controlled airfield standard departure 2.

A.4 Test Data for Reduced-Power Flight Range Demonstration, April 28, 2016

L-band demonstration flight test data at the 10-mW output power level, over hilly terrain, are presented in Figures A.44. to A.48.

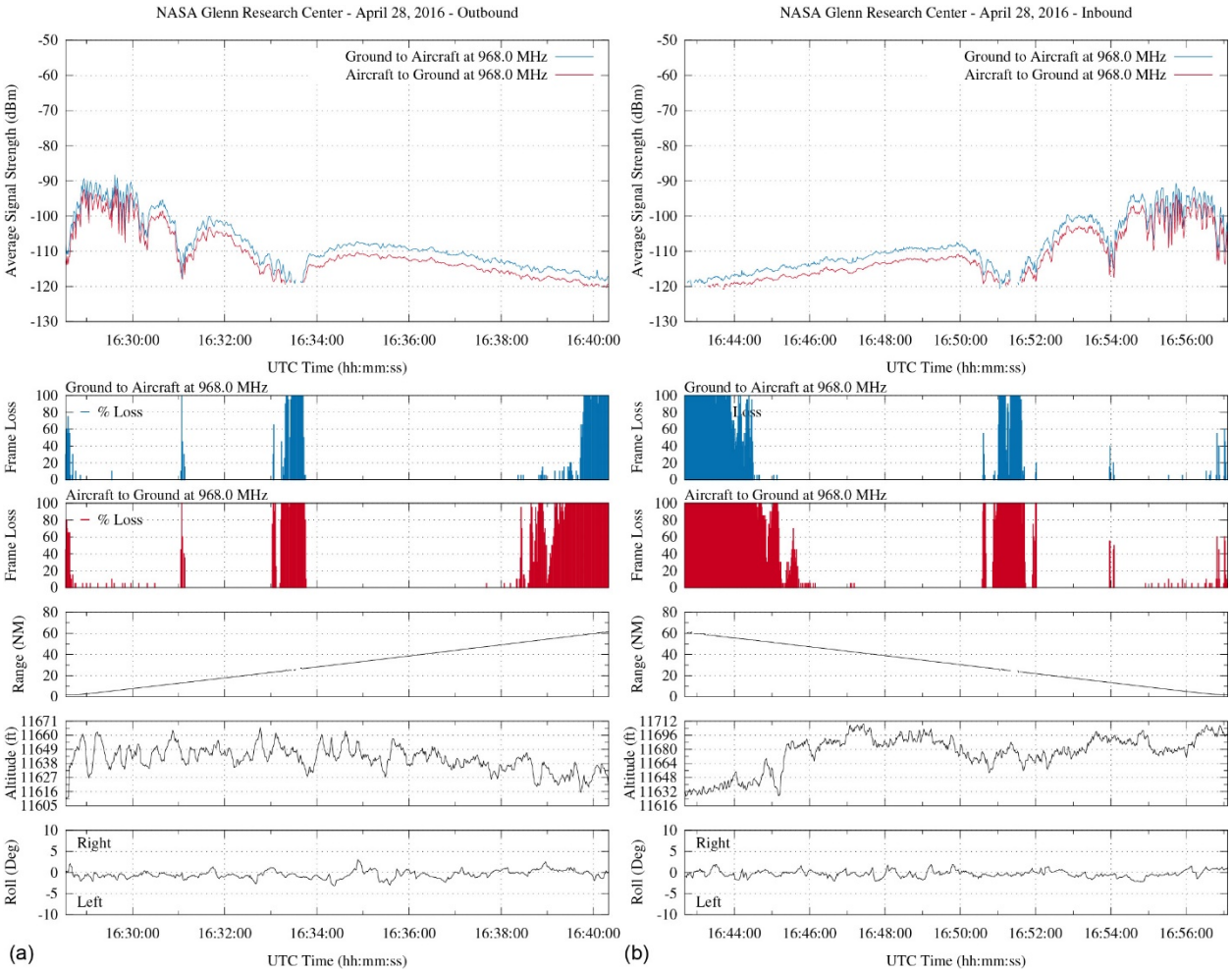

Figure A.44.—L-band signal strength and frame loss over hilly terrain during outbound track. (a) From ground station 2 (GS2). (b) Toward GS2.

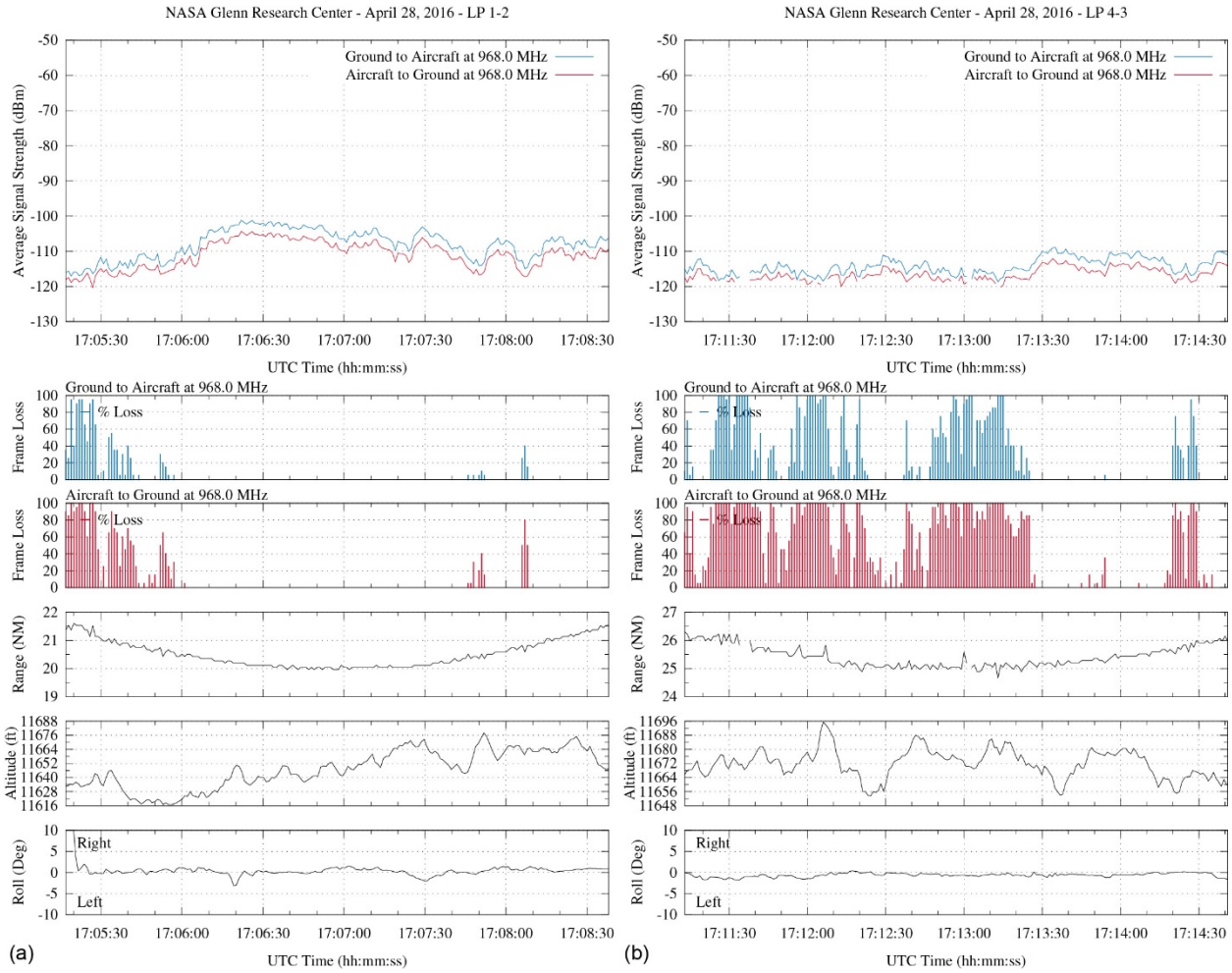

Figure A.45.—L-band signal strength and frame loss over hilly terrain. (a) At 20-nmi range and 11,600-ft altitude. (b) At 25-nmi range and 11,600-ft altitude.

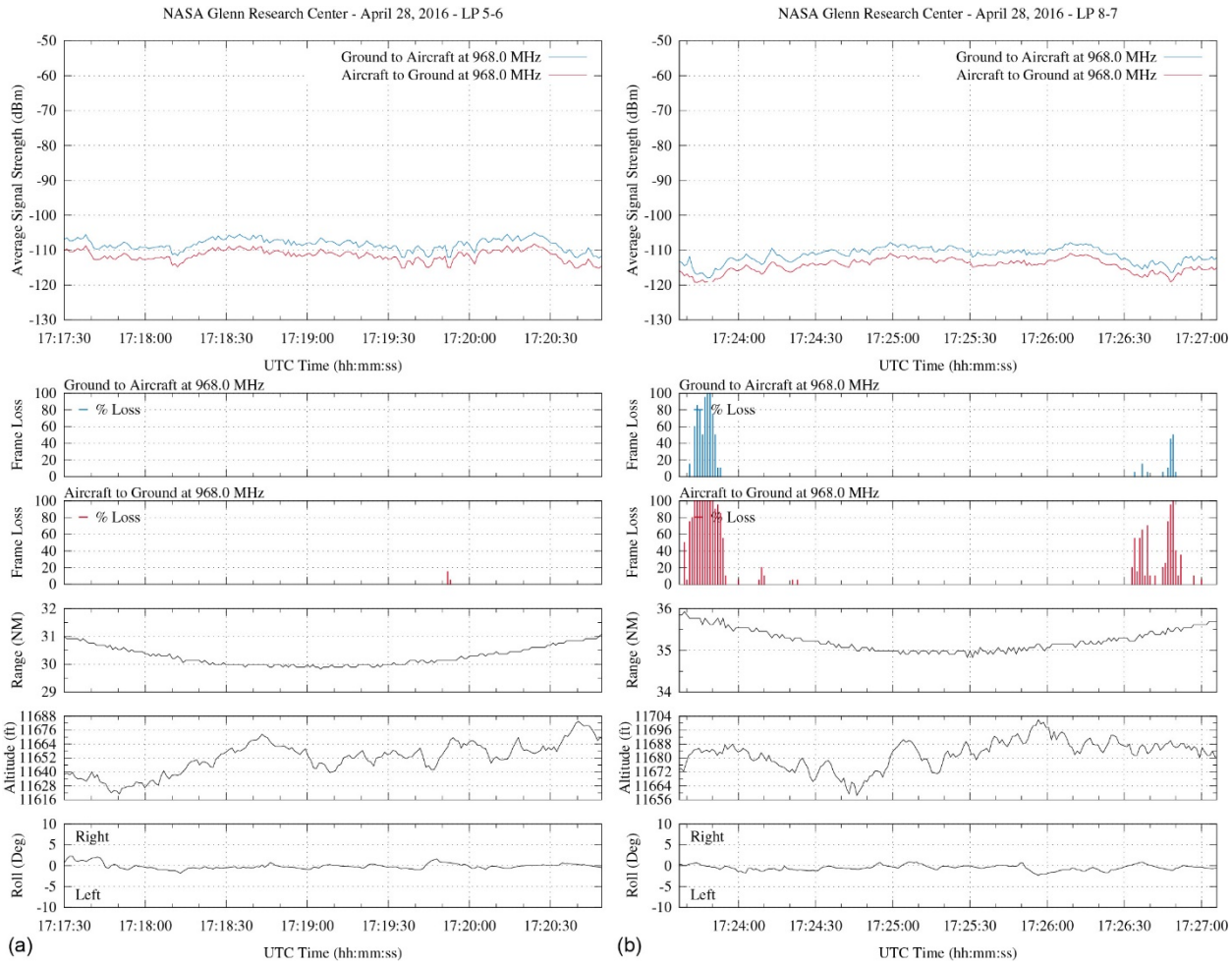

Figure A.46.—L-band signal strength and frame loss over hilly terrain. (a) At 30-nmi range and 11,600-ft altitude. (b) At 35-nmi range and 11,600-ft altitude.

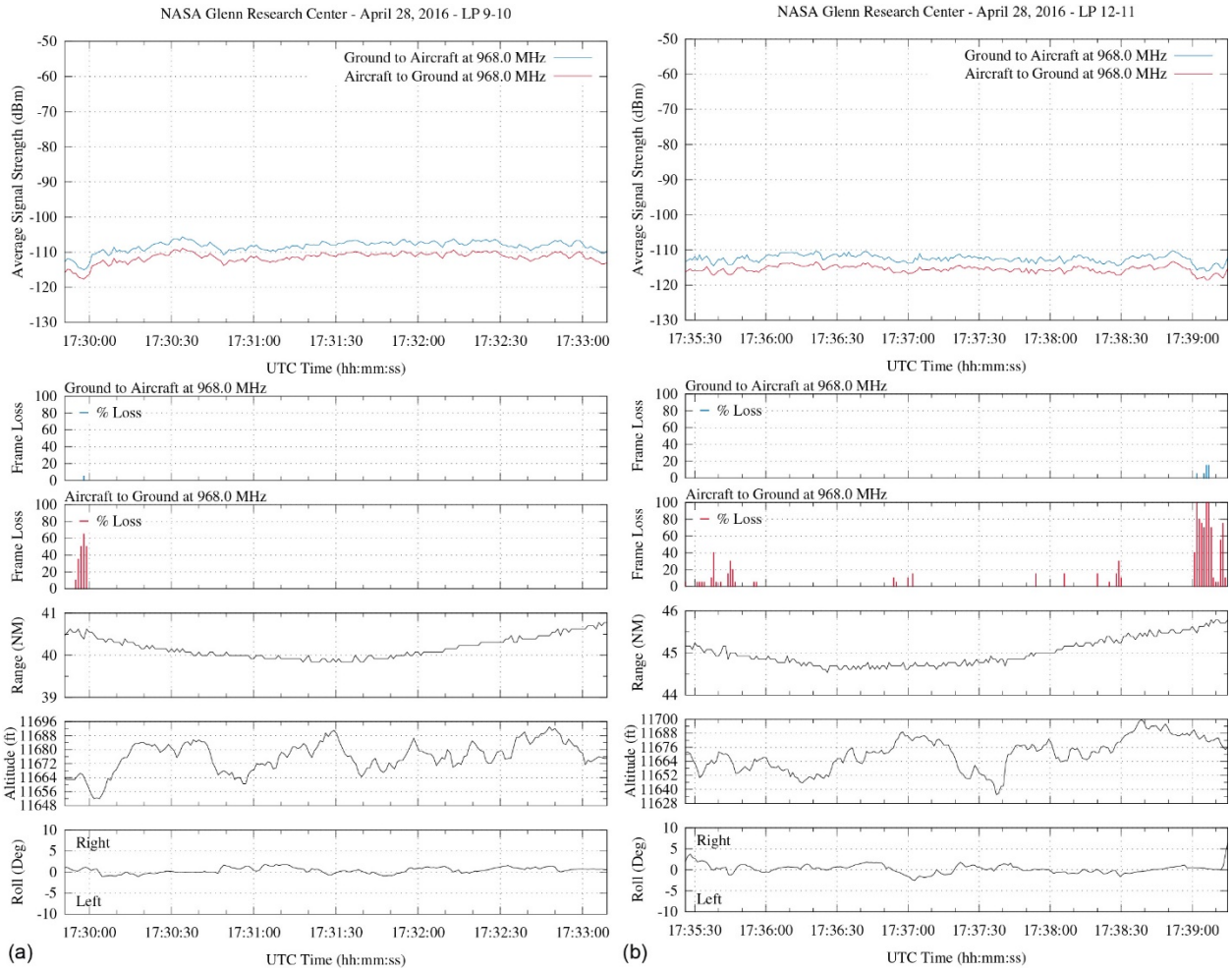

Figure A.47.—L-band signal strength and frame loss over hilly terrain. (a) At 40-nmi range and 11,600-ft altitude. (b) At 45-nmi range and 11,600-ft altitude.

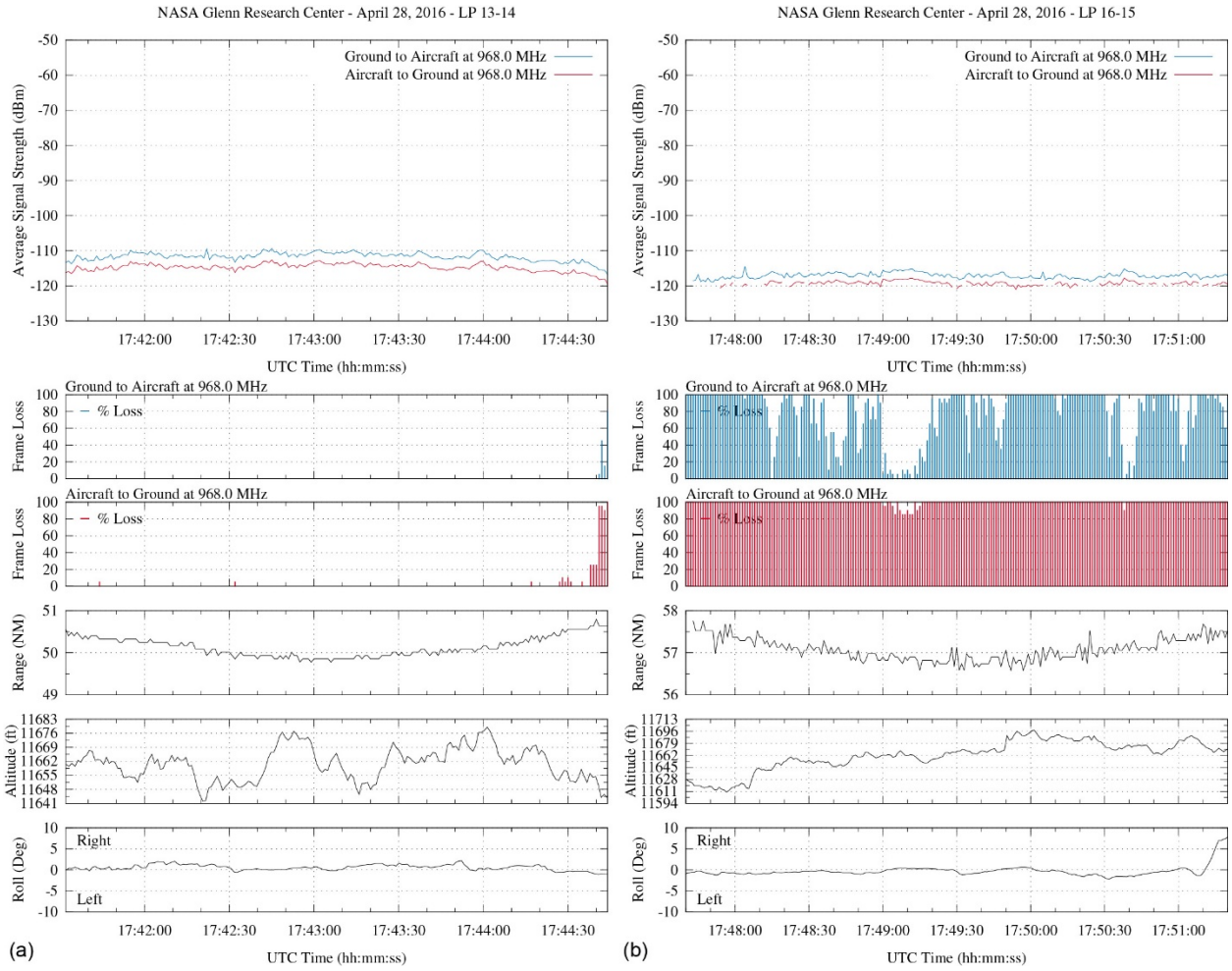

Figure A.48.—L-band signal strength and frame loss over hilly terrain. (a) At 50-nmi range and 11,600-ft altitude. (b) At 56-nmi range and 11,600-ft altitude.

Appendix B.—Abbreviations, Acronyms, and Symbols

6in4	Protocol 41
ACK	acknowledgment
AES–GCM	Advanced Encryption Standard in Galois/Counter Mode
AH	authentication headers
AR	access router
ATC	air traffic control
BU	binding update
C2	command and control
CDF	cumulative distribution function
CMAC	Cryptographic Message Authentication Code
CN	correspondent node
CNPC	Control and Non-Payload Communications
CoA	care-of address
ECDSA	Elliptic Curve Digital Signature Algorithm
EPL	excess path loss
ESP	Encapsulating Security Payload
FAA	Federal Aviation Administration
GMSK	Gaussian minimum shift keying
GPS	Global Positioning System
GS1	ground station 1
GS2	ground station 2
GS3	ground station 3
HA	home agent
HoA	home address
IKEv2	Internet Key Exchange version 2
IP	Internet Protocol
IPv4	Internet Protocol version 4
IPv6	Internet Protocol version 6
IPMI	Intelligent Platform Management Interface
LAN	local area network
MOPS	Minimum Operational Performance Standards
MR	mobile router
MSL	mean sea level
NAS	National Airspace System
NAVAID	navigational aid
RA	Router Advertisement
RF	radiofrequency
ROHC	Robust Header Compression
RTP	Real-time Transport Protocol
SATCOM	satellite communications
SMA	SubMiniature version a

STANAG	NATO Standardization Agreement
TCP	Transmission Control Protocol
TNC	Threaded Neill-Concelman
UA	unmanned aircraft
UAS	Unmanned Aircraft Systems
UDP	User Datagram Protocol
UPS	uninterruptible power supply
USB	Universal Serial Bus
VPN	virtual private network
WAN	wide area network

Symbols:

G_{rx}	receiver antenna gain
G_{tx}	transmitter antenna gain
$L_{path\ loss}$	path loss
$L_{rx\ cable}$	receiver cable loss
$L_{tx\ cable}$	transmitter cable loss
m	total number of UAs
P_r	theoretical received power
P_t	transmit power

References

1. Command and Control (C2) Data Link Minimum Operational Performance Standards (MOPS) (Terrestrial). RTCA Paper No. DO–362, 2016.
2. Shalkhauser, Kurt A., et al.: Control and Non-Payload Communications Generation 1 Prototype Radio Flight Test Report. NASA/TM—2014-218099, 2014. http://ntrs.nasa.gov
3. Ishac, Joseph A., et al.: Control and Non-Payload Communications Prototype Radio—Generation 2 Flight Test Report. NASA/TM—2014-218391, 2014. http://ntrs.nasa.gov
4. U.S. Department of the Interior: National Atlas of the United States, March 5, 2003. http://nationalatlas.gov Accessed Nov. 22, 2016.
5. Map data ©2016 Google. Google, Inc., 1600 Amphitheatre Parkway, Mountain View, CA 94043, http://www.google.com/earth/
6. Standard Interfaces of UAV Control System (UCS) for NATO UAV Interoperability. STANAG 4586 (Edition 3), STO–EN–SCI–271, 2012.
7. IPv6 Python Extension Module. NASA LEW19323–1, 2017. https://software.nasa.gov/software/LEW-19323-1 Accessed April 28, 2017.